AD

USAAVLABS TECHNICAL REPORT 70-14

AN INVESTIGATION OF EFFICIENCY LIMITS FOR SMALL, COOLED TURBINES

By

A. F. Carter
F. K. Lenherr

August 1970

U. S. ARMY AVIATION MATERIEL LABORATORIES
FORT EUSTIS, VIRGINIA

CONTRACT DAAJ02-68-C-0050

NORTHERN RESEARCH AND ENGINEERING CORPORATION

CAMBRIDGE, MASSACHUSETTS

DISCLAIMERS

The findings in this report are not to be construed as an official Department of the Army position unless so designated by other authorized documents.

When Government drawings, specifications, or other data are used for any purpose other than in connection with a definitely related Government procurement operation, the United States Government thereby incurs no responsibility nor any obligation whatsoever; and the fact that the Government may have formulated, furnished, or in any way supplied the said drawings, specifications, or other data is not to be regarded by implication or otherwise as in any manner licensing the holder or any other person or corporation, or conveying any rights or permission, to manufacture, use, or sell any patented invention that may in any way be related thereto.

Trade names cited in this report do not constitute an official endorsement or approval of the use of such commercial hardware or software.

DISPOSITION INSTRUCTIONS

Destroy this report when no longer needed. Do not return it to the originator.

DEPARTMENT OF THE ARMY
HEADQUARTERS US ARMY AVIATION MATERIEL LABORATORIES
FORT EUSTIS VIRGINIA 23604

The research described herein was conducted by Northern Research and Engineering Corporation under Contract DAAJ02-68-C-0050 with the U. S. Army Aviation Materiel Laboratories.

The object of this research effort was to investigate, both analytically and experimentally, the efficiency limits of nine small cooled axial turbine stages. The nine turbine stages were designed for optimum performance and then fabricated into cascade vane and blade rows. These cascades were tested to determine both the profile and total loss coefficients, and the results of the test were used to determine the accuracy of the prediction technique.

Appropriate technical personnel of the U. S. Army Aviation Materiel Laboratories have reviewed this report and concur with the conclusions contained herein.

The findings and recommendations outlined herein will be taken into account in the planning of future small cooled axial turbine programs.

Task 1G162203D14413
Contract DAAJ02-68-C-0050
USAAVLABS Technical Report 70-14
August 1970

AN INVESTIGATION OF EFFICIENCY LIMITS FOR SMALL, COOLED TURBINES

NREC Report No. 1137-1

by

A. F. Carter
F. K. Lenherr

Prepared by

Northern Research and Engineering Corporation
Cambridge, Massachusetts

for

U. S. ARMY AVIATION MATERIEL LABORATORIES
FORT EUSTIS, VIRGINIA

SUMMARY

This report describes the results of a combined analytical and experimental investigation of the efficiency limits of small, cooled turbines. The first section of the report is concerned with the design procedure whereby optimal stage aerodynamic and blade designs were established for nine representative turbine stages. Three levels of corrected work output at each of three annulus heights were considered. The second section contains the results obtained in cascade tests of the resulting stator and rotor mean section blading and six additional rotor root profiles. Both total and profile losses were measured in each case. In the third section, a correlation of blade row total-pressure-loss coefficient is obtained from the experimental data. Stage efficiencies are then recalculated for the nine original stages based on the derived correlation. The achievable stage efficiencies are presented and discussed in the fourth major section of the report. Results indicate that the aspect ratio penalties associated with small annulus heights are considerably less severe than previous studies would suggest.

TABLE OF CONTENTS

LIST OF ILLUSTRATIONS

LIST OF TABLES

LIST OF SYMBOLS

Symbols	Description	Units
A	Annulus area	sq in.
A_W	Annulus wall area	sq in.
A_B	Blade surface area	sq in.
C	Blade chord	in.
C_p	Specific heat at constant pressure	Btu/lbm/^oR
f	Arbitrary function	-
F	Additional loss, or correction, factor	-
g_o	Constant in Newton's law	lbm-ft/lbf-sec^2
ΔH	Specific stagnation enthalpy drop	Btu/lbm
H	Annulus height	in.
h	Heat transfer coefficient	Btu/sq ft/hr/^oR
J	Mechanical equivalent of heat	ft-lbf/Btu
k	Rotor tip clearance	in.
K	Constant determining coolant radial temperature distribution	per ft
K_S	Stator additional secondary loss factor	-
K_R	Rotor additional secondary loss factor	-
K_1	Constant relating total-to-profile loss ratio to wall-to-blade area ratio	-
K_2	Constant relating total-to-profile loss ratio to passage aspect ratio	-

Symbols	Description	Units
ℓ	Blade suction surface length	in.
N	Rotational speed	rpm
N_B	Number of blades	-
N_c	Number of coolant passages in a blade	-
o	Throat width	in.
p	Static pressure	psi
P	Perimeter	ft
P_o	Total pressure	psi
r	Radius	ft
R	Gas constant	lbf-ft/lbm/^{o}R
γ	Specific heat ratio	-
Re	Reynolds number	-
s	Pitch	in.
T	Static temperature	^{o}R
T_o	Total temperature	^{o}R
t_e	Trailing-edge thickness	in.
U	Blade speed	ft/sec
V	Velocity	ft/sec
W	Coolant flow rate in a passage	lbm/hr
x	Axial distance	in.
y	Tangential distance	in.
Y	Total-pressure-loss coefficient	-
z	Radial distance	in.
β	Flow angle	deg

Symbols	Description	Units
δ	Ratio of inlet total pressure to standard sea level conditions	-
D	Hub-to-tip diameter ratio	-
θ_{cr}	Temperature correction factor for standard sea level conditions	-
μ	Viscosity	lbm/ft-hr
ξ	Rotor blade area taper ratio	-
ρ	Density	lbm/cu ft
η	Efficiency	-

Subscripts	Description
c	Coolant
c_o	Coolant at inlet
D	Datum
ex	Exit
hub	Conditions at hub
in	Inlet
m	Metal or mean line
mp	Mean line with suction
p	Profile
s	Gas or secondary
T	Total
w	Wall
$*$	Reduced or extreme value
1	Traverse station
2	Fully mixed station
$Isen$	Isentropic

INTRODUCTION

One of the problems identified by previous programs of work ultimately directed toward the development of small gas turbines of advanced design has been the relatively low level of efficiency obtained from small, cooled turbines. To achieve lighter, more compact power plants, the trend has been toward higher pressure ratio and higher turbine inlet temperatures and the resultant increase in engine specific power output. One objective of the U. S. Army Aviation Materiel Laboratories is to develop an engine with a specific power output in excess of 200 hp sec/lbm of airflow. For the power output range of interest, the engine mass flow range under consideration is from 2 to 5 lbm/sec. The combination of a low mass flow rate and a high turbine inlet pressure results in small turbine annulus areas, while the high temperature levels necessitate blade cooling. Since it is desirable to drive a single-shaft, high-pressure-ratio compressor with a single-stage turbine, the high loading of the turbine stage is an additional factor that has to be considered.

The principal reasons for the relatively low efficiency of the type of turbine of interest are the relatively low aspect ratio of the blading, the relatively high trailing-edge blockage of the blading, and the level of work output. Because of the cooling requirements and manufacturing limitations, blade chords and trailing-edge thicknesses are dictated by mechanical, rather than aerodynamic, considerations. Since blade row aspect ratios will be lower and trailing-edge blockages will be higher than those occurring in larger engines and since both factors will influence the row total-pressure-loss coefficients, it is extremely unlikely that the efficiency of the small turbines can be as high as that achieved in larger engines with comparable turbine work output levels. The primary objective of the program reported herein was to derive a correlation of row total-pressure-loss coefficients that could be applied in the prediction of the efficiency of turbines of the type having application to small engines of advanced design; the secondary objective was to define the level of achievable efficiency for three levels of corrected work output as a function of selected blade height.

The investigation is based on nine possible turbine designs for the first-stage turbine of an engine having a mass flow rate of 5 lbm/sec, a cycle pressure ratio of 10:1, and a turbine inlet temperature of 2500 ^{o}F. For each of three specified corrected work outputs, three values of annulus height were also specified. The corrected work outputs ($\Delta H/\theta_{CT}$) are 27, 22, and 17 Btu/lbm; the highest work output corresponds to the case in which the compressor is driven by a single-stage turbine, while the lowest level is approximately that which would be used for the first stage of a two-stage compressor turbine. The three selected annulus heights are 1.0, 0.7, and 0.4 in. To complete the design-point specifications, a rotational speed has to be selected for each of the nine designs. Since the engine pressure ratio and mass flow are common to all nine designs, each turbine was assumed to have the same design-point rotational speed. To

select the speed, the design of the compressor for a 5-lbm/sec, 10:1-pressure-ratio engine was considered. While a variety of compressor configurations are possible, a single-stage centrifugal was chosen as the basis for the rotational speed selection. From consideration of the compressor specific speed, a design-point rotational speed of 50,000 rpm was assumed for all nine turbine designs.

All turbines will be of relatively small annulus height. However, annulus height is a design variable that can be selected directly or indirectly by the turbine designer. Designs selected to have low values of the stage loading parameter, $g_c J \Delta H / U^2$, will have small blade heights. In these designs it is probable that the adverse effects on stage efficiency of low-blade-row aspect ratios will offset the advantages of low stage loading. Conversely, if a design is selected to have larger values of blade height and blade aspect ratio, stress considerations will dictate a smaller value of mean radius and a higher stage loading. For the investigation, the values of annulus height chosen for the designs are 1.0, 0.7, and 0.4 in. The designs of 1.0 in. annulus height will have relatively high stage loadings and will be of relatively low hub-to-tip diameter ratio. For the lowest value of annulus height, the stages will have moderate stage loading parameters. Since the blade chords are dictated by the cooling and manufacturing requirements, the small annulus height designs will have low-aspect-ratio blading; the losses associated with low-aspect-ratio blading will possibly offset the benefits of the selection of a moderate value of stage loading.

Following stage aerodynamic and blade design for each stage, two-dimensional cascades of the nine stator mean sections, the nine rotor mean sections, and the six rotor hub sections of the 0.7- and 1.0-in.-annulus-height designs were manufactured. Two additional cascades in which the stator mean of the 0.7-in.-annulus-height, 22-Btu/lbm stage was leaned 10 and 20 deg with respect to a normal to the end walls were also manufactured. The cascades were tested at design values of exit Mach number both with solid end walls and with a porous end wall which allowed the removal of end-wall boundary layers. These cascade tests have provided the total and profile loss coefficient data upon which a correlation of loss coefficient has been based.

In the final phase of the program, the loss coefficient correlation that has been developed has been applied to the prediction of stage efficiencies. Since the measured cascade loss coefficients are significantly lower than those that can be deduced from stage tests of the type of turbine under consideration, it has been necessary to define the efficiency limits of the small, cooled turbines in terms of empirical constants which nominally relate the magnitude of secondary losses measured in a two-dimensional cascade to those existing in turbine blade rows in a stage.

STAGE AERODYNAMIC AND BLADE DESIGN

INTRODUCTION

In order to ensure that the cascades to be tested in the experimental program would be representative of the blade sections that would be used in an actual small, cooled engine application, the design of the basic stages is treated as such. Each stage design was based on the achievement of the required life of the turbine of 1000 hr using air cooling. Hence, the selection of blade chords, blade maximum and trailing-edge thickness, rotor blade area taper ratios, and number of blades per row was based on both aerodynamic and mechanical design requirements.

To ensure that fully consistent designs were obtained, the initial phase made use of a loss coefficient correlation that had been demonstrated to be applicable to the type of stage involved. In particular, the correlation had been used in the successful prediction of the stage efficiencies of three low-aspect-ratio turbines tested by Continental Aviation and Engineering Corporation (Reference 1) as part of an earlier program of work for USAAVLABS.

The selection of a constant rotational speed for all nine stage designs has two basic advantages. One, the selection of a turbine design standard is set in the context of a design problem frequently faced by the turbine designer when the gas generator speed is selected from compressor design considerations. Two, the combination of a constant rotational speed with ranges of corrected work output and annulus height produces a wide range of blading types. As a result, the cascade testing of representative bladings will adequately cover the range of parameters necessary to derive a loss correlation that could subsequently be applied to a wide range of small, cooled turbine design requirements. As previously stated, the selected speed is 50,000 rpm. While the selection of any other speed for all designs or individual design speeds would have resulted in a different set of cascades on which the correlation is based, the resultant correlation should not be dependent on the choice of rpm. In the current investigation, the predicted achievable stage efficiencies are for the original designs. However, the correlation of total-pressure-loss coefficients could be used in design optimization studies in which rotational speed is a variable. Similarly, the selection of a mass flow rate of 5 lbm/sec will not preclude the application of the loss correlation to engines of different flow rate, provided the range of aspect ratios investigated in the cascade test program adequately covers the range that is encountered in the design of small, cooled turbines.

STAGE DESIGN SPECIFICATIONS

The turbine design specifications common to all nine turbines are:

Mass Flow Rate	5 lbm/sec
Turbine Inlet Total Pressure	142 psia
Turbine Inlet Total Temperature	2,500 °F
Rotational Speed	50,000 rpm

The three levels of corrected work output are 27, 22, and 17 Btu/lbm corresponding to actual power outputs of 1125, 917, and 709 hp. As previously stated, for each work output level the three annulus heights considered are 1.0, 0.7, and 0.4 in.

The level of the inlet temperature necessitates blade cooling, and it was assumed that blade trailing-edge thickness would have to be limited to 0.030 in. in order to ensure the manufacturing feasibility of the cooled blading.

THE ORIGINAL STAGE DESIGNS

Selection of Annulus Dimensions

With the rotational speed held constant for all designs, the selection of the annulus dimensions for each design must be made principally on the basis of the minimum area that is aerodynamically acceptable. The critical stress level in a turbine design is at or near the rotor hub section, and this level is dependent upon N^2A, where N is the selected rotational speed and A is the mean annulus area of the rotor. The taper ratio of the rotor blading will influence the stress level, and the allowable stress level will depend on the gas relative total temperature at the critical section. Hence, the final selection of the annulus dimensions was made on the basis of the coolant flow requirements of each stage, the objective being that the coolant flow required for each design to achieve the specified life of the engine would be a constant percentage of the engine mass flow.

Since the permissible variation in annulus area between designs of differing annulus heights but constant work output is relatively small, the large annulus height design (1.0 in.) is forced to be a relatively low hub-to-tip diameter ratio stage, while the small annulus height necessitates a high hub-to-tip ratio stage. Similarly, the choice of annulus dimension is influenced by the required work output. The highest work output designs (at 27-Btu/lbm corrected work output) have the lowest exit total pressure levels. Hence, to provide the necessary flow area at turbine exit, the mean radius for a 27-Btu/lbm design is necessarily greater than that required for the 17-Btu/lbm design of the same annulus height. Thus, the general pattern of annulus dimensions for the nine stages is that the mean radius of the design will increase with a decrease of annulus height and with an increase of work output. The trend is illustrated in Figure 1, where the selected annulus dimensions are diagrammatically represented.

The final selection of annulus dimensions were based on the detailed design of each stage. For example, it was found necessary to increase the annulus area of the large blade height designs compared to the value used for the 0.4-in. design in order to avoid impulse conditions at the rotor hub section.

Although there are possible aerodynamic advantages associated with the selection of an annulus geometry other than one of constant inside and outside diameters through the stage, this annulus type was selected for all designs. The principal reasons for this choice are (1) the blade sections were eventually to be tested in a two-dimensional cascade, and (2) the approach leads to a wider range of design parameters to be investigated in the experimental program. The choice of the constant-annulus configuration does not directly affect any final design selection, in that the experimental data are to be correlated in a form that makes these data of general applicability.

The Originally Assumed Total-Pressure-Loss Coefficient Correlation

It was assumed initially that an existing correlation of total-pressure loss, developed for use in the design-point analysis computer program of References 2 and 3, would be applicable to small turbines provided that loss levels were corrected for the probable effects of low aspect ratio and large trailing-edge blockage. That is, it was assumed that a row total pressure loss could be expressed as the product of a datum level of loss applicable to large turbines and two correction factors.

$$Y_T = Y_D f\left(\frac{t_e}{s}\right) \cdot F \qquad (1)$$

where Y_T is the row loss coefficient
Y_D is a datum loss level applicable to large turbines
$f\left(\frac{t_e}{s}\right)$ is a correction factor for the effect of trailing-edge thickness-to-pitch ratio on the loss level
F is a correction factor for the loss increases associated with low aspect ratio and tip clearance effects.

The correlation for the datum loss used in the design-point analysis is that derived in Reference 2 and is as follows:

$$Y_D = \frac{|\tan\beta_m - \tan\beta_{ex}|}{0.6 + 0.8\cos\beta_{ex}} f\left(\frac{V_{in}}{V_{ex}}\right) \qquad (2)$$

where

$$f\left(\frac{V_{in}}{V_{ex}}\right) = 0.035 \quad \text{if} \quad \frac{V_{in}}{V_{ex}} \leq 0.5$$

and

$$f\left(\frac{V_{in}}{V_{ex}}\right) = 0.035 + 0.15\left(\frac{V_{in}}{V_{ex}} - 0.5\right) \quad \text{if} \quad \frac{V_{in}}{V_{ex}} > 0.5$$

The subscripts **in** and **ex** denote inlet and exit conditions relative to a blade row, β is the relative flow angle measured from the axial direction, and V denotes the relative velocity.* In this correlation, the assumption is made that the loss is proportional to the tangential momentum change across the blade row, dependent on the overall acceleration across the row, and that trailing-edge loss is related to the blade exit angle in that aerodynamic blockage is dependent on the ratio of trailing-edge thickness to throat width.

An assumption made in deriving the above correlation is that the datum loss level is applicable to blade rows in which the trailing-edge-to-pitch ratio is 0.02, where this number is representative of "large engine" design practice. The correction for larger values of blockage, $f(te/s)$, was obtained from the Ainley-Mathieson turbine prediction procedure of Reference 4. In the experimental portion of the program, the loss coefficient measured at the midheight of a large-aspect-ratio blade row (or a small-aspect-ratio blade row with end-wall boundary-layer suction) is defined as a profile loss, Y_p . Since the loss includes that due to the trailing-edge thickness, the profile loss will be equal to the product $Y_D f(te/s)$. Hence,

$$f\left(\frac{te}{s}\right) = \frac{Y_p}{Y_D} \tag{3}$$

The assumed correction for the trailing-edge blockage effect is shown in Figure 2. This figure shows a second scale using the ratio te/o where o is the throat width. The ratio of trailing-edge thickness-to-throat width is considered to be more directly related to the trailing-edge loss mechanism than the ratio te/s. To obtain the second scale, it was assumed that the Ainley correlation based on te/s is valid for a 60-deg exit angle blade for which the value of o/s is approximately 0.5.

The second correction, F , of Equation 1 was assumed to be given by the equation

$$F = \left[0.6 + 2.4\,\frac{o}{H} + \frac{100}{3}\,\frac{k}{H}\right] f\left(\frac{te}{s}\right) \tag{4}$$

where H/o is the blade row passage aspect ratio, and k/H is the ratio of tip clearance to blade height for an unshrouded rotor blade.

---

* For stator blading, the relative angles and velocities are, of course, the absolute values.

Equation 3 was derived from the stage test data of Reference 1. In the series of tests reported in Reference 1, blade aspect ratios and tip clearances were varied and stage efficiencies measured. It was found that successive reductions of blade height from 1.086 to 0.724 and 0.362 in. decreased the stage efficiency from 86.7 to 82.2 and 73.2 percent, respectively. The constants 0.6 and 2.4 of Equation 3 produce an acceptably accurate prediction of the observed results. Similarly, the constant 100/3 was derived from the experimental results of the series of tests in which stage efficiencies were measured at various levels of tip clearance.

Selection of Number of Blades

If the loss correlation selected correctly represents the variations of loss with passage aspect ratio and trailing-edge blockage, the additional loss factor variation with number of blades can be used to select an aerodynamic optimum number of blades. Increasing the number of blades reduces the loss as a result of the increase in passage aspect ratio, while the accompanying increase in trailing-edge blockage will tend to increase the loss. Typical variations of the additional loss factor with number of blades (based on the originally assumed loss correlation) are illustrated in Figure 3. The data shown in the figure were obtained from Equation 3 for two stage aerodynamic designs of the intermediate work output level; the largest and smallest blade height designs were considered. For each stator and rotor blade row, the height and trailing-edge thicknesses were held constant and the throat width and pitch varied with the number of blades. The basic profile loss was assumed to be constant in each case. Hence, an increase in the number of blades implies a reduction in the blade chord with the row solidity held constant. The figure illustrates the relative insensitivity of loss to the selected number of blades in the vicinity of the optimum and the considerable difference in the optimum number of blades, depending on the choice of annulus height. The large value of the optimum number of blades for the small annulus height reflects the assumed strong dependence of the loss level on aspect ratio where the aspect ratio is low. While it would appear that an aerodynamic optimum or near-optimum number of blades could be selected for the larger value of annulus height, it is evident that for the 0.4-in.-annulus-height designs, the basis for selection of the number of blades must be the mechanical feasibility of cooling the blading. Thus, the approach adopted was to evaluate the minimum chord for which blade cooling would be possible and to use this minimum chord unless the aerodynamic optimum number of blades would produce a larger, more readily cooled blade chord.

In the initial design of the stages, the uncertainty associated with the loss coefficient correlation was such that the selection of the number of blades was not considered to be critical to the overall success of the investigation. Rather, there was some virtue in selecting blading for cascade tests that would provide a wide range of parameters for the experimental program, provided no chord length was selected that would lead to blading which could not be cooled. The number of blades in the stator and rotor rows for each of the nine designs is shown in Table I.

Thermomechanical Design

Previous small turbine investigations have shown the interdependence of turbine efficiency and the adequacy of turbine cooling. The aerodynamic compromises made to achieve adequate cooling have resulted in very low turbine efficiencies. Conversely, if the design standards had been set by aerodynamic efficiency considerations, it is extremely unlikely that adequate cooling, and hence life, would have been achieved. It was considered important, therefore, to compare designs which could be expected to meet the life requirements. Since the quantity of coolant flow required to achieve the necessary life will affect the basic engine cycle efficiency, an additional constraint that approximately equal coolant flow rates would be used was also imposed. If this design objective is met, then both the effect of coolant flow rate on turbine stage performance and the effect of a cooled flow bleed on the engine cycle can be expected to be approximately constant for all nine designs.

The choice of the number of blades only slightly affects the gross cooling requirement, assuming that the effectiveness of the cooling system is not greatly changed from design to design. However, the distribution of cooling is important, and to cool the hottest parts of the blading becomes more difficult as the size of the blade decreases. For example, in the case of convective cooling in which a minimum coolant hole size is selected, approximately the same number of coolant holes is required irrespective of the number of blades; and as the number of coolant passages per blade decreases, the temperature distribution problem increases. When the distribution problem becomes serious, the amount of coolant flow has to be increased to produce sufficient local cooling.

For convection-cooled blades, a practical limit on blade chord was assumed to be approximately 0.6 in. For transpiration cooling, which might be used in view of the large coolant flows required for convective cooling, a similar chord limitation exists. Therefore, the number of blades in any row was set near the calculated optimum or at a value for which a chord of not less than 0.6 in. would be obtained during the detailed design of the blading. This selection required the assumption of values of pitch/chord ratio for each row. During the detailed design of the blading, somewhat larger chords were shown to be necessary for the selected number of blades. The actual chords of the sections tested in the experimental phase of the program are listed in Table II, from which it will be seen that the minimum chord used is 0.66 in. Selected stator chords vary from 0.660 to 0.840 in., and the rotor root sections of the 0.7- and 1.0-in. annulus designs have chords ranging from 0.850 to 1.060 in.

To demonstrate that these blades could be cooled, calculations assuming convective cooling were undertaken. The procedure is presented in Appendix I together with the results from three rotor blade analyses. Although it had been an objective to have approximately the same coolant flow in each design, the calculated rotor coolant flows varied from 7 to 10 percent. The largest annulus height design requires more coolant flow, but

the larger coolant flow is in part due to the larger annulus area specified for this blade height. Figure 4 presents computed rotor hub section centrifugal stress and gas relative temperature for each design. This figure also shows the allowable metal temperature as a function of stress level for one possible blading material (MAR-M200). It will be seen that the gas relative temperatures are between 600 and 750 deg above the allowable metal temperatures required for a 1000-hr life. The designs for a 27-Btu/lbm specific work output have higher levels of stress than the designs of corresponding height for the 17-Btu/lbm work output. However, the disadvantages of higher stresses (resulting from the larger annulus area requirement) are offset by lower rotor relative gas temperatures which accompany the larger stage total temperature drop. Although Figure 4 indicates the need for varying levels of cooling, the variation is relatively small. Hence, it is reasonable to assume that the selected designs would require approximately the same quantity of coolant and would have approximately the same efficiency penalty associated with their cooling requirements.

Stage Aerodynamic Designs

Each of the designs was completed using the design-point analysis computer program of References 2 and 3. Aerodynamically consistent designs were completed by specifying additional loss factors for the selected number of blades. Although the annulus dimensions had previously been selected on the basis of a required stage exit Mach number, some midradius changes were made during the course of finalizing each design. In particular, the hub loading of the 1.0-in.-annulus design forced an increase in the originally selected values of mean radius. Each design was selected on the basis of varying the stage reaction to optimize the stage total-to-total efficiency. The total-to-total efficiency is calculated from the ratio of actual total temperature drop to the isentropic value based on the stage total pressure ratio ignoring the addition of any coolant flow to the main flow through the turbine stage. Hence, the total-to-total efficiency, η, is given by

$$\eta = \frac{\Delta T_0}{\Delta T_{0\,ISEN}} = \frac{\Delta T_0}{T_{00}} \Big/ \left\{ 1 - \left(\frac{P_{02}}{P_{00}} \right)^{\frac{\gamma-1}{\gamma}} \right\} \qquad (5)$$

where P_{00}/P_{02} is the stage total-to-total pressure ratio.

The mean-line aerodynamics of the selected designs are presented in Table III. The table contains flow angles, Mach numbers, the mean stage loading ($g_c J \Delta H/U^2$), and the value of stage efficiency consistent with the originally assumed row total-pressure-loss coefficient correlation of Equations 2 and 3. Table IV presents the hub-line aerodynamic data for the 0.7- and 1.0-in. designs. Hub-line aerodynamic data for the 0.4-in. designs have not been included in Table IV; these stages have relatively high hub-to-tip diameter ratios, and the flow conditions at the hub differ but little from the mean-line data of Table III.

DETAILED BLADE DESIGN

Blade profiles were designed using a prescribed surface Mach number procedure. The Stanitz channel design method of Reference 5 forms the basis of the method incorporated into an NREC computer program. The Stanitz method obtains the geometry of a channel which satisfies specified channel wall velocity distributions; the island formed by two adjacent channels defines a blade profile. To obtain the solution of the channel geometry, linearized compressible flow is assumed. A number of improvements were made to the original Stanitz method when it was programmed. These improvements are mainly associated with the application of the basic solution technique to the profile design problem. The most significant change is in the treatment of the upstream stagnation streamline. The improved method eliminates the upstream cusp formed when a blade profile is defined by two channels. As a result, the Stanitz channel design procedure has been modified to yield a profile design method. To obtain turbine blade profiles, surface Mach number distributions are specified at points along the pressure and suction surfaces of the blade. While an arbitrary selection of surface Mach number distributions will in all probability yield an unacceptable profile, techniques have been developed that permit logical modifications of the prescribed distribution to obtain desired profile characteristics. The principal characteristics are trailing-edge thickness, profile chord, and profile cross-sectional area. Each profile was designed to have the preselected 0.030-in. trailing-edge thickness. In the design of the rotors, chords and sectional areas of root and tip profiles were selected to yield mechanically acceptable blading from both manufacturing and stress considerations. The root-to-tip sectional area ratios for 0.4-, 0.7-, and 1.0-in. designs were chosen to be 1.5, 1.75, and 2.0, respectively. The increase in taper ratio accompanies the decrease in stage hub-to-tip diameter ratio, and actual values were selected to reflect standard design practice. Although the parameter N^2A has a strange influence on blade root section stress levels, stage hub-to-tip diameter and blade taper ratios also influence the level of maximum stress. By increasing the blade taper ratio with decreasing stage hub-to-tip diameter ratio, the detailed blade design attempted to satisfy the requirement that stages of differing blade height could be considered as valid alternatives meeting the stage loading and life specifications with approximately equal coolant flow rates.

Typical blade sections are shown in Figures 5 and 6. The first of these is the stator mean section of the 17-Btu/lbm work output design of 0.4-in. annulus height; Figure 6 shows the three basic sections of the rotor of the same stage. In Figure 7, the surface Mach number distributions used to obtain the profiles shown in the two preceding figures are presented. The actual surface Mach number specifications for the 24 cascade sections are presented in tabular form. Table V lists the Mach number distributions for the two surfaces as a function of the selected normalized surface lengths for the stator mean sections; between each of the listed change points, the Mach number versus length variation is assumed to be linear, as illustrated in Figure 7. Table VI presents the Mach number

distribution specification for the rotor means, and Table VII presents the specification for the six rotor hub sections. For each design, the maximum surface Mach number and diffusion rate were each held to as low a value as possible. The basic intent is, of course, that boundary-layer growth should be minimized and that shock-induced separation should be avoided if possible in the designs of high subsonic exit Mach number.

The profile coordinates for the 24 sections tested in the cascade rig are given in Appendix II. The **x-y** coordinates for the surfaces, the surface lengths, and the cross-sectional area of the profiles are listed. These coordinates correspond to points at 5 percent of surface length increments.

The blade section geometries of the profiles that were cascade-tested are listed in Table VIII. This table presents the numbering system used to identify the cascades and the pitch, pitch/chord ratio, chordal aspect ratio, and passage aspect ratio of each of the 24 rectangular cascades. Cascades 19 and 20 are leaned versions of cascade 9 (the 0.7/22 stator mean section); the first of these is leaned 10 deg with respect to the normal to the end wall, while the second is leaned 20 deg.

CASCADE TESTING

INTRODUCTION

The objectives of the cascade test program were to determine the three-dimensional and two-dimensional total-pressure-loss coefficients of each of the selected cascades.

The three-dimensional loss includes the secondary losses which were expected to be significant in low-aspect-ratio blades. The two-dimensional loss, or profile loss, is the loss that would be measured in an infinite-aspect-ratio cascade in which end-wall effects would not influence the level of loss. In any cascade or blade row, any boundary layer at the end wall is under the influence of the static pressure field. Any fluid whose velocity is less than that of the free stream at a corresponding location in the flow passage will be forced toward the suction surface side of the flow passage. The resultant secondary flow is known to give rise to large values of secondary flow losses. In the experimental program it was the intention to remove end-wall boundary layers by the use of wall suction in a second test of each cascade. By removing the end-wall boundary layer, it was believed that any accumulation of low-momentum fluid at the junction of the suction surface and end wall would be sufficiently reduced that measurements of total-pressure-loss coefficients made at the midheight of the cascade would be representative of a large-aspect-ratio cascade. Thus, the original test of the cascade with solid end walls would yield the total, or three-dimensional, loss; a subsequent test with end-wall suction was expected to yield a profile, or two-dimensional, loss at the midheight of the cascade. As defined in the preceding chapter, the profile loss includes the trailing-edge loss.

CASCADE RIG DESIGN

The principal features of the cascade rig are a large inlet plenum, a cascade inlet section, the cascade block, and the exit traverse mechanism. Air at the required pressure is supplied to the inlet plenum, and, for the suction tests, air is sucked from small plenum chambers adjacent to each of the cascade end walls. Exploded views of the cascade rig assembly are shown in Figures 8 and 9. Figure 8 shows the plenum and the parts external to the plenum, while Figure 9 shows the inlet section which is inserted into the plenum. The cascade blading is machined from a solid aluminum piece, with seven blades and eight flow passages in each cascade. To provide for interchangeability between solid-wall and porous-wall tests, the cascade blading is machined to a depth approximately 0.2 in. below the lower wall. Thus, the alternative end walls can be fitted over the cascade. The top section of the cascade rig carries the traverse mechanisms and is used throughout all tests. The lower section of the cascade assembly, to which the cascade blocks are mounted, has a separate downstream plate, which is used to adjust the row exit height to 0.7 and 0.4 in. from

the maximum value of 1.0 in. The inlet section pieces shown in Figure 9 comprise two plates, two involutes to reduce the upstream inlet height from 2.0 in. to the 0.4-, 0.7-, or 1.0-in. value, and two inlet side walls.

The inlet side walls are constructed from a series of plates which permit the setup of the required inlet flow angle and the total width of the eight-passage cascades for the individual cascades. Sectional views for the inlet configuration for the three cascade heights are shown in Figure 10. The involute transition walls which reduce the passage height were selected to provide a controlled acceleration ahead of the cascade. While a relatively long inlet length is required to ensure that the design inlet flow angles were achieved in each case, long inlets would have produced a significant boundary-layer buildup at the cascade inlet. However, the contraction of the passage height (from 2 in. to 1.0, 0.7, or 0.4, depending on the cascade) using the involute transition walls will reduce wall boundary-layer thickness at the cascade inlet to acceptably small values. No attempt was made to measure the inlet profile. However, from past experience, this design approach is known to result in an extremely good quality of velocity and pressure profile at the inlet to the cascade. A typical cascade assembly is shown in Figure 11. The downstream traverse plane is in each case a chord length in the design exit flow direction downstream of the trailing edge. The selected exit traverse probe dimensions limit the measurement locations to 0.025 in. from the wall. However, actual measurements were never attempted at less than 0.050 in. from the wall.

The traverse mechanisms are illustrated diagrammatically in Figure 12. Part of the upper wall can be translated horizontally to provide the tangential direction traverse. The vertical and flow angle traverse mechanisms are carried on the moving wall. The angular traverse is about the tip of the exit probe. Remote drive and the remote indication of the horizontal, vertical, and angular positioning are provided by three independent hydraulic/potentiometer systems. While the accuracy of each of the systems is very good, traverses are calibrated in terms of indicated dial readings and actual x, z, and β measurements. Accurate positioning of the probe to within 0.001 in. and 0.1 deg is achieved with the traverse mechanism.

TEST PROCEDURE

Each cascade was tested at the appropriate design values of inlet total-to-exit static pressure ratio and inlet flow angle. Since the cascade flow exhausts to ambient pressure, actual inlet pressures were set at the design value of inlet total-to-exit static for the individual cascade times the barometric pressure. Design values of total-to-static pressure ratio for each cascade are listed in Table IX. The inlet total temperature was not a controlled quantity. Inlet temperatures varied with the point of operation of the air-supply compressor. In general, the inlet temperature increased with increasing pressure ratio requirement

for the cascade being tested; temperatures were always within the range 230° to 300°F. The instrumentation standard was maintained throughout. The inlet total pressure is assumed to be equal to the measured plenum static pressure. Exit total pressure, exit static pressure, and flow angle measurements are obtained from the exit traverse instrument. Since traverses at 0.050 in. from the wall were required, the selected probe was the modified conical probe shown in Figure 11. The probe is known to record accurately the local total pressure up to high subsonic Mach numbers. All exit total pressures were recorded as the total pressure drop (ΔP_0) from the measured upstream total pressure.

Angle measurements are made with the two side pressures balanced; any small error in angular position, due to the probe side tap configuration, was eliminated by the *in situ* calibration of the probe using a calibration block in place of a cascade. The apparent dynamic head based on the measured total and side tap pressure is corrected to a true dynamic head (and hence local static pressure is obtained), based on a calibration provided by the instrument manufacturer, United Sensor and Control Corporation.

Traverses With Solid End Walls

To determine total-pressure-loss coefficients, horizontal traverses covering approximately two pitches about the central profile of the cascade were undertaken at four depths from the upper wall. For the 1.0-in.-height cascades, the depths of immersion were 0.071, 0.214, 0.357, and 0.5 in.; for the 0.7-in. cascades, the depths were 0.05, 0.15, 0.25, and 0.35 in. These depth settings correspond to centers of equal area where the height of the cascade is divided into seven equal strips. For the 0.4-in.-height cascades, the depth settings were 0.05, 0.10, 0.15, and 0.20 in. rather than at centers of seven strips because of the inherent difficulties of making measurements at less than 0.030 in. from the wall.

The upper half of the cascade was assumed to be representative of the complete cascade. To check this assumption, a complete depth traverse at approximately the maximum total-pressure-loss position was undertaken to confirm the existence of symmetry about the mean line. In general, acceptable agreement between points equidistant from the two end walls was obtained. Where any significant difference was recorded, the lack of symmetry was found to be due to either a small leakage between the blade profile and the upper wall or a recirculation occurring at the lower wall where the passage end-wall plate fits over the cascade blading. It was found that a perfect seal was required around the blade profile at both the end walls. Any small leakage path at the lower wall from a region of high pressure to a region of low pressure that caused a flow into the blade passage resulted in extremely high losses. Similarly, where the cascade was not perfectly sealed at the upper wall and a small tip leakage was possible, very high losses were observed.

In the initial testing, before the tremendous importance of the end-wall

sealing had been realized, loss coefficients as much as ten times as high as those finally measured were recorded. These results were an unanticipated byproduct of the experimental program. It must be concluded that the turbulent mixing losses associated with the introduction of extremely small quantities of flow with a velocity component normal to the local flow direction can result in total-pressure-loss coefficients that are an order of magnitude greater than those measured in the absence of these secondary flows. In no case in which these high losses were measured were the leakage flows greater than 1 percent of the cascade through-flow based on the probable leakage areas either at the tip of the blade or near the blade profile at the lower wall. The most probable explanation of the high losses is that the introduction of flow normal to the main flow direction triggers a massive flow separation from the blading; the nature of the blade wakes and the variation of measured static pressure in the plane of the downstream traverse confirm the belief that the small leakage flows create a flow separation.

For any cascade in which the loss and the flow angle distribution were not symmetrical, the assembly was rebuilt to eliminate leakage paths. Only the results from cascade tests in which all leakage was eliminated were considered to be valid. While the results from tests in which leakage occurs are of some interest, no detailed analysis would be possible because of the difficulty associated with estimating or calculating the extremely small leakage flow areas and leakage flows that generate the high losses.

Traverses With Porous End Wall

As previously noted, the objective of applying wall suction was to suppress the secondary flow of end-wall boundary layer from the pressure surface side of the end-wall passages to the suction surface. By suppressing this flow, it was believed that valid two-dimensional losses would be measured at the midheight of even the lowest-aspect-ratio cascade. The end-wall configurations for these tests consist of a 40-percent-porosity "electroplate" perforated metal. The porous material is attached to the wall block; and in the region in which suction is to be applied, the material is supported by a honeycomb structure between the porous wall and the suction cavity.

The level of suction to be applied was computed from the assumed design value of the minimum level of static pressure occurring on the suction surface of each profile. The traverses were to be undertaken at the midheight of the cascade, again covering the central blade pitch in the horizontal direction. Additional traverses at one-third and two-thirds of the blade height were selected to confirm the uniformity of the exit flow conditions over the central two-thirds of the passage height. During the initial testing in which the entire wall passage areas between the blade leading and trailing edges and the suction and pressure surfaces were porous, high levels of midsection loss and considerable nonuniformity

were measured. It was concluded, therefore, that this configuration resulted in too large a quantity of air being removed from the flow passage. The most probable cause of the increased loss level is the increase in the inlet-to-exit velocity ratio of the cascade accompanying the removal of too much flow from the cascade. To remedy the situation, the area of porous end wall was considerably reduced. In the finally selected configuration, only the region of low static pressure adjacent to the suction surface is left porous. The porous area was standardized to be of one-quarter pitch in width in the tangential direction and extending along the suction surface from one-third of the axial distance through the cascade to the trailing-edge line.

With this porous end-wall configuration, exit traverses were undertaken at the midheight and two adjacent stations for each cascade. At least two levels of suction pressure were used in each series of tests. In general, these traverses showed an acceptable degree of uniformity of loss over the central part of the blading, indicating that the application of end-wall suction produced a midheight loss which could be considered as a true profile loss. However, in a number of cases, the midheight traverses showed higher levels of loss than had been measured in the corresponding test with solid end walls. This phenomenon is discussed later in the analysis section of the report.

DATA REDUCTION

The traverse data were initially processed to yield local values of total pressure, static pressure, and flow angle for each traverse. Data corresponding to one pitch about the total-pressure wake of the central blade were then selected for the evaluation of total-pressure-loss coefficients. Values of total-pressure-loss coefficients were computed for each horizontal traverse and, in the case of the total loss number, from mass-flow-weighted values of flow quantities covering the half blade height. Since a flow distance of one chord had been selected for the plane of the traverses, these data include the losses due to mixing which occur between the plane of the trailing edge and the plane of the traverse. In addition to the loss coefficients based on measurements in the plane of the traverse, the fully mixed loss coefficients were also computed. These calculations of the "fully mixed" loss coefficients follow the standard method for cascade testing; the method is outlined in Appendix III.

The total-pressure-loss coefficient data are summarized in Table X. Values of total-pressure-loss coefficient are given for four traverse sections (A, B, C, and D) for the tests with solid end walls, the midheight loss coefficient for the tests with applied end-wall suction, and a total loss coefficient for the cascade. The loss coefficients in the last three columns of Table X comprise the data subsequently used in the analysis, where the total loss coefficient is a mass-flow-weighted value for the complete row based on traverses at the four depths of immersion. The data of Table X are grouped into sets of three. For example, the results for

the three 0.4-in.-height stator mean section cascades are listed first, and these are followed by the three rotor mean sections from the 0.4-in.-annulus height stages. In each case, the order in which results are presented is in the order of increasing stage work output. Results from the tests of the two leaned cascades (cascades 19 and 20) are presented and discussed in Appendix IV.

The data concerning the distribution of loss with blade height are of some interest, although these data do not contribute directly to the loss correlations derived later in the report. In only 8 of the 24 cascades listed in Table X is the loss coefficient for the traverse closest to an end wall (section A) the largest of the four measured values. In all but 1 of the remaining 16 cascades, the highest value of local loss coefficient based on the complete constant-depth traverse was at either position B or position C. Cascade number 5 is the only cascade shown to have its maximum value of local loss coefficient at the midheight position. Since there was no obvious reason why this cascade should have different characteristics from the others, the test was repeated following a rebuild of the cascade assembly. However, similar results were obtained. It is of interest that this cascade was designed for, and tested at, the highest value of exit Mach number occurring in the series of cascades. A tentative conclusion would be that a shock-induced separation produced the high level of midheight loss. Although an attempt was made to relate the position of maximum loss to blade chord or passage aspect ratio, cascade height, and loading, no readily established trend was discovered. It would appear that it would be necessary to undertake a considerably more detailed analysis to relate loss distributions to secondary flows. Since such an analysis based on planar cascade tests would not of itself contribute to a greater accuracy in the prediction of stage efficiencies, the attempt to rationalize the measured loss distributions was not pursued further.

To illustrate the variety of distributions measured, the measured total-pressure-loss distributions are shown in Figures 13, 14, and 15 for three cascades. Figure 13 is for cascade number 3, a 0.4-in.-height stator mean section from a stage of 22-Btu/lbm loading. This figure shows the most typical result, in that the highest loss is at section B (which in this case is 0.10 in. from the wall). Figure 14 is for cascade number 12, which is a 0.7-in.-height rotor mean section. In this case, the highest level of loss is measured at section C, 0.25 in. from a wall. The third illustrative example is for cascade number 24, a 1.0-in.-height rotor root section from the 17-Btu/lbm corrected work output stage design. The total-pressure-loss traverse data for this cascade are shown in Figure 15. These data show high end-wall loss and high loss at an immersion depth of 0.357 in.

It should be pointed out that these three cascades are not necessarily representative of their type; for example, the distribution for cascade number 3 cannot be considered to be typical of 0.4-in.-height blade rows, stators, or blade sections from the stages of 22-Btu/lbm work output. Indirectly, the figures illustrate the inherent difficulty of establishing values of total loss coefficients and profile loss coefficients for the cascades.

DATA ANALYSIS AND DERIVATION OF A CORRELATION

INTRODUCTION

The experimental data were expected to yield values of three-dimensional and two-dimensional losses for typical blade sections having possible application to the type of turbine of interest to USAAVLABS in its advanced engine program. These data are to be correlated so that the achievable efficiency of possible alternative designs can be predicted.

Although the data are obtained from two-dimensional cascade tests, and hence are not truly representative of blading in a stage environment, the principal objective was to establish a correlation for secondary losses of low-aspect-ratio blading and for the profile loss of the type of blading necessary in a small, cooled turbine application. However, the correlation obtained from the experimental portion of the investigation must be regarded as a correlation for profile and end-wall losses rather than profile and secondary flow losses. The data for the leaned stator cascades presented in Appendix IV illustrate the fact that the additional secondary flow driving forces usually occurring in a stage environment will increase secondary losses.

TOTAL-PRESSURE-LOSS COEFFICIENT DATA

The data presented in Table X comprise the average total-pressure-loss coefficients for the solid wall test, the midheight loss coefficient from solid wall test., and the midheight loss coefficients measured during tests with end-wall suction. The first of these will be identified as γ_T, the second as γ_m, and the third as γ_{mp}. It was originally believed that γ_T would be representative of the sum of profile and secondary loss, $\gamma_p + \gamma_s$, that γ_m would equal or exceed the profile loss γ_p, and that the measured midheight loss from end-wall suction tests γ_{mp} would equal γ_p. However, from Table X it will be seen that for 5 of the 24 cascades the value of γ_{mp} is greater than γ_T, that for 3 cascades the value of γ_m is greater than γ_T, and that in 12 out of 24 cases the value of γ_{mp} is greater than γ_m.

It is quite obvious that there is a need to explain the apparent anomalies in these results. Clearly, the most serious cases are those in which the mean-line profile loss measured in the suction test γ_{mp} exceeded the total loss with solid end walls. This was observed in the results from cascades 9, 11, 15, 18, and 26. A detailed investigation of one cascade, cascade 9, showed a loss core adjacent to the suction surface but separate from the blade wake. The magnitude of this additional loss could be reduced by lowering the level of suction pressure, but it could not be eliminated altogether. Examination of the cascade test hardware showed that a small area of the porous wall ahead of the row inlet was depressed below the plane of the cascade end wall. The maximum depth of this discontinuity was approximately 0.005 in. It was concluded that a step of the order of

0.005 in. introduced a wall boundary layer and resultant secondary flow which could not be suppressed by end-wall suction. In the worst case, cascade number 26, the level of loss with end-wall suction applied was approximately 70 percent higher than the previously measured total loss. These results are therefore similar to the initial tests with solid walls, where extremely small leakage flows produced large increases in loss. Hence, the principal conclusion drawn from the attempts to trace the causes of apparent anomalies was that any of a number of mechanisms leading to locally thickened boundary layers could lead to large secondary flow losses. The three mechanisms specifically identified in the series of tests were:

1. Leakage flows from pressure to suction surface in any cascade in which a gap existed between the blading and the end wall.

2. A flow into the main stream through the porous end wall in regions of low static pressure adjacent to a blade suction surface when the applied suction pressure was insufficient to ensure the removal of all end-wall boundary-layer flow.

3. End-wall surface irregularities, particularly in the case of the tests with porous end walls, which produce more low-momentum flow than could be removed by applying end-wall suction.

From Table X it will be seen that for cascades 5, 12, and 23, the local loss coefficient at the midheight position (see Column D) is greater than the total loss which is the average for the row. These profiles are all from stage designs of the highest work output (27 Btu/lbm). Hence, these blades are among the most highly loaded in terms of the row deflections and row exit Mach numbers. It is, therefore, to be expected that the flow disturbance due to end-wall secondary flow would extend furthest from the end walls for these designs. The original decision to measure profile loss coefficients using wall suction was of course based on the anticipation that midheight loss of the solid cascades would be greater than the purely profile loss. Since lower levels of midheight loss were in fact obtained during the suction tests of these cascades, the original plan of assuming Y_{mp} to be the true profile loss was retained.

The cases in which Y_{mp} is greater than Y_m, which occurred in half the total number of tests, represent the final anomaly. There are at least two possible explanations of these results: (1) the value of Y_{mp} is increased above a true profile loss value either by secondary flow effects introduced by irregularities in the porous wall or by an increase in the inlet-to-exit row velocity ratio as a result of wall suction; or (2) the levels of midheight loss from the original solid-wall tests are lower than actual profile loss in some instances due to the fact that the presence of end-wall loss increases the overall acceleration of the midheight flow. Unfortunately, there is no way in which it can be validly established which of the two alternatives is correct for a particular cascade. Hence, it was decided to correlate the data on the assumption that the smaller of

Y_m or Y_{mp} would be more representative of the true profile loss, Y_p. This course of action is reasonably valid provided that the points appearing in later presentations of possible correlations clearly identify the two types of "profile" loss coefficients.

DATA CORRELATION

The assumptions made throughout the attempt to correlate the data are that the total-loss coefficient is the sum of profile and secondary loss and that the parameters which influence profile loss also influence secondary loss. The latter assumption makes it possible to consider the total loss as a product of the profile loss and a factor. The attempt to correlate the data is therefore considered first in terms of a correlation for the ratio Y_T/Y_p and a correlation for Y_p.

Aspect Ratio Correlation

Earlier work of NACA personnel (Reference 6) suggests that the secondary loss is purely a viscous wall loss, and hence it is assumed that

$$Y_T = Y_p + Y_w$$

and

$$\frac{Y_T}{Y_p} = 1 + \frac{Y_w}{Y_p} \tag{6}$$

where Y_w is the wall total-pressure-loss coefficient.

Assuming that the losses are purely viscous losses and are related to wetted areas, the ratio Y_w/Y_p would equal A_w/A_B where A_w and A_B are end-wall and blade-surface wetted areas, respectively. Hence, values of $(Y_T/Y_p)/(1 + \frac{A_w}{A_B})$ were obtained for each of the 24 cascades. These values are shown in Figure 16, where the cascade number is used as the ordinate. Cascades 1 to 6 are the 0.4-in. blades, 7 to 12 are the 0.7-in. blades, and 12 to 18 are the 1.0-in. blades. In view of the lack of any systematic trend, it was concluded that the best correlation which could be obtained from these data is

$$\frac{Y_T}{Y_p} = K_1\left[1 + \frac{A_w}{A_B}\right] \tag{7}$$

where K_1 is the arithmetic mean of points shown in Figure 16. The mean value is less than unity (0.894), which is most probably explained by the fact that the profile loss will include a trailing-edge blockage loss. Although there is considerable scatter about the mean value, the fact that blade sections with widely differing deflections, velocity ratios, and design exit Mach number levels have approximately the same value of $(Y_T/Y_p)/(1 + \frac{A_w}{A_B})$ is a good indication that in the cascade tests, the total-loss

coefficient includes a wall friction loss rather than a loss due to secondary flow.

While the correlation based on the ratio $\frac{A_W}{A_B}$ is a useful correlation, in general it is not suitable for preliminary turbine design investigations. In the present case, all the information necessary to calculate $\frac{A_W}{A_B}$ is available. However, for stage aerodynamic designs, it would be more advantageous to use a parameter that does not depend on the detailed design of the blading. It can be shown, although not analytically proven, that the wall-to-blade area ratio is in general approximately equal to the ratio of throat opening to the blade height ($\frac{o}{H}$).

It was, therefore, assumed that the originally selected correlation with passage aspect ratio was correct in its general form; that is,

$$\frac{\gamma_T}{\gamma_P} = \left[1 + \frac{1}{K_2\left(\frac{H}{o}\right)}\right] \tag{8}$$

The values of $\frac{\gamma_T}{\gamma_P}$ have been plotted in Figure 17 against the blade passage aspect ratio. For each point, a value of K_2 was evaluated. For 12 of the 24 cascades, the values of K_2 were in the range 1.0 to 2.0; cascades 7 and 26 had low values of K_2, and cascades 18 and 22 had extremely high values. In obtaining the best fit of the data, the results from cascades 7, 26, 18, and 22 were disregarded. An arithmetic mean of the remaining 20 values of K_2 is 1.6, and this value has been used in the finally selected correlation shown in the figure. In view of the fact that it is difficult to explain why a stator mean section of 0.7-in. blade height from a stage of 17-Btu/lbm work output and a 1.0-in.-height rotor-root section from a stage of 27-Btu/lbm output should have a high total loss and a low profile loss coefficient compared to the other cascades, it must unfortunately be concluded that for these cascades, valid profile loss coefficients have not been obtained. The following correlation is a reasonable fit of the experimental data:

$$\frac{\gamma_T}{\gamma_P} = \left[1 + \frac{1}{1.6\left(\frac{H}{o}\right)}\right] \tag{9}$$

Correlation of Profile Loss

Although there is some uncertainty as to what constitutes the profile loss of each of the cascades tested, it was decided to proceed on the basis that the lower of the values of γ_m and γ_{mp} is in fact the profile loss. At the start of the present program, a correlation for total loss of the following form was used:

$$Y_T = \frac{|\tan\beta_1 - \tan\beta_2|}{0.6+0.8\cos\beta_2} f\left[\frac{V_1}{V_2}\right] f\left[\frac{t_e}{s}\right] f\left[\frac{H}{O}\right] \qquad (10)$$

where $f\left(\frac{V_1}{V_2}\right)$, $f\left(\frac{t_e}{s}\right)$, and $f\left(\frac{H}{O}\right)$ were corrections of a datum level of loss, where this datum level is principally dependent on the tangential loading of a blade section. On the assumptions that the preceding section has established a relationship between profile loss, total loss, and aspect ratio, and that the correction for trailing-edge thickness effects of Figure 2 could be expected to be valid, reduced loss coefficients Y_* were computed for each data point, where

$$Y_* = \frac{Y_p(0.6 + 0.8\cos\beta_2)}{f\left(\frac{t_e}{s}\right)|\tan\beta_1 - \tan\beta_2|} \qquad (11)$$

The Y_* data points were plotted against design values of velocity ratio ($\frac{V_1}{V_2}$) for each section. It was seen that the level of Y_* generally increased with $\frac{V_1}{V_2}$ but that the scatter of points would be reduced if profile losses were reduced using the correction based on the aerodynamic blockage, $\frac{t_e}{O}$. Therefore, a revised version of the reduced loss coefficient Y_*', where

$$Y_*' = \frac{Y_p(0.6 + 0.8\cos\beta_2)}{f\left(\frac{t_e}{O}\right)|\tan\beta_1 - \tan\beta_2|} \qquad (12)$$

was plotted against velocity ratio as shown in Figure 18. The expected increase of loss with velocity ratio is clearly evident. The points corresponding to cascades 18 and 26 have previously been identified as having the most questionable values of profile loss, and these points also lie furthest from the finally selected linear variation of Y_*' with $\frac{V_1}{V_2}$. Therefore, the correlation of profile loss is as follows:

$$Y_p = \frac{|\tan\beta_1 - \tan\beta_2|}{0.6 + 0.8\cos\beta_2} f\left[\frac{t_e}{O}\right] f\left[\frac{V_1}{V_2}\right]$$

where (from Figure 2)

$$f\left(\frac{t_e}{O}\right) = 0.8 + 3.6\left(\frac{t_e}{O}\right) \text{ if } \frac{t_e}{O} > 0.08 \qquad (13)$$

and (from Figure 18)

$$f\left(\frac{V_1}{V_2}\right) = 0.007 + 0.044\left(\frac{V_1}{V_2}\right)$$

The residual scatter of the various test points shown in Figure 18 may simply represent experimental accuracy in the determination of the performance of the actual blading. On the other hand, it could indicate the presence of an additional factor influencing profile loss besides the four employed in the correlation. An obvious parameter of importance in the control of blade boundary-layer thickness is the rate of suction surface

diffusion, defined as the nondimensional Mach number reduction specified over the latter part of the suction surface divided by the fractional surface length over which the diffusion occurs.

Diffusion rate was therefore plotted versus row velocity ratio for each of the cascades. It can be seen in Figure 19 that the rate of diffusion tended generally to increase with overall velocity ratio. However, a fairly wide range of diffusion rates was employed for cascades with similar values of velocity ratio. Hence, the diffusion rate represents an independent parameter which could have affected the measured profile losses.

Two kinds of effect on profile loss could have occurred. First, it is possible that diffusion rate alone caused the observed variation in reduced profile loss coefficient. Second, the correlation of profile loss with velocity ratio may have been fundamentally valid, with the effect of high diffusion rates being simply to elevate the level of the correlation shown in Figure 18. Both of these possibilities were accordingly investigated.

Figure 20 presents the variation of reduced loss coefficient with suction surface diffusion rate. Although there is clearly a trend toward high losses when the diffusion rate is high, the amount of scatter of the test points is greater than that seen in Figure 18. Hence, velocity ratio was retained as the basic correlating parameter.

To investigate the second possible effect mentioned earlier, a best straight line was fitted to the data of Figure 19, separating the cascades into two equal groups of relatively higher or lower diffusion. In 11 cases, cascades having high or low diffusion rates also had respectively high or low reduced profile losses. However, in 13 cases, the opposite relation held. It was therefore concluded that no contribution to the scatter shown in Figure 18 occurred as a result of diffusion rate. Hence, the profile loss correlation given in Equation 13 was retained unchanged.

The Final Correlation

Based on the derived correlations of $\frac{Y_T}{Y_P}$ and Y_P, the final correlation for row total-loss coefficient based on cascade loss is as follows:

$$Y_T = \frac{|\tan\beta_1 - \tan\beta_2|}{0.6 + 0.8\cos\beta_2}\left[1 + \frac{1}{1.6\left(\frac{H}{S}\right)}\right]\left[0.8 + 3.6\left(\frac{t_e}{S}\right)\right]\left[0.007 + 0.044\left(\frac{V_1}{V_2}\right)\right] \quad (14)$$

In the case of rotor blading, tip clearance loss would have to be included in the correlation. Since the source of a tip clearance loss correlation can only be stage tests, it will be assumed that tip clearance loss can be treated in the manner originally assumed in Equation 4.

In investigating the correlation in greater detail, it is evident that the contributions of both velocity ratio and aspect ratio are considerably

different from those assumed in the preliminary aerodynamic design. Over the range of velocity ratios tested, from approximately 0.1 to 1.0, the original correlation (Equations 2 and 3) assumed a loss increase of approximately 200 percent whereas the final correlation predicts an increase of approximately 350 percent. On the other hand, for the range of passage aspect ratios considered in the experimental program (from 9 to 1), the original correlation assumed a 250-percent increase in loss. The new correlation predicts only a 50-percent increase over the same range. Hence, the relative importance of aspect ratio has been considerably deemphasized, and that of velocity ratio has been increased, in the final results. However, only one secondary flow driving force (that from pressure to suction surface at the end walls) is present in planar cascade tests, and only relatively small quantities of flow are subjected to this force when a uniform profile exists at the inlet to the row. A recent USAAVLABS report (Reference 10) reproduces experimental data from Reference 11 that show a doubling of the end-wall loss coefficient in the case in which the row inlet boundary-layer thickness is less than 1 percent of the blade height. It must be concluded, therefore, that the factor $\left(1+\frac{1}{1.2(H/c)}\right)$ derived as an aspect ratio correction from planar cascade tests will underestimate the detrimental effects of low aspect ratio in a turbine stage. In the case of stator blading, additional secondary losses might reasonably be expected because of the radial static pressure gradient (which is demonstrated to be significant in the cascade tests of leaned stators discussed in Appendix IV). For rotor blades, the total-pressure profile existing at the stator exit will influence the level of loss. It is therefore proposed that the correlation factor for aspect ratio effects in a stage environment be expressed as $\left(1+\frac{K_S+K_R}{1.2(H/c)}\right)$, where K_S and K_R are additional secondary loss factors; these factors can be derived only from stage test data. In the case of rotor blading, the performance of the rotor is known to depend on the detailed performance of the stator row.

ACHIEVABLE STAGE EFFICIENCIES

INTRODUCTION

It is well known that the direct use of cascade loss data to evaluate the efficiency of a corresponding turbine design can lead to highly optimistic predictions of actual stage performance. The reasons for this phenomenon are not fully understood. One factor is undoubtedly the presence, in the typical stage environment, of significant radial transport of low-momentum fluid, due to the static pressure gradients at the stator exit and the centrifugal forces in the rotating row. A second major factor was inadvertently demonstrated in the course of the cascade test program. This was the effect mentioned earlier of a substantial increase in row loss level when a thickened-wall boundary layer entered the cascade. In this case, an irregularity in the inlet section was identified as the source of the boundary layer. Additional factors, which can be expected to contribute to the difference between stage test data and predictions based solely on isolated cascade data, are: radial flow components introduced by the annulus geometry, blade row interference effects dependent on interblade row gaps, intrablade row effects dependent on blade twist and taper, and tip clearance effects dependent on the detailed design of the blading. Even though it is not possible to consider individual effects in current prediction procedures, it is convenient to group the resultant losses into a single secondary loss.

Before proceeding to the calculation of achievable stage efficiencies as a function of selected annulus blade height and corrected work output, it is necessary to estimate the additional secondary loss factors K_S and K_R.

On the assumption that the values for K_S and K_R can be obtained to convert the desired cascade loss correlation to one which is for blade rows in a stage, the correlation could be used to predict the performance of any turbine. However, in the current program only, the nine original designs have been considered. Hence, the calculated achievable stage efficiencies which are presented and discussed later apply only to a series of designs in which rotational speed, inlet mass flow, inlet total temperature, and inlet total pressure are held constant. As previously discussed, each set of three designs, of a particular level of stage work output, can be considered as alternative turbines which satisfy the power and speed requirements of a compressor.

POSSIBLE VALUES OF THE ADDITIONAL SECONDARY LOSS FACTORS

The series of tests reported in Reference 1, which cover a range of blade row aspect ratios and stage efficiencies, has been used as the basis for the selection of the factors K_S and K_R. Considering three stages of differing annulus height, three values of stage efficiency are available for the calculation of two empirical factors, assuming that these factors are

constant. Thus, any two tests will yield values for K_S and K_R, assuming that the derived correlation of the datum loss is applicable and that the aspect-ratio-dependent correction factors are as follows:

$$f\left(\frac{H}{D}\right) = 1 + \frac{K_S}{1.6\left(\frac{H}{D}\right)} \qquad \text{for stators} \qquad (15a)$$

and

$$f\left\{\left(\frac{H}{D}\right), \left(\frac{k}{H}\right)\right\} = 1 + \frac{K_R}{1.6\left(\frac{H}{D}\right)} + 56\left(\frac{k}{H}\right) \qquad \text{for rotors} \qquad (15b)$$

(The coefficient of the tip clearance term is based on the initially derived correlation, which is in agreement with the test results of Reference 1, where tip clearance effects were also investigated.)

For the highest and lowest aspect ratio stages of Reference 1, values of 3.4 and 4.2 were obtained for K_S and K_R, respectively. However, these values will not predict with sufficient accuracy the test results of the intermediate aspect ratio stage. By considering the various combinations of stage results, it was concluded that an acceptably good fit of the experimental data would be obtained with values of 2 and 6 for K_S and K_R, respectively. With an assumed value of 2 for K_S, the derived values of are 5.3, 5.9, and 5.5 for the three stage tests reported in Reference 1, in which the tip clearance was held at 1.5 percent of the rotor blade height. While the above variation of K_R might be considered to be relatively large, it must be appreciated that a 10-percent variation in one component of the rotor row total loss can in some circumstances result in a change of stage efficiency which is within the limits of experimental accuracy.

While values of 2 and 6 have been selected as the most probable values for the row additional secondary loss factors, alternative values have been assumed for the reprediction of the nine original selected turbines.

STAGE EFFICIENCY PREDICTIONS

It must be emphasized that the design-point specifications for the nine turbines are identically those used to define the cascades on which the loss correlation is based. The common specifications for the nine stages are repeated below:

Mass Flow Rate	5 lbm/sec
Turbine Inlet Total Pressure	142 psia
Turbine Inlet Total Temperature	2,500 °F
Rotational Speed	50,000 rpm

The originally selected annulus geometries together with the selected number of blades were retained for the final phase of the investigation. It

could be argued that each design could have been reevaluated using the derived loss correlation with the annulus dimensions (in particular, the stage mean radius) and number of blades as design analysis variables. However, since the originally selected annulus dimensions are representative of the range of turbines that would be considered if annulus blade heights of 0.4, 0.7, and 1.0 in. were respecified as alternatives for the three levels of corrected work output, the original designs will satisfactorily indicate the trend of efficiency with blade height. Thus, the design-point performance of the original nine turbines was predicted.

For each design requirement, five design-point analyses were performed. The first computer run employed the data from the cascade tests without modification; that is, K_S and K_R were set equal to unity. The second and third runs employed the derived value of K_R (6.0) with K_S set equal to 1 and then 2. The final two runs retained K_S equal to 2 and used alternative values of 4 and 8 for K_R. Resulting efficiencies for the 17-, 22-, and 27-Btu/lbm stages have been plotted along with chosen stage loading as functions of annulus height in Figures 21, 22, and 23, respectively. These same results have also been presented as functions of corrected work output in Figure 24 for two pairs of values of K_S and K_R, together with the corresponding values of stage mean radius for the stages.

When the data presented in Figures 21, 22, and 23 are considered as a group, the efficiency of stages of 0.4-in. annulus height is always greater than that of the corresponding stages of 0.7- and 1.0-in. annulus height. Corresponding stages in this context are stages having the same work output level and for which the same values were assumed for the stator and rotor additional loss factors. There is, of course, the possibility that actual values of K_S and K_R will depend on specific features of the individual stage designs. For example, the 1.0-in.-annulus designs, which are of relatively low hub-to-tip diameter ratio, might be less sensitive to any wall boundary layers at stage inlet. Therefore, it is of some importance to compare the predicted efficiency of the 0.4-in. stage using the pessimistic assumptions ($K_S = 2$ and $K_R = 8$) with the efficiency of the 1.0-in. stages predicted with the optimistic secondary loss assumptions ($K_S = 1$ and $K_R = 1.0$). At two of the three work output levels, the 0.4-in. stages still have higher efficiencies than the most optimistic efficiency predicted for the 1.0-in. designs. Only in the case of the highest work level, 27 Btu/lbm, is the highest achievable efficiency greater than that for the 0.4-in. design's predicted efficiency based on the pessimistic loss assumption. However, in this case the difference in efficiency is less than one-half a percentage point. Therefore, it is reasonable to conclude that for the design specifications considered, the lowest blade height in the range considered will produce the most efficient turbine stage.

The variation of the stage loading factor is shown in each of the three figures. In each case, the stage loading factor, $\frac{g_c J \Delta h}{U_t^2}$, is approximately 2.0 for the 1.0-in. design and 1.0 for the larger diameter designs using the 0.4-in. blade height. Thus, the conclusion to be drawn is that the inherent benefits of reducing the stage loading factor are greater than

the detrimental effect of the lower aspect ratios which accompany the selection of a higher mean radius design in the range of blade heights considered. It is worthy of note that the results presented in Reference 1 are not necessarily in disagreement with this conclusion. Although reducing an annulus height from 1.07 to 0.37 in. produced a very large efficiency drop in that case, the stage loading factor actually increased rather than decreased. The lowest height design in that case has a substantially lower corrected inlet flow $W\sqrt{\theta}/\delta$ than the large annulus stage, whereas in the current investigation a common value of corrected inlet flow is used in each of the nine designs.

Considering the data of Figure 24, which presents what might be considered the most optimistic and most pessimistic predictions of stage efficiency as a function of corrected stage work output, it will be seen that the efficiency is predicted to be not greatly dependent on work output, provided a mean radius is selected that maintains a particular value of $g_c J \Delta H/U^2$. The figure illustrates the uncertainty of the prediction of the efficiency level with an approximate 5-percentage-point spread with the assumed variations of the additional secondary loss factor; the most optimistic efficiency for a 1.0-in.-height stage is less than 86 percent, and the most pessimistic efficiency for a 0.4-in. stage is within 1 percent of that value. The higher efficiency of the 0.4-in.-height stages for a particular assumption is fundamentally due to the higher mean radius of the design. Thus, the trade-off between turbine efficiency and overall physical dimensions remains an important aspect of turbine selection. A stage loading parameter, $g_c J \Delta H/U^2$, of 1.0 has produced the highest values of predicted efficiency at each work output level in the current investigation. To achieve that loading level, it was necessary to increase the outside diameter of the turbine by as much as 30 percent compared with the more highly loaded designs having 1.0-in. blades. Because of the variation in stage hub-to-tip diameter ratios and the change in hub diameters, the disk rim speeds have been increased by an even greater percentage.

CONCLUDING REMARKS

Despite the uncertainty concerning the relative magnitude of secondary loss in planar cascades and in stages, and hence the uncertainty in which levels of efficiency are achievable in the small turbines of interest to USAAVLABS, the current investigation provides the basis for the eventual determination of achievable efficiency levels. It should also be emphasized that the results of the design analyses presented herein are for a particular value of the turbine flow parameter corresponding to a flow rate of 5 lbm/sec, an inlet temperature of 2960 °R, and an inlet total pressure of 142 psia. Thus, the principal result of the investigation must be regarded as the derivation of a loss correlation, even though there is uncertainty concerning the value of the empirical constant in the secondary loss term. For designs of lower mass flow or higher inlet pressure levels which are of interest to the designers of high-performance, small gas turbine engines, it is reasonable to conclude that blade heights of considerably less than 0.4

in. will still correspond to optimum designs even though their efficiencies are lower than those that would be obtained in larger capacity turbines having the same value of stage loading factor.

CONCLUSIONS

1. A correlation of total-pressure-loss coefficients for low-aspect-ratio turbine blading has been obtained. The correlation contains an empirical factor relating the magnitude of aspect-ratio-dependent secondary loss measured in planar cascades to the secondary flow loss in turbine stage blading.

2. Even though the level of achievable efficiency is dependent on the additional secondary loss factor introduced into the correlation, the current investigation has shown that the benefits of the reduced stage loading factor outweigh the detrimental effects of reducing the blade height in the range considered.

3. The most probable level of efficiency for a stage having a 0.4-in. annulus for the selected design-point requirements, irrespective of the level of corrected stage work output, is 87 percent. This is approximately 5 percentage points higher than designs of comparable inlet flow capacity, in which a 1.0-in. blade height is selected in order to achieve high-blade-row aspect ratio but in which the level of the stage loading factor is approximately doubled.

4. The cascade test program has shown that the level of loss in low-aspect-ratio and highly loaded rows is extremely sensitive to small disturbances of the main flow field. Small irregularities in the end wall which produce boundary-layer separation, small tip clearance leakages, and small quantities of flow entering the cascade normal to an end wall were found to increase the level of total-loss coefficient by as much as a factor of 5. These results were an unexpected byproduct of the experimental program, in that neither the small discontinuity in some of the porous-wall configurations nor the small leakage flows that resulted from imperfect assemblies of particular cascades would have been previously considered to be of such large importance.

5. The tests of leaned cascades, although limited to two leaned standards for one stator cascade profile geometry, have shown that the introduction of a relatively small force normal to the end walls significantly affects the level of loss, its distribution with height, and the variation of tangential and through-flow velocity components. Although the row that was leaned 20 deg with respect to the end walls had a level of total loss which was more than 50 percent higher than that of the normal cascade, the indications are that leaned stator blades could be used to advantage in a turbine stage to suppress the secondary flows and losses created by the strong radial gradient of static pressure across the stator exit annulus.

RECOMMENDATIONS

1. A series of stage performance tests should be undertaken to validate the principal conclusions of the investigation and to provide more data on the additional secondary loss factor assumed in the derived correlation of the total-pressure-loss coefficient.

2. As part of the stage test program above, or as a separate investigation, the effects of stator lean in an annular cascade and/or in a complete stage should be further investigated. Any such program should be integrated with a thorough analytical analysis so that the results of the investigation might be applied to the optimization of stage performance generally.

3. While further cascade testing with a high quality of inlet profile would not be recommended due to the fact that the secondary losses would not necessarily be representative of stage performance, a more detailed evaluation of partiuclar cascades with various standards of inlet total-pressure profile is a logical and useful extension of the original program. The results of such an investigation would provide a better understanding of the secondary flow effects, which undoubtedly have a significant influence on the level of efficiency that is achievable in a small turbine having low-aspect-ratio blading.

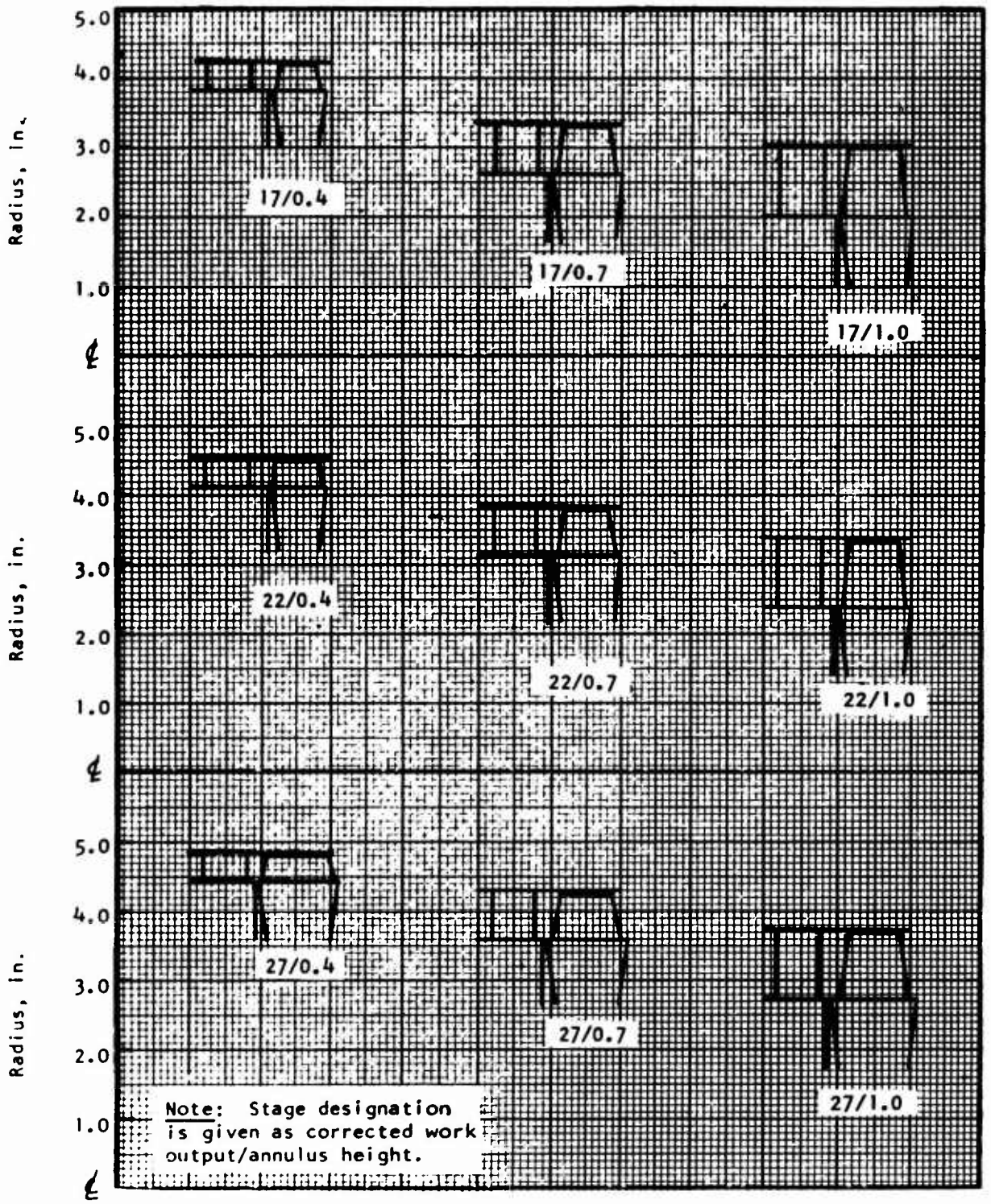

Figure 1. Selected Annulus Dimensions of Nine Turbines.

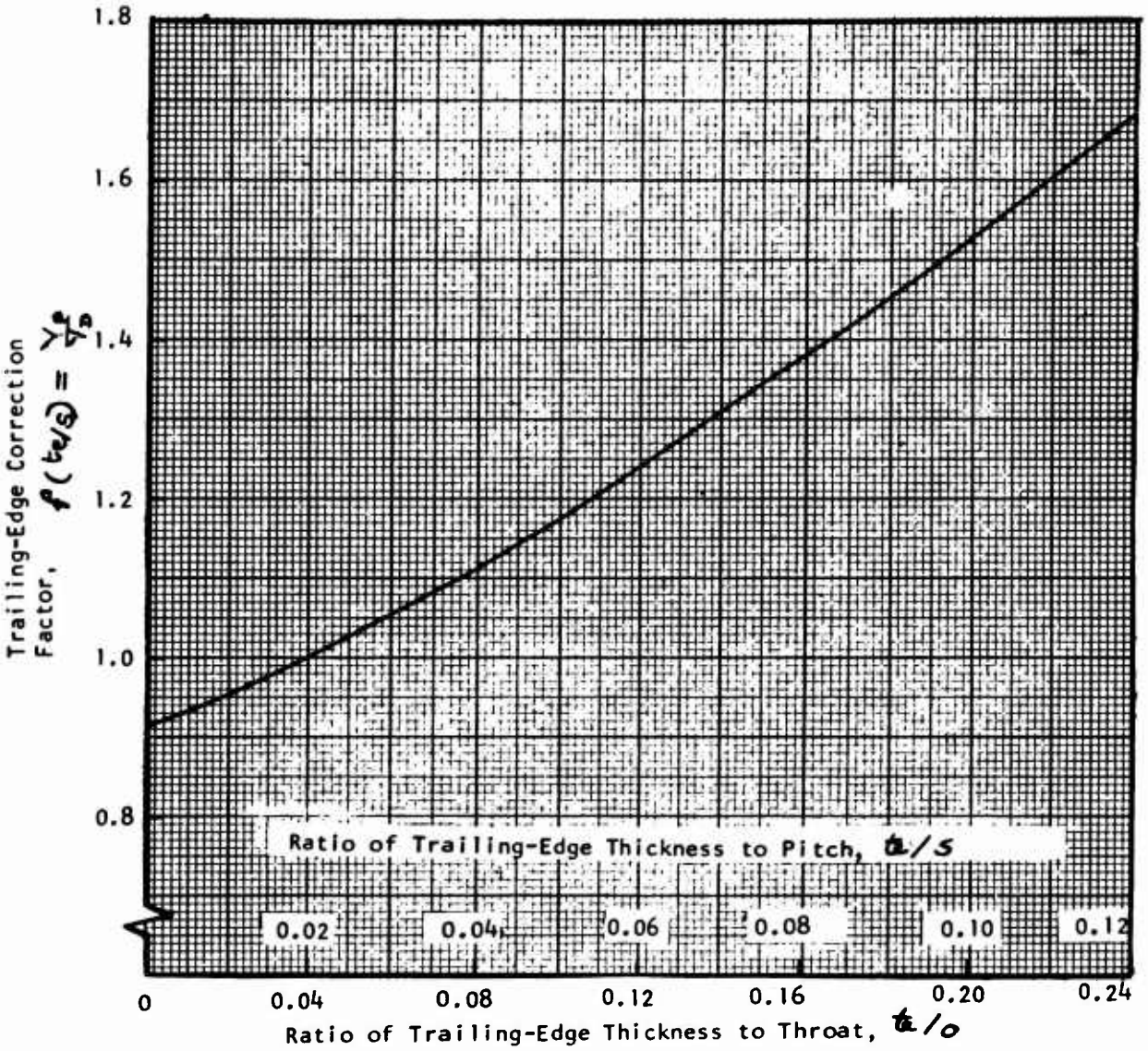

Figure 2. Effect of Trailing-Edge Thickness on Overall Pressure-Loss Coefficient.

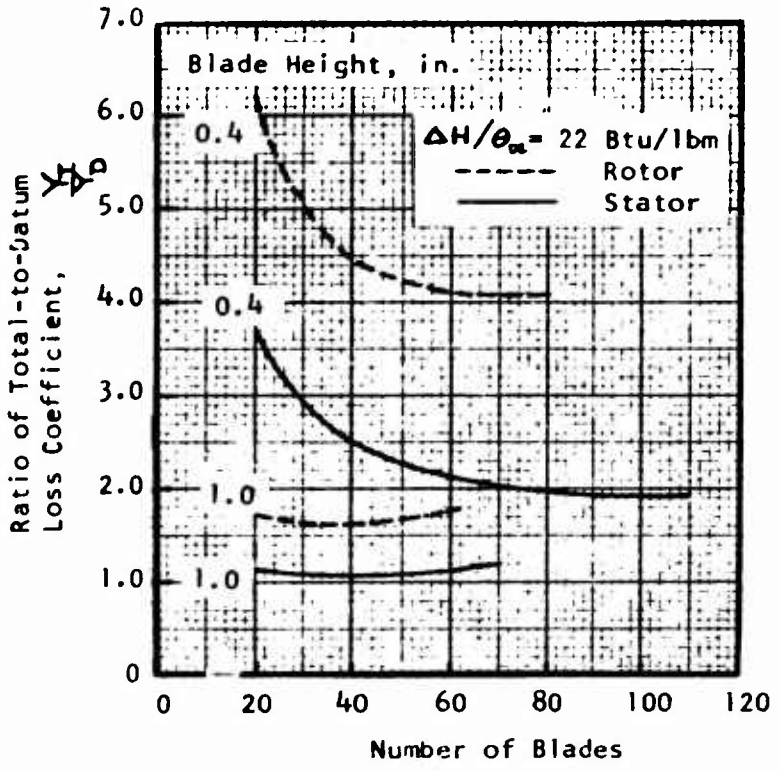

Figure 3. Effect of Number of Blades on Additional Loss Factor.

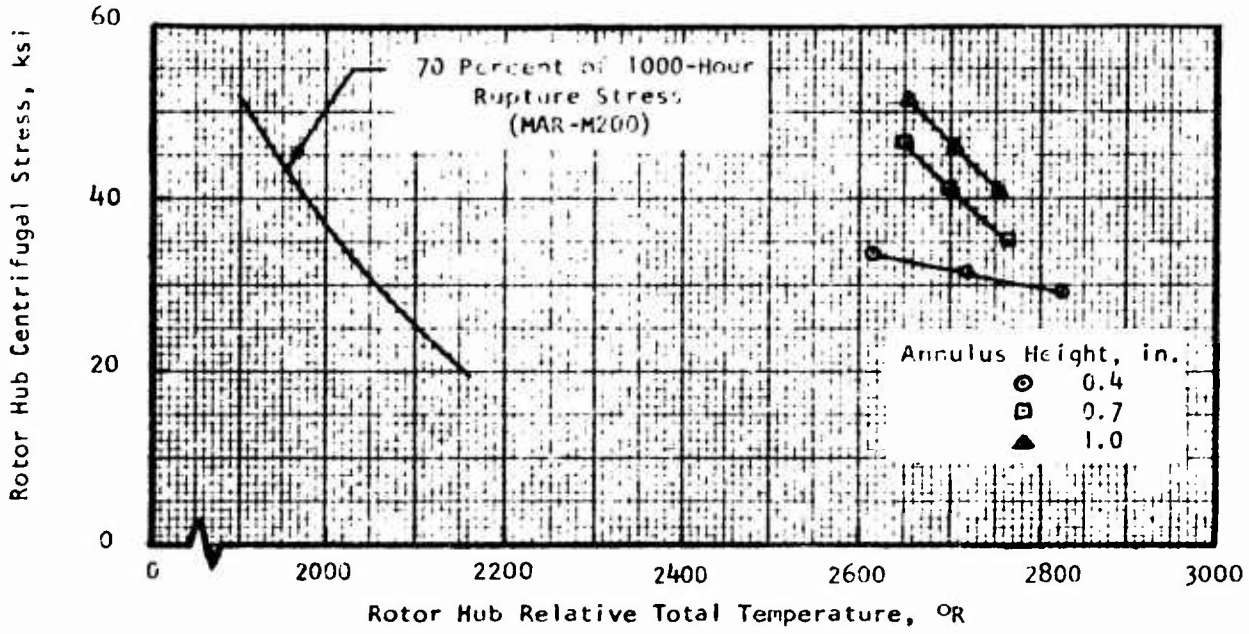

Figure 4. Rotor Hub Section Stress and Uncooled Temperature Level for the Original Designs.

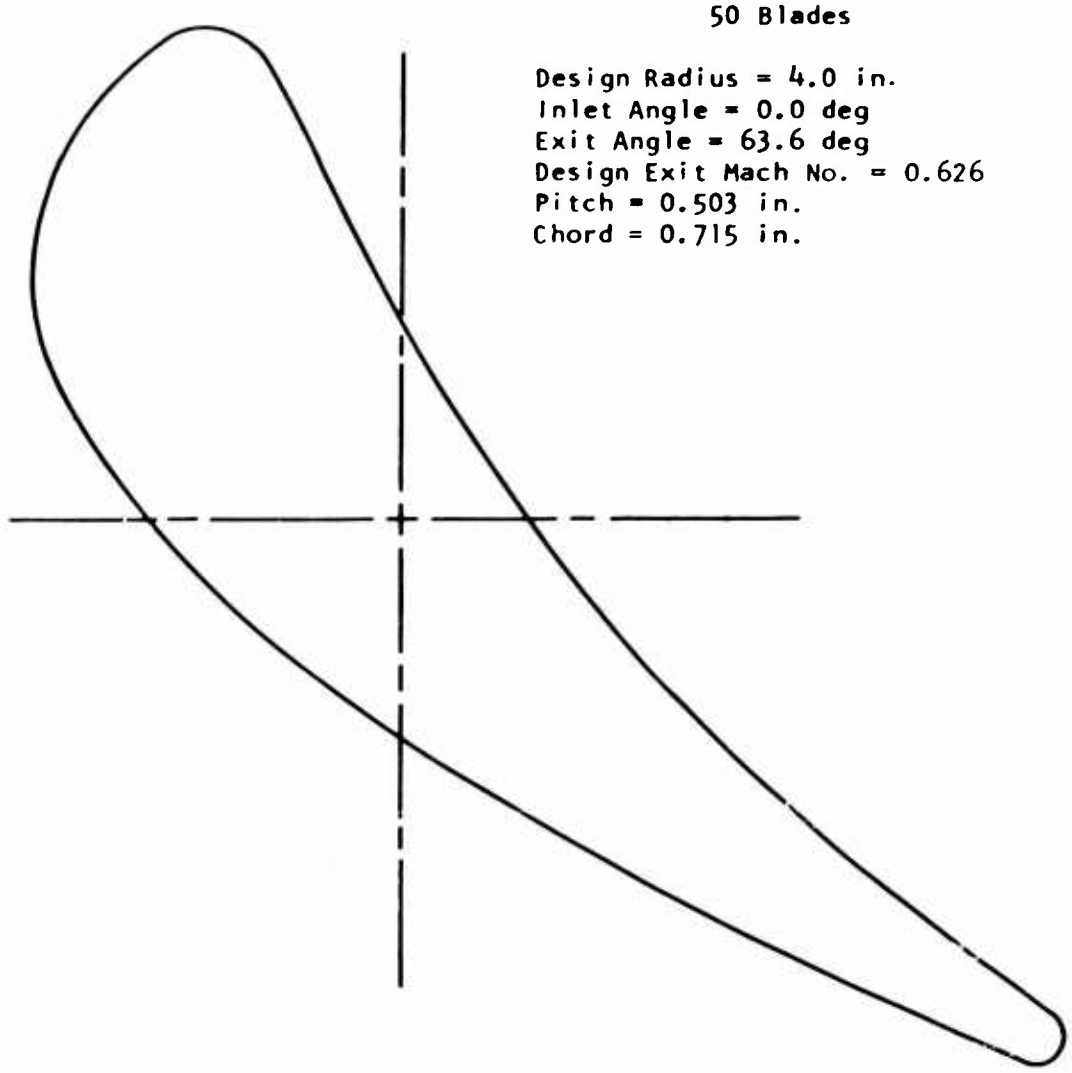

Figure 5. Stator Mean Section, 17/0.4 (Scale = 10:1).

47 Blades

	Root	Mean	Tip
Design Radius, in.	3.8	4.0	4.2
Inlet Angle, deg	-15.84	-26.57	-35.68
Exit Angle, deg	-60.775	-60.80	-60.78
Design Exit Mach No.	0.824	0.858	0.890
Pitch, in.	0.508	0.535	0.561
Chord, in.	0.79	0.773	0.74

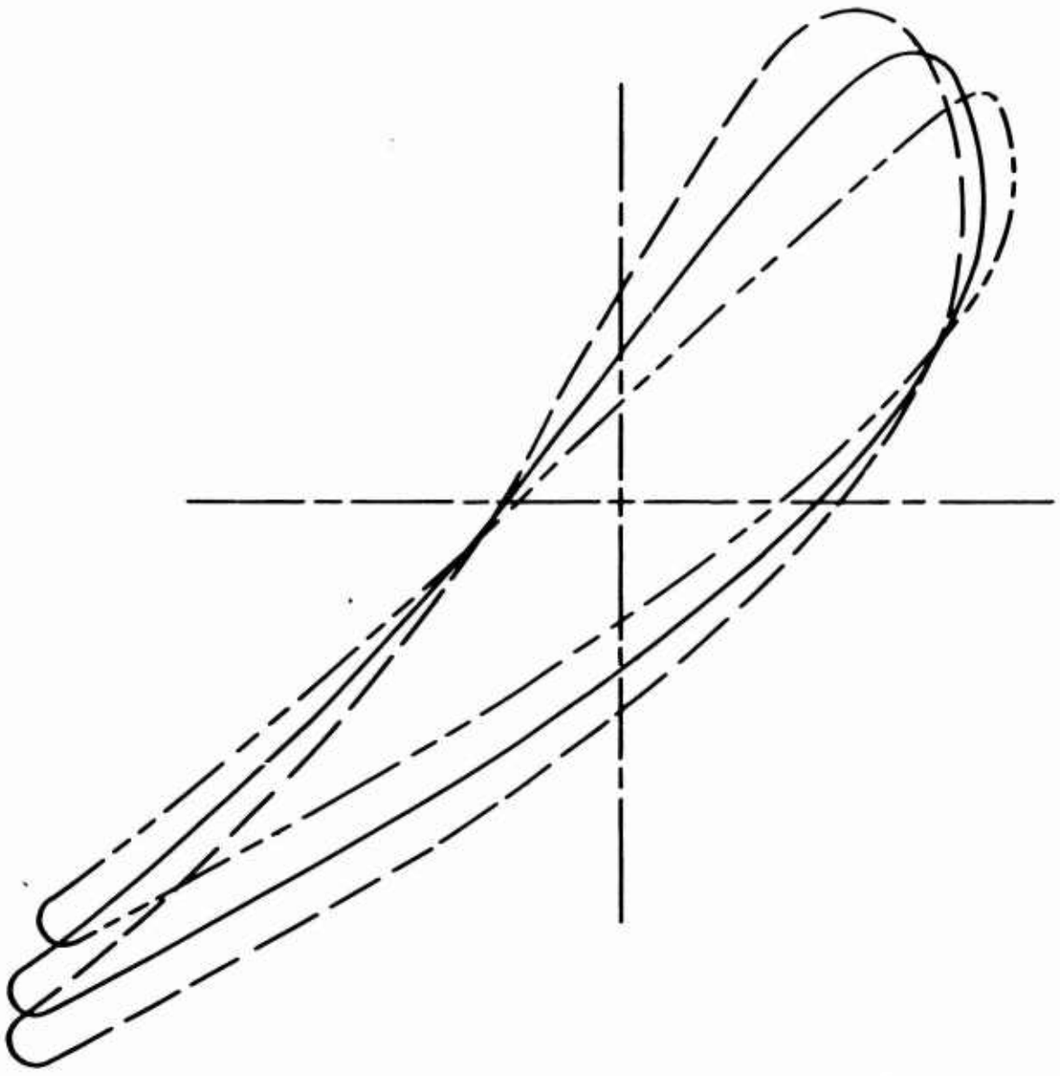

Figure 6. Rotor Sections, 17/0.4 (Scale = 10:1).

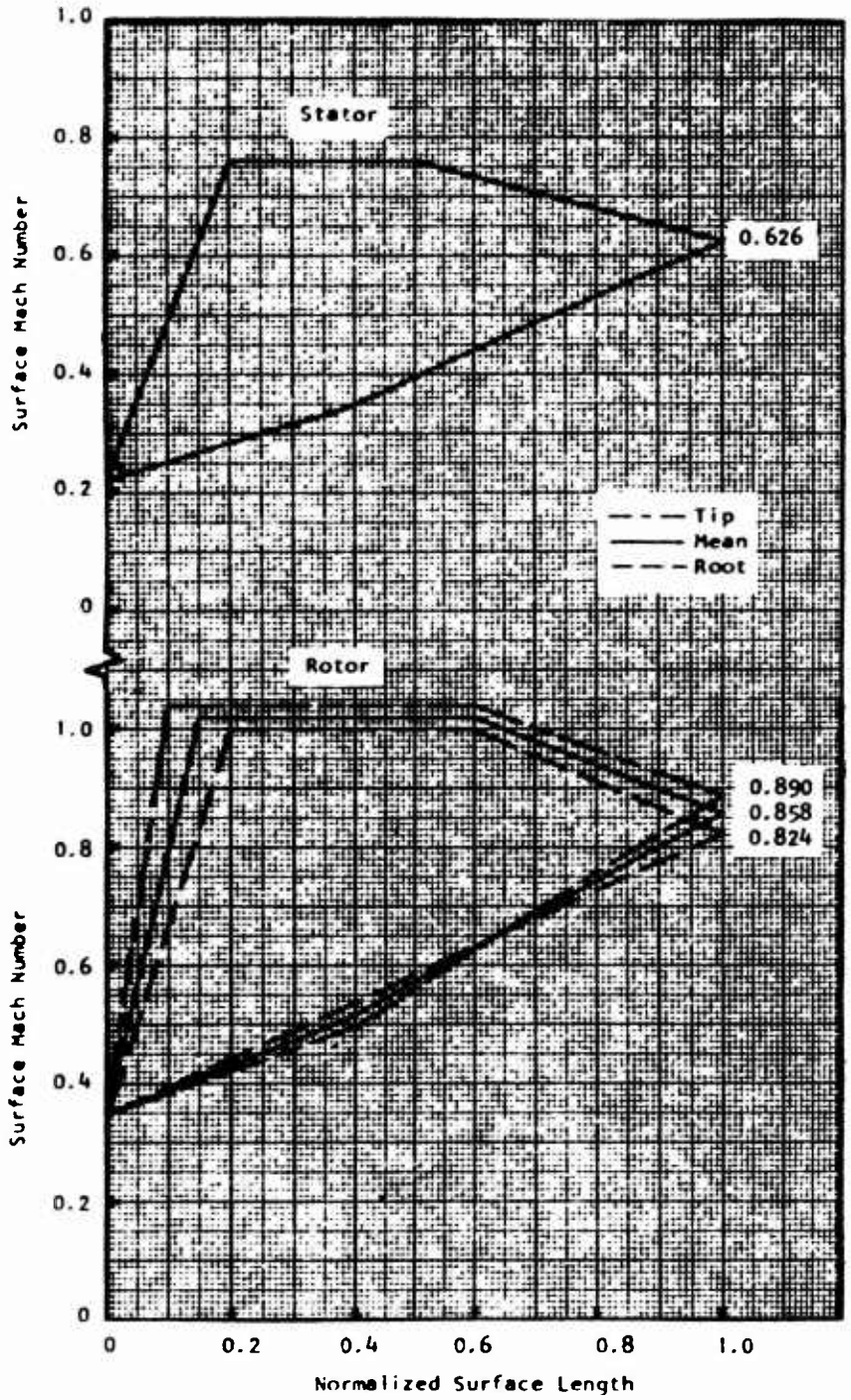

Figure 7. Prescribed Mach Number Distribution for Stator Mean and Rotor Profiles (17/0.4/4.0).

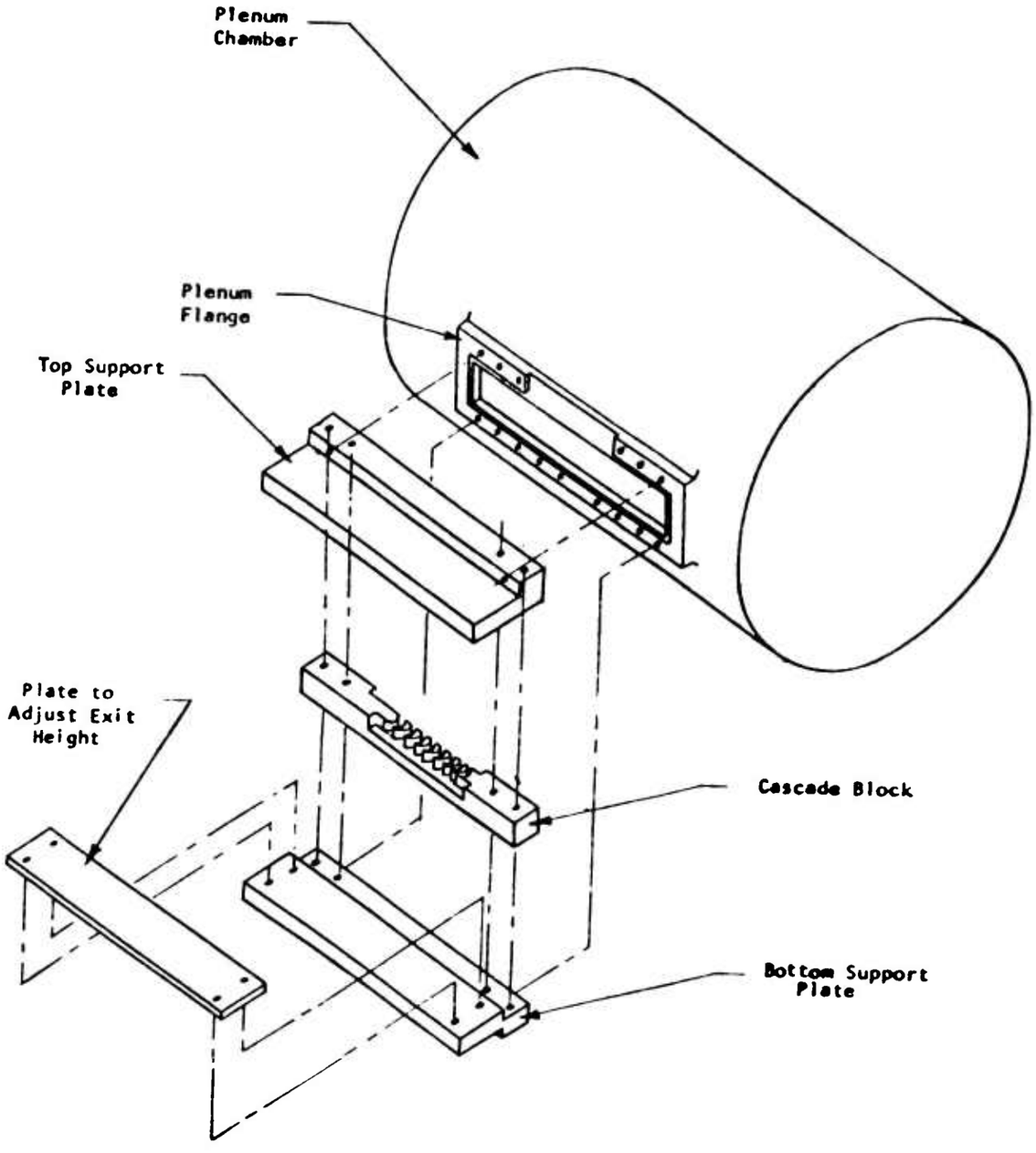

Figure 8. Exploded View of Cascade Assembly.

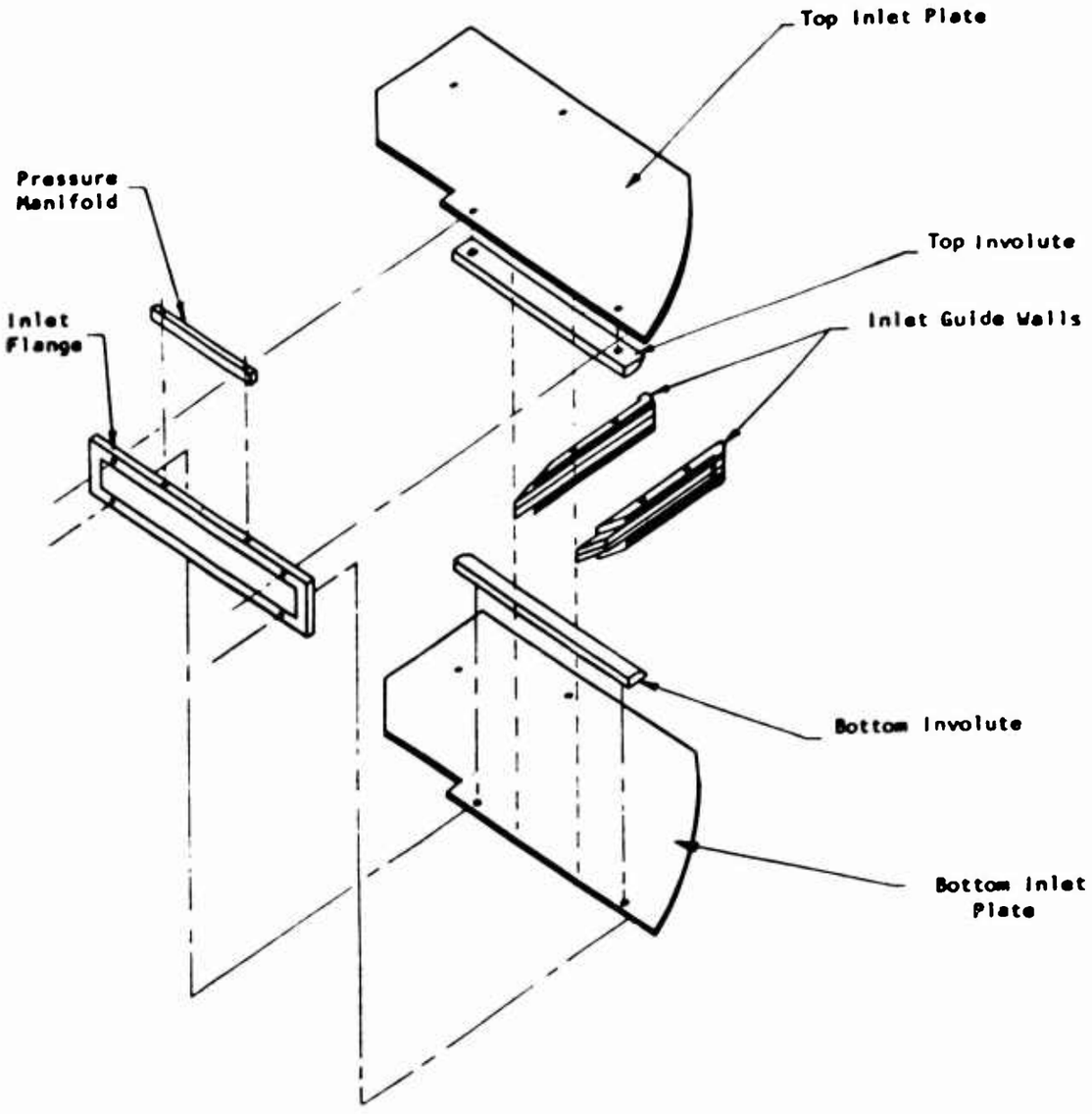

Figure 9. Exploded View of the Inlet Section to the Cascade.

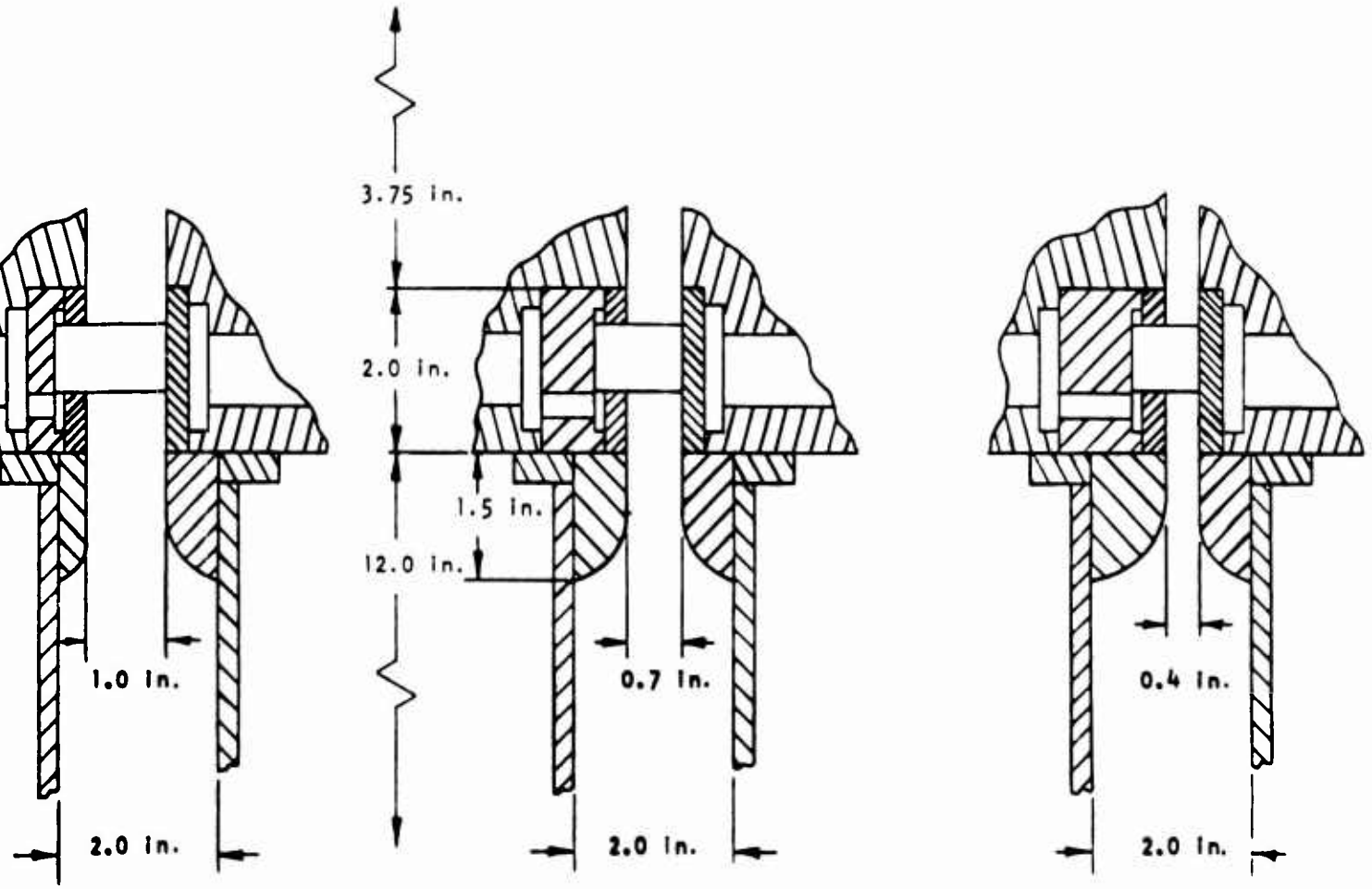

Figure 10. Sectional View of Cascade Assembly for Three Blade Heights.

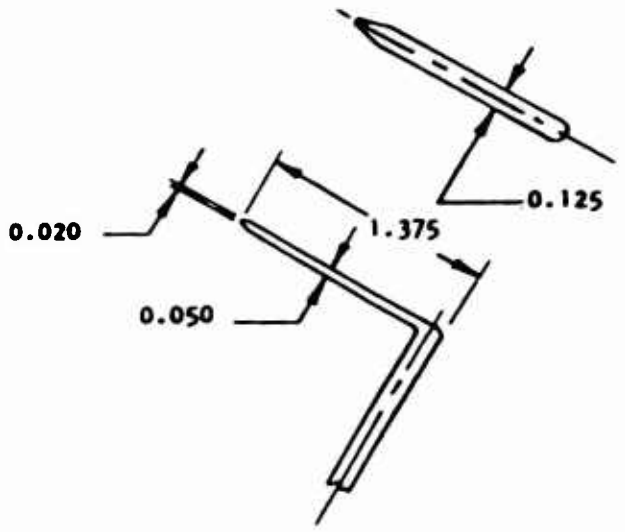

Probe Dimensions, in.

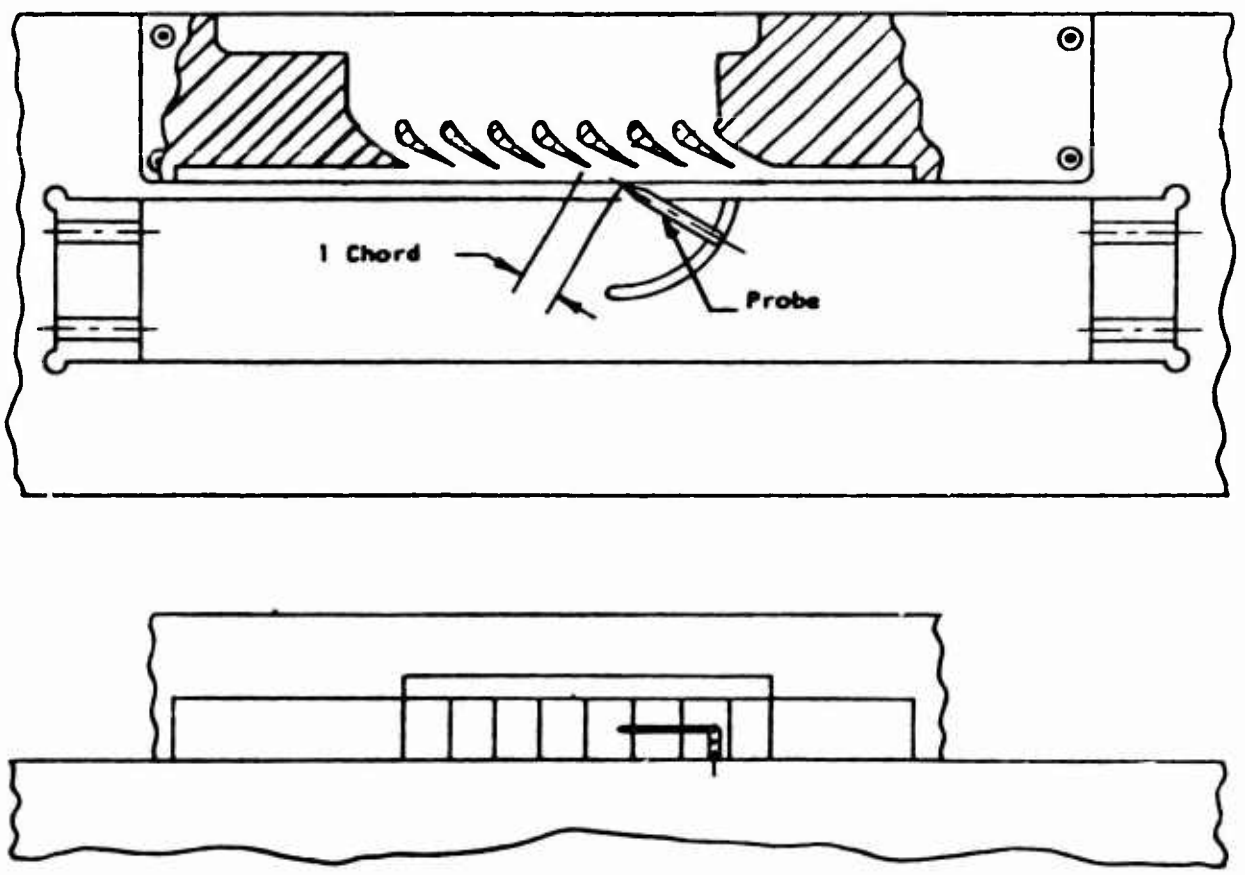

Figure 11. Cascade and Probe.

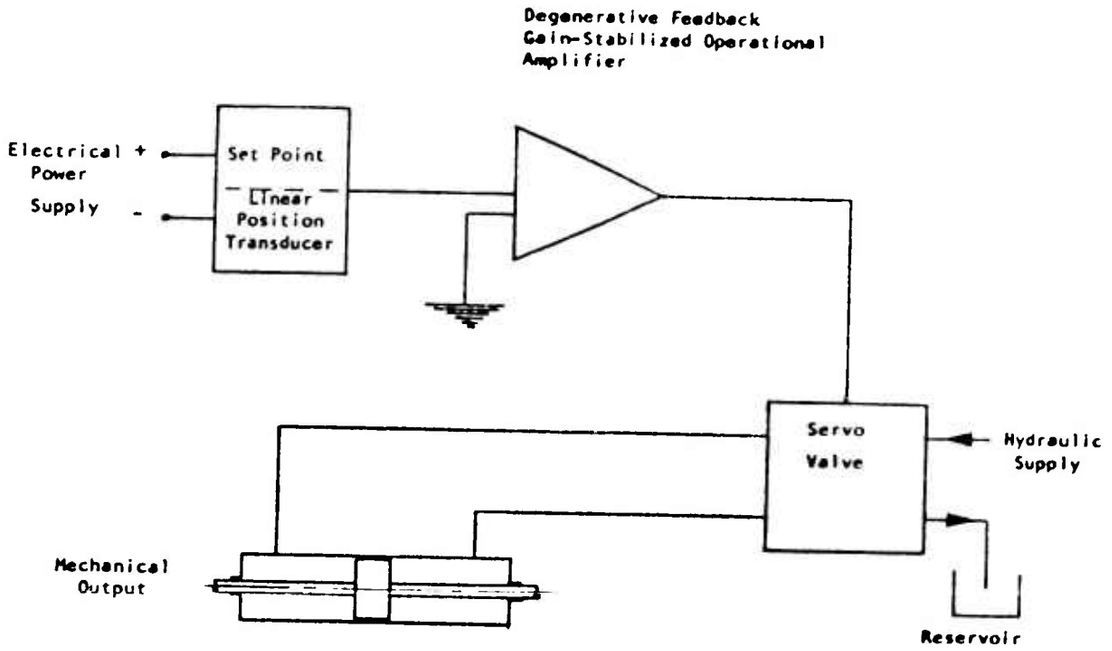

Figure 12. Schematic of the Traversing Actuator System.

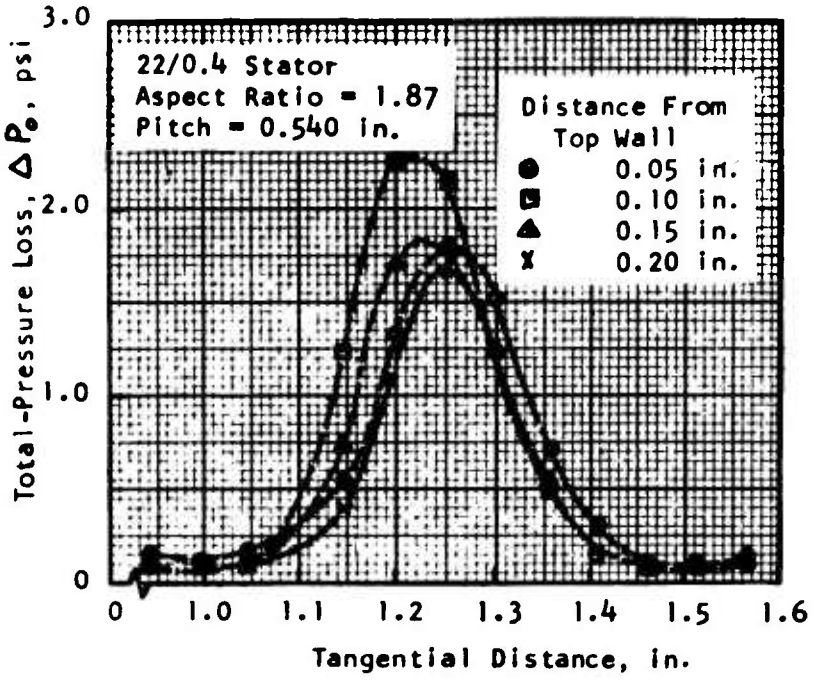

Figure 13. Total-Pressure Defect Profile (Solid Wall Test of Cascade 3).

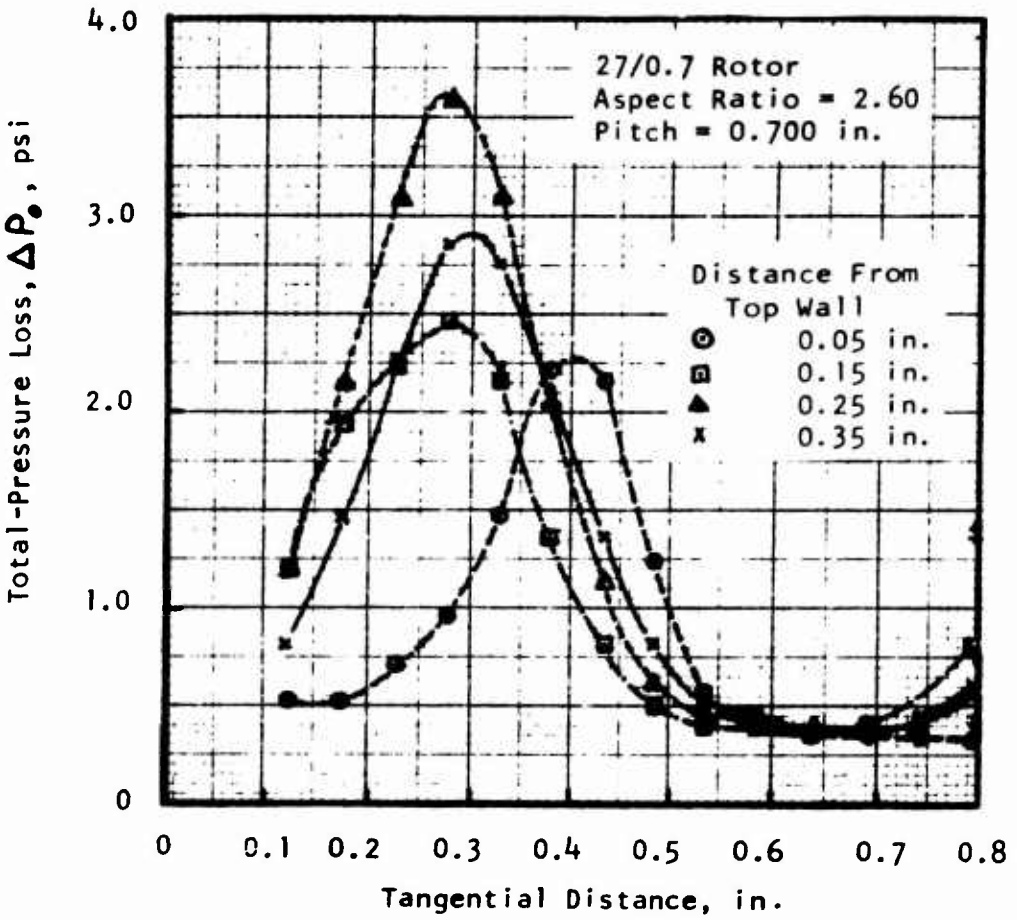

Figure 14. Total-Pressure Defect Profile (Solid Wall Test of Cascade 12).

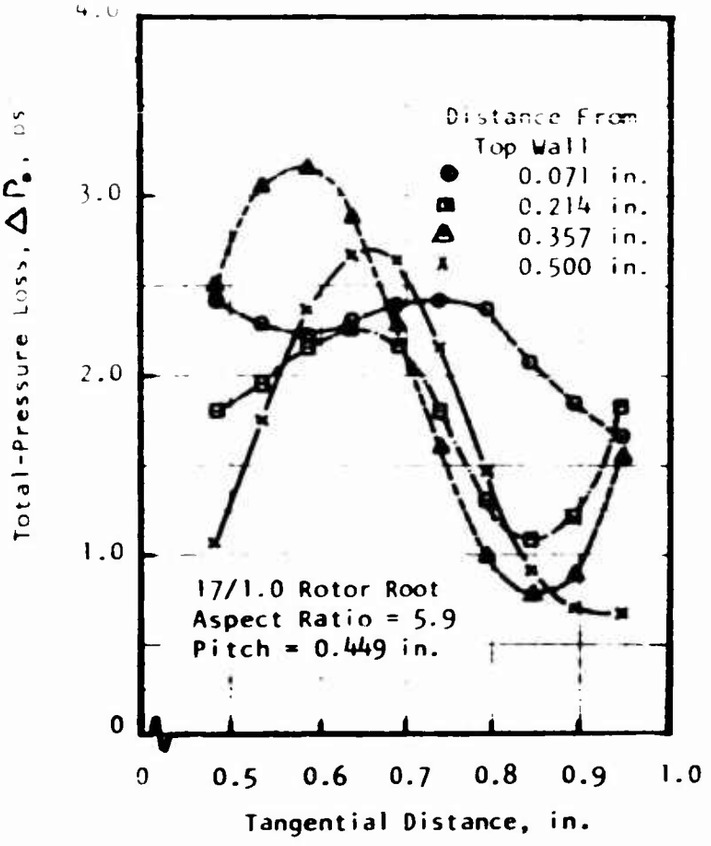

Figure 15. Total-Pressure Defect Profile (Solid Wall Test of Cascade 24).

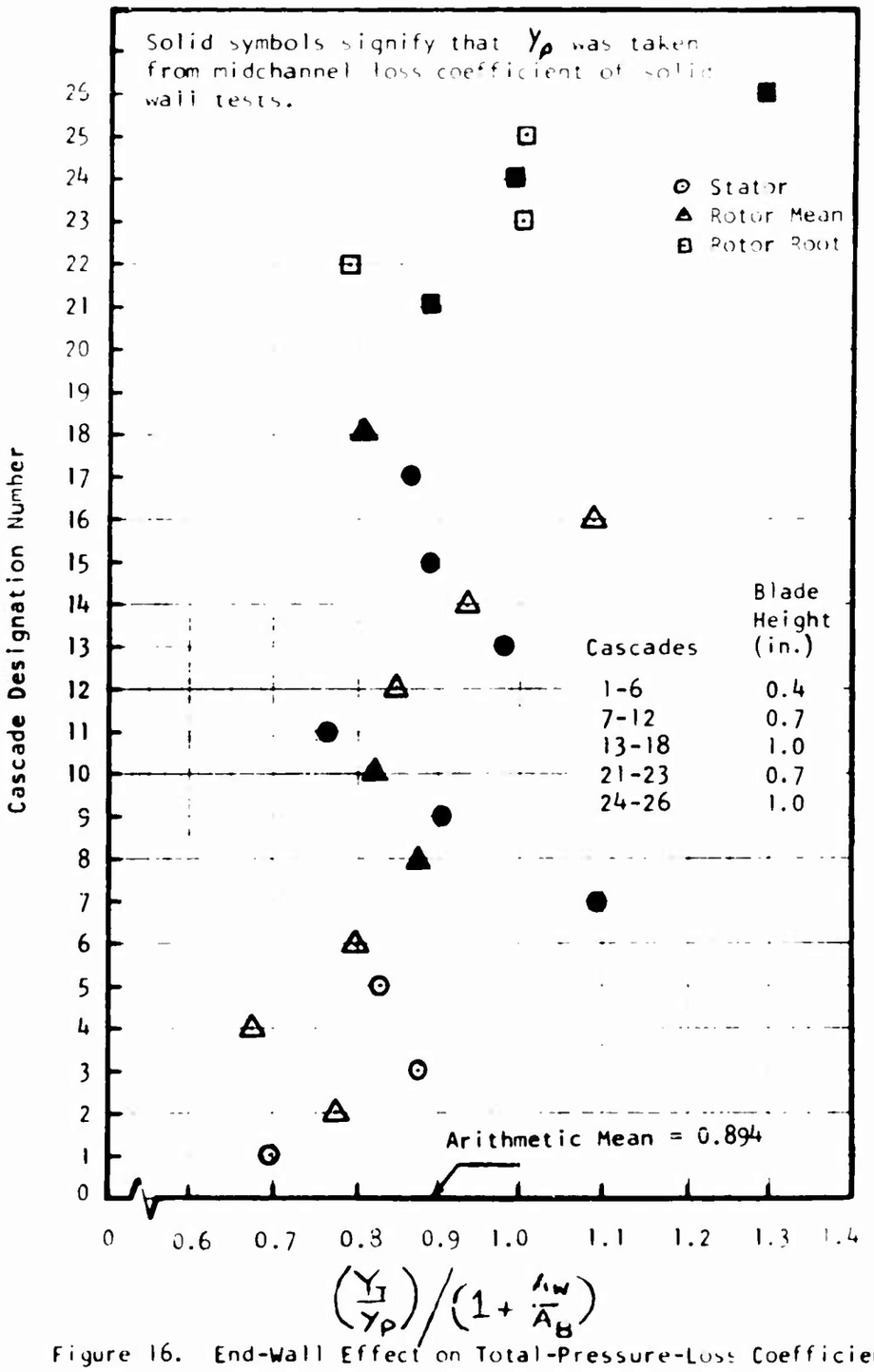

Figure 16. End-Wall Effect on Total-Pressure-Loss Coefficient.

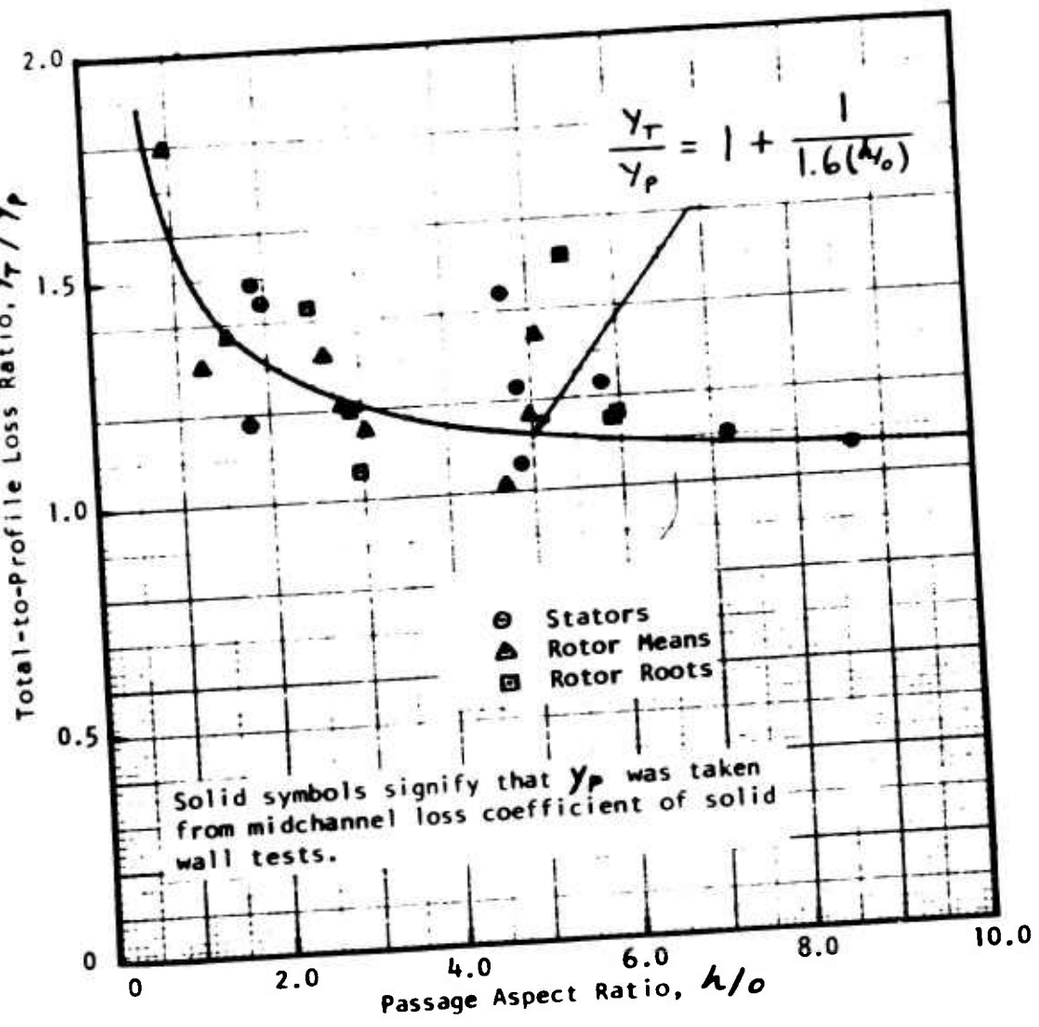

Figure 17. Aspect Ratio Effect on Total-to-Profile Loss Ratio.

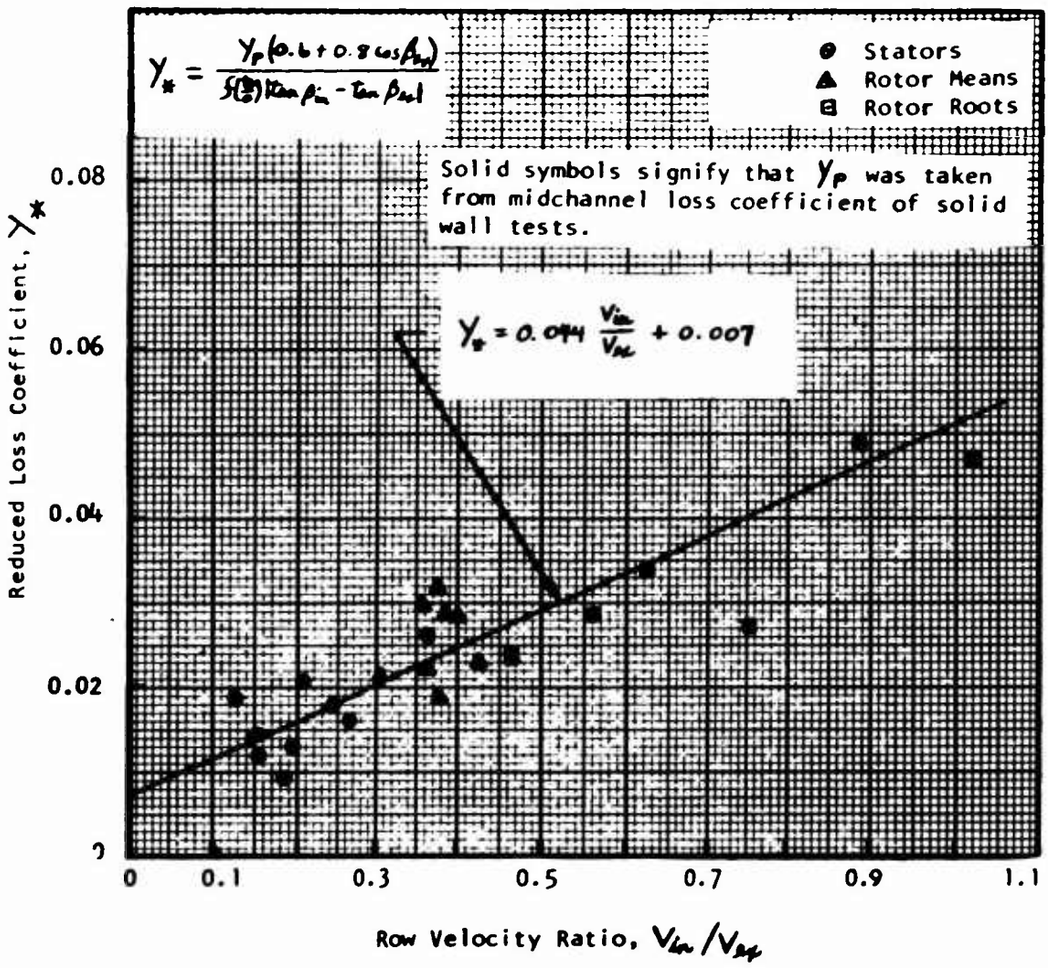

Figure 18. Profile Loss Correlation.

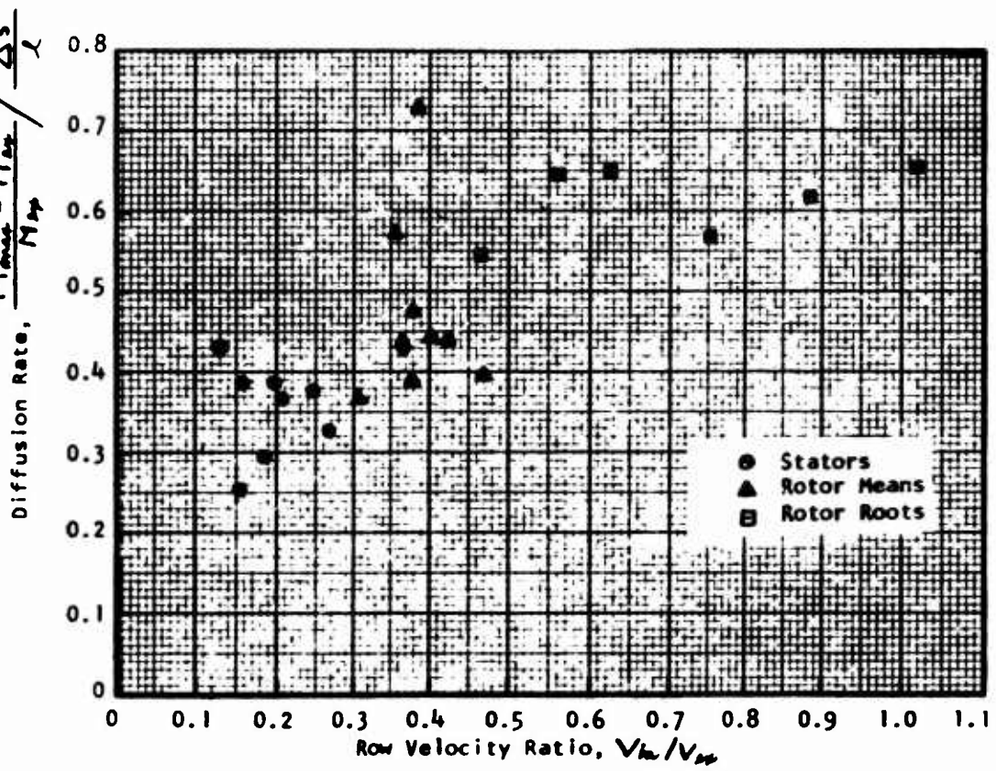

Figure 19. Design Diffusion Rate.

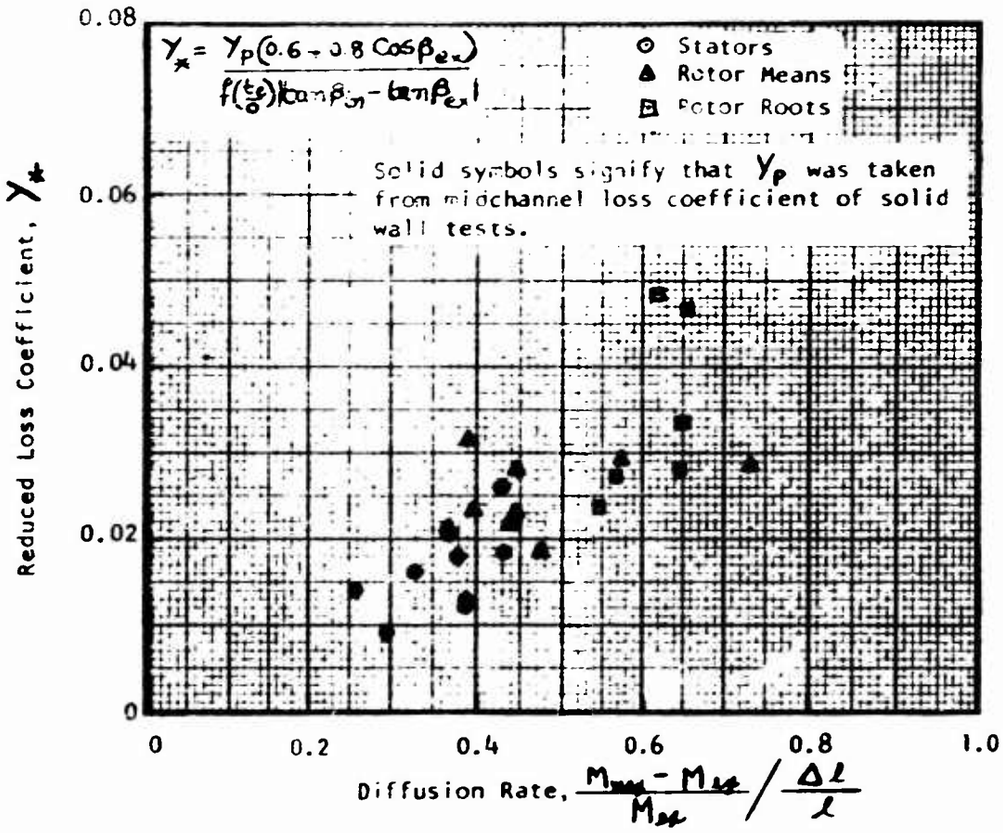

Figure 20. Effect of Diffusion Rate on the Reduced Loss Coefficient.

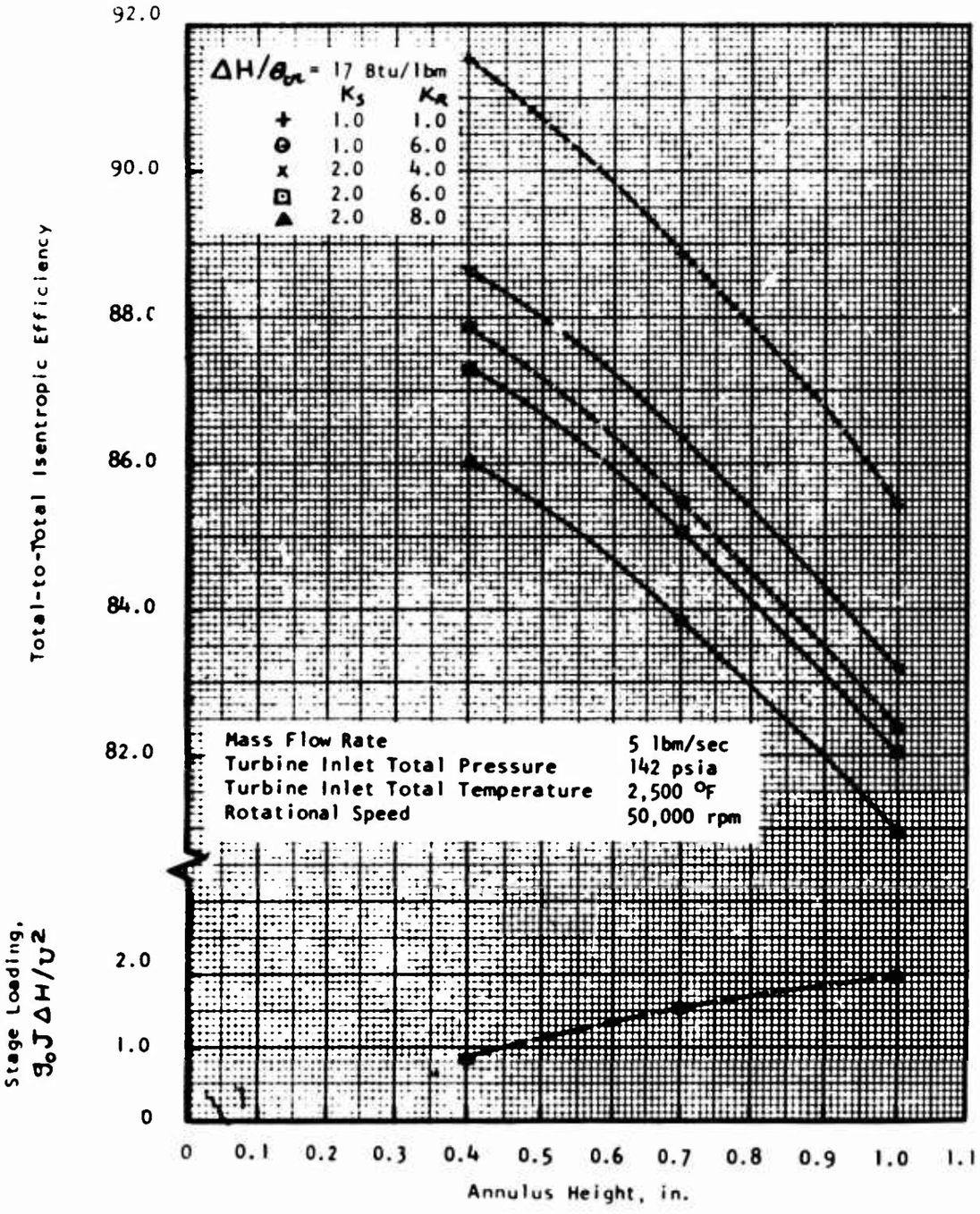

Figure 21. Achievable Efficiency for Corrected Work Output of 17 Btu/lbm.

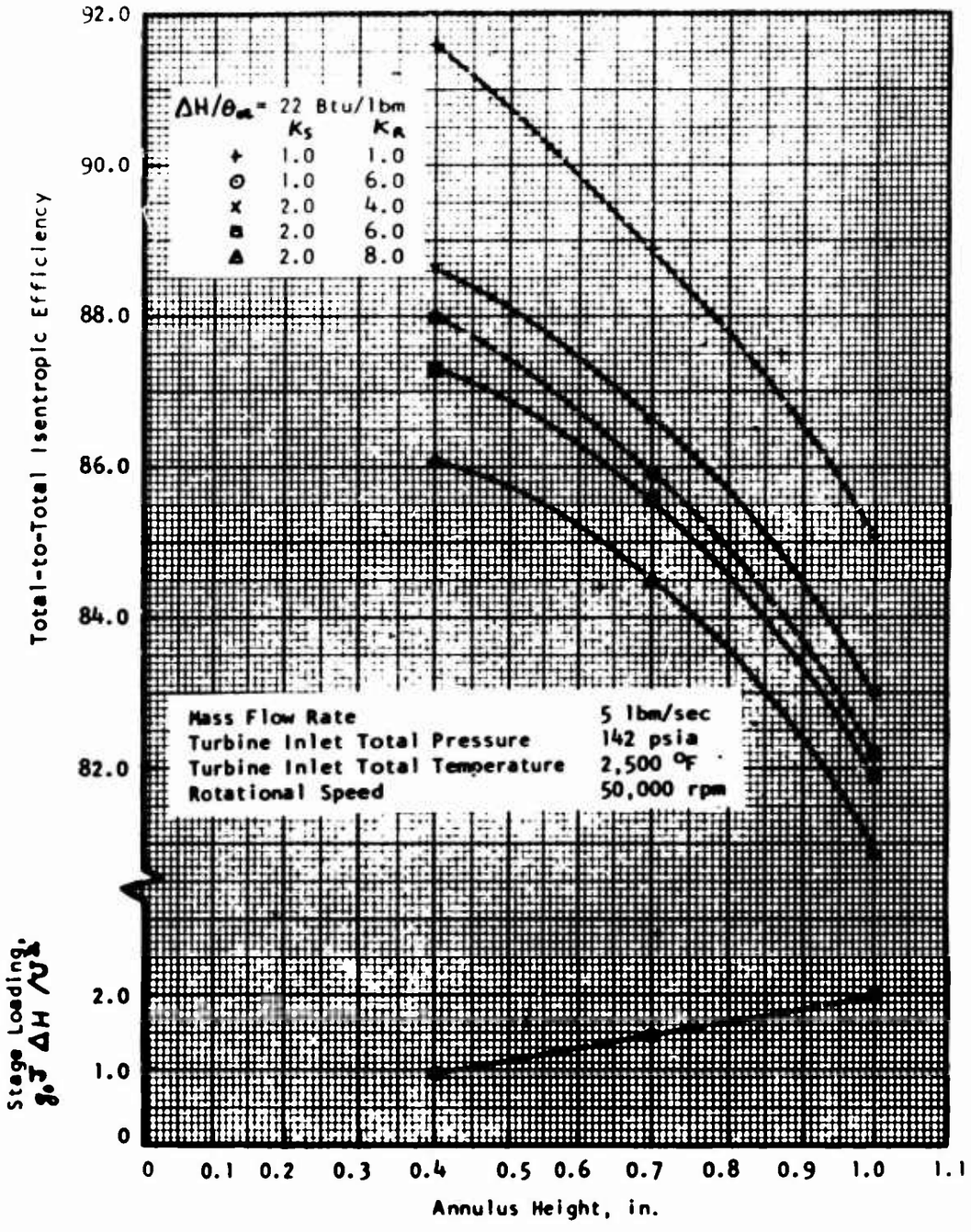

Figure 22. Achievable Efficiency for Corrected Work Output of 22 Btu/lbm.

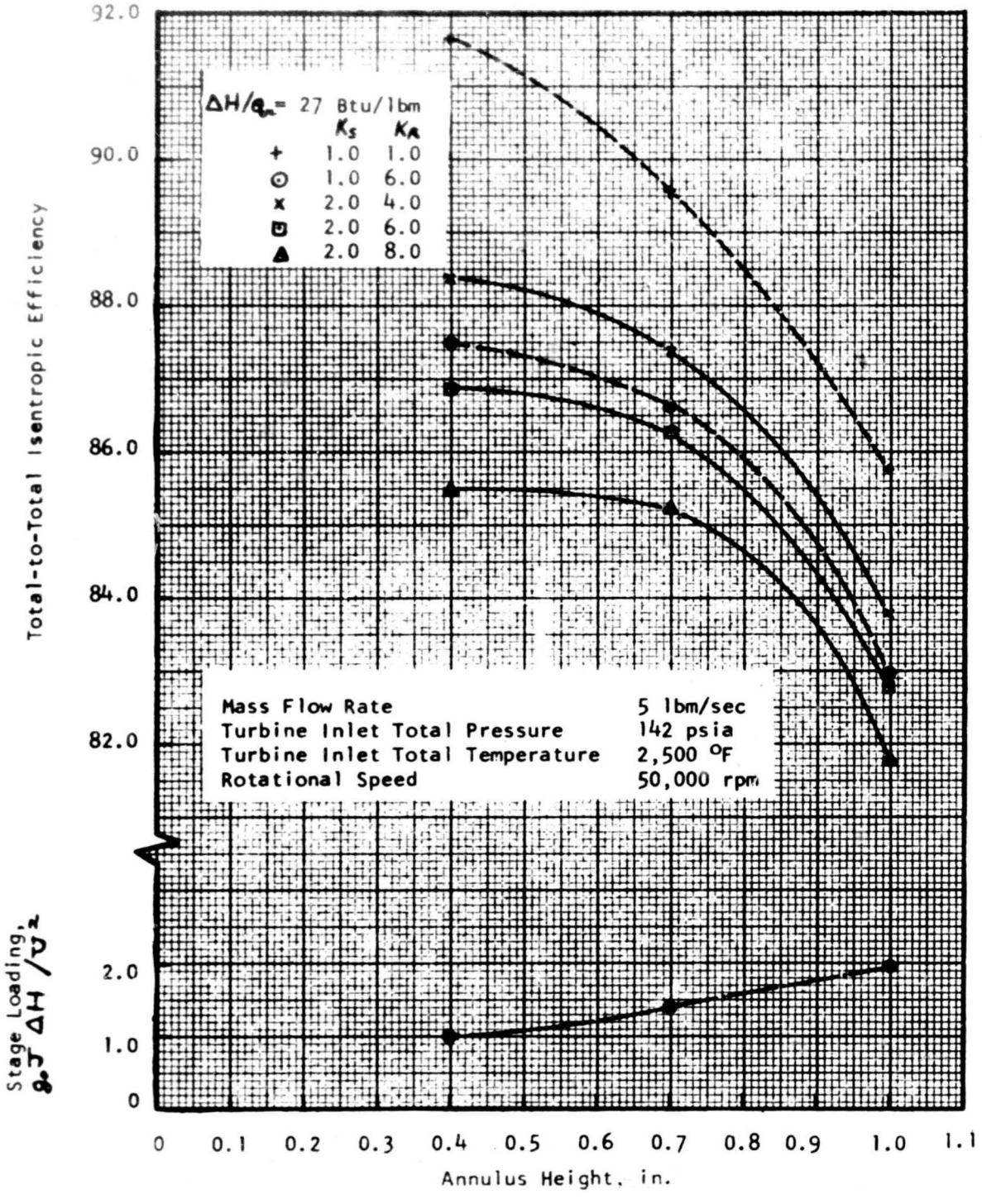

Figure 23. Achievable Efficiency for Corrected Work Output of 27 Btu/lbm.

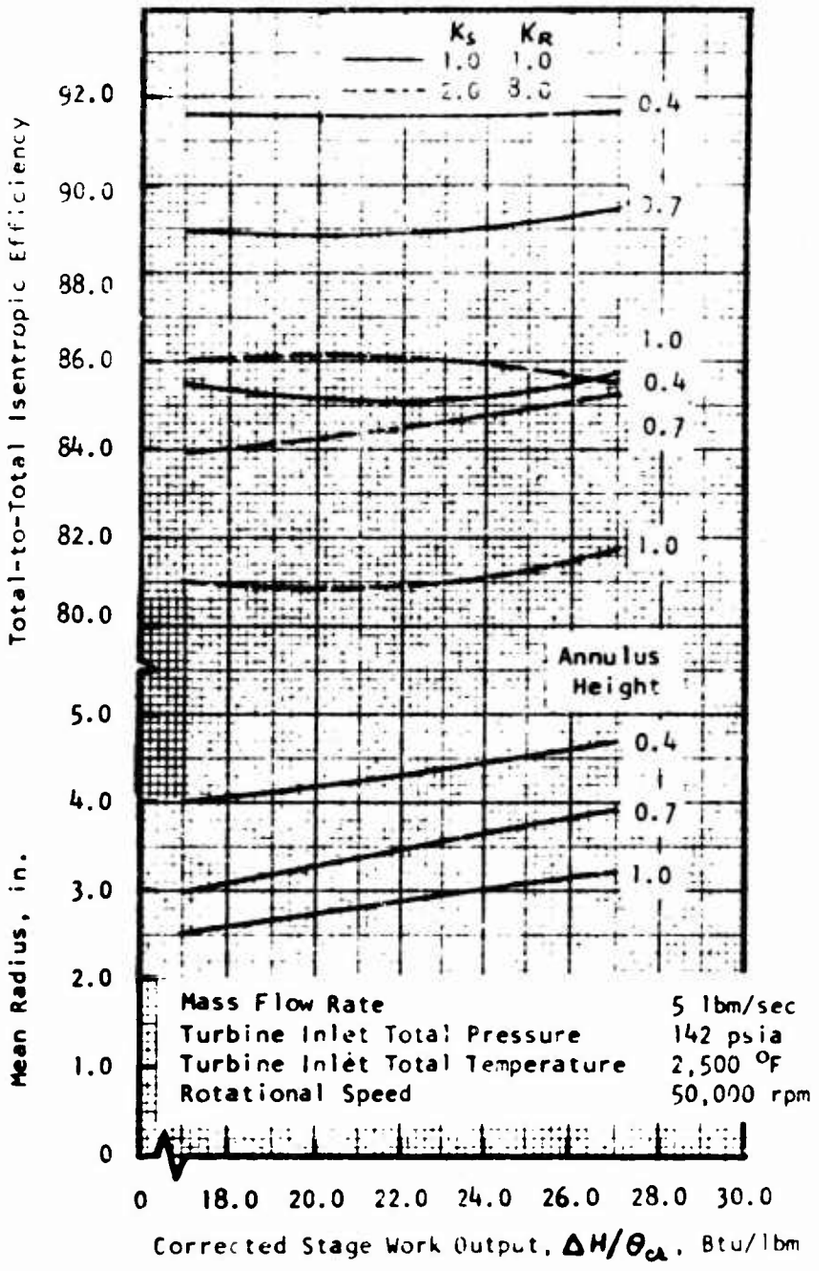

Figure 24. Achievable Efficiency for Various Blade Heights.

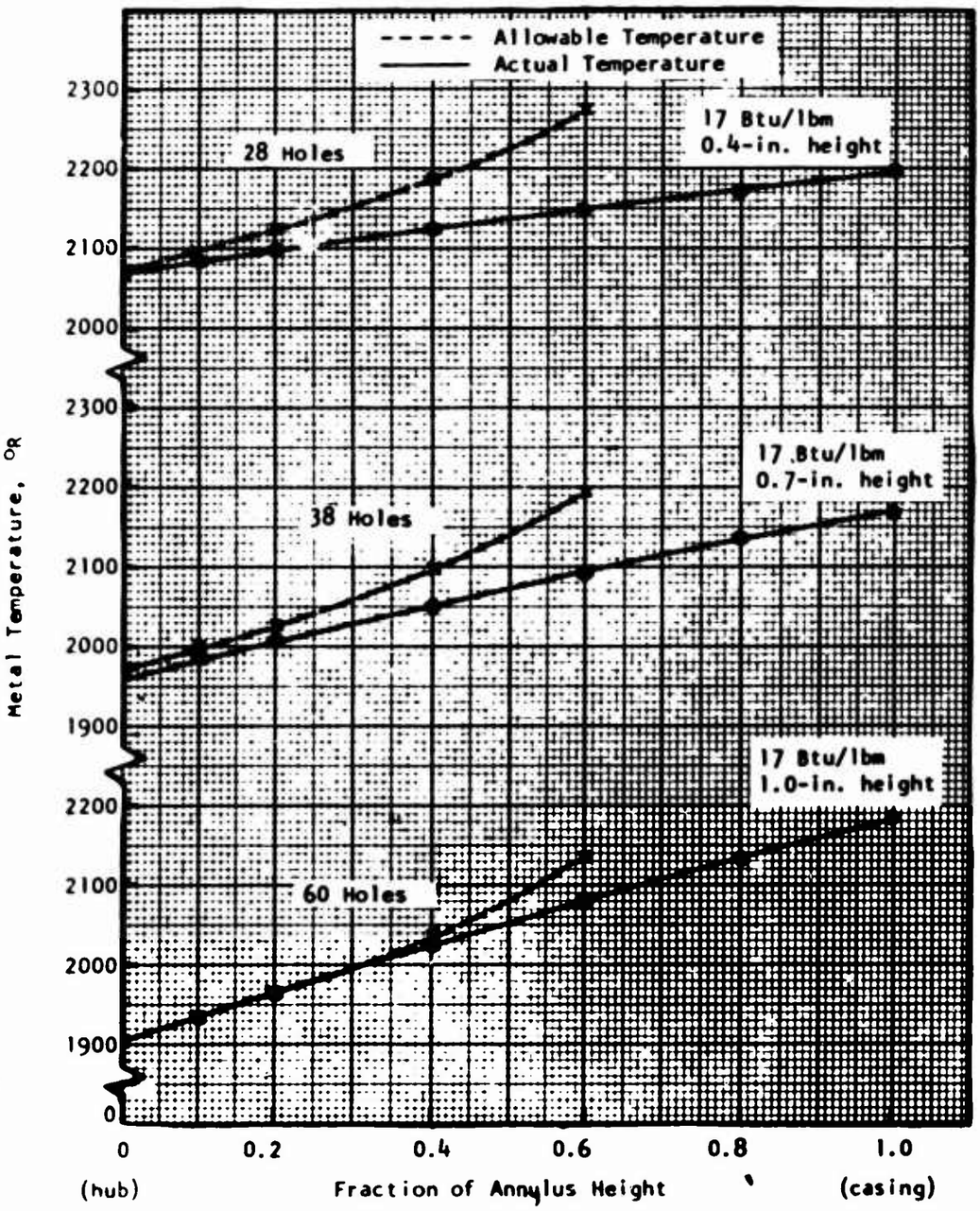

Figure 25. Radial Variation of Allowable and Actual Rotor Metal Temperatures (Minimum Required Number of Coolant Passages).

TABLE I. NUMBER OF BLADES

Corrected Work Output (Btu/lbm)	Annulus Height (in.)	Number of Stators	Number of Rotors
17	0.4	50	47
	0.7	40	38
	1.0	29	28
22	0.4	50	47
	0.7	40	38
	1.0	32	31
27	0.4	50	47
	0.7	40	35
	1.0	35	31

TABLE 11. BLADE CHORD LENGTHS

Corrected Work Output (Btu/lbm)	Annulus Height (in.)	Chord Length (in.)		
		Stator Mean	Rotor Mean	Rotor Root
17	0.4	0.715	0.773	0.790
	0.7	0.660	0.880	0.930
	1.0	0.750	0.810	0.850
22	0.4	0.733	0.850	0.855
	0.7	0.740	0.800	0.910
	1.0	0.725	0.860	0.910
27	0.4	0.830	1.070	1.130
	0.7	0.840	1.010	1.060
	1.0	0.750	0.920	1.000

TABLE III. MEAN-LINE AERODYNAMICS OF THE ORIGINAL STAGE DESIGNS

Corrected Work Output (Btu/lbm)	Annulus Height (in.)	Angles (deg)				Mach Numbers				Stage Loading Factor	Efficiency
		Stator Exit	Rotor Inlet	Rotor Exit	Stage Exit	Stator Exit	Rotor Inlet	Rotor Exit	Stage Exit		
17	0.4	63.60	-26.60	-60.70	- 2.10	0.626	0.311	0.858	0.420	0.820	84.99
	0.7	71.20	34.27	-64.22	-19.44	0.719	0.280	0.722	0.333	1.504	84.68
	1.0	74.70	54.00	-68.00	-37.50	0.746	0.335	0.738	0.349	1.981	80.02
22	0.4	67.80	- 3.20	-57.20	5.40	0.809	0.306	0.906	0.493	0.920	84.20
	0.7	74.50	38.28	-66.02	-15.96	0.821	0.279	0.803	0.339	1.433	84.60
	1.0	76.90	57.40	-69.50	-40.90	0.832	0.350	0.863	0.400	1.990	79.94
27	0.4	69.55	14.53	-52.41	10.10	0.990	0.357	0.986	0.611	0.990	83.64
	0.7	76.38	37.36	-67.39	-16.51	0.888	0.263	0.913	0.366	1.375	84.49
	1.0	78.38	58.90	-70.50	-42.70	0.902	0.352	0.985	0.448	1.953	80.86

TABLE IV. HUB-LINE AERODYNAMICS OF THE ORIGINAL STAGE DESIGN

Corrected Work Output (Btu/lbm)	Annulus Height (in.)	Angles (deg)				Mach Numbers				Hub Loading Factor
		Stator Exit	Rotor Inlet	Rotor Exit	Stage Exit	Stator Exit	Rotor Inlet	Rotor Exit	Stage Exit	
17	0.7	71.20	49.23	-60.94	-17.15	0.808	0.399	0.651	0.331	1.539
	1.0	74.70	65.40	-67.30	-37.70	0.932	0.591	0.579	0.283	1.981
22	0.7	74.50	52.66	-62.41	-12.78	0.910	0.401	0.734	0.349	1.454
	1.0	76.90	67.70	-69.10	-40.80	1.016	0.606	0.690	0.325	1.990
27	0.7	76.38	52.86	-63.70	-13.79	0.976	0.381	0.852	0.389	1.393
	1.0	78.38	68.80	-69.50	-42.00	1.081	0.603	0.817	0.385	1.953

TABLE V. PRESCRIBED SURFACE MACH NUMBER DISTRIBUTIONS - STATORS

Blade Height (in.)	Corrected Work Output (Btu/lbm)	Suction		Pressure	
		Fractional Length	Mach Number	Fractional Length	Mach Number
0.4	17	0.0000	0.2200	0.0000	0.2200
		0.2000	0.7600	0.4000	0.3500
		0.5000	0.7600	1.0000	0.6260
		1.0000	0.6260	-	-
	22	0.0000	0.2000	0.0000	0.2000
		0.2500	0.9415	0.4000	0.3100
		0.5000	0.9415	1.0000	0.8097
		1.0000	0.8097	-	-
	27	0.0000	0.1800	0.0000	0.1800
		0.3000	1.1000	0.4000	0.3400
		0.7000	1.1000	1.0000	0.9909
		1.0000	0.9909	-	-
0.7	17	0.0000	0.1600	0.0000	0.1600
		0.3000	0.8000	0.4000	0.2800
		0.7000	0.8000	1.0000	0.7190
		1.0000	0.7190	-	-
	22	0.0000	0.1200	0.0000	0.1200
		0.3500	0.9000	0.3500	0.2300
		0.6700	0.9000	0.5500	0.3400
		1.0000	0.8207	1.0000	0.8207
	27	0.0000	0.1000	0.0000	0.1000
		0.4000	0.9600	0.3000	0.1900
		0.6800	0.9600	0.6000	0.3700
		1.0000	0.8880	1.0000	0.8880
1.0	17	0.0000	0.1200	0.0000	0.1200
		0.3500	0.8000	0.3000	0.1900
		0.8200	0.8000	0.6000	0.3600
		1.0000	0.7480	1.0000	0.7480
	22	0.0000	0.1000	0.0000	0.1000
		0.3500	0.8900	0.3000	0.1700
		0.8200	0.8900	0.6000	0.3500
		1.0000	0.8320	1.0000	0.8320
	27	0.0000	0.0900	0.0000	0.0900
		0.4000	0.9600	0.3000	0.1600
		0.8500	0.9600	0.6000	0.3400
		1.0000	0.9020	1.0000	0.9020

TABLE VI. PRESCRIBED SURFACE MACH NUMBER DISTRIBUTIONS - ROTOR MEANS

Blade Height (in.)	Corrected Work Output (Btu/lbm)	Suction		Pressure	
		Fractional Length	Mach Number	Fractional Length	Mach Number
0.4	17	0.0000	0.3500	0.0000	0.3500
		0.1500	1.0200	0.4000	0.5200
		0.6000	1.0200	1.0000	0.8577
		1.0000	0.8577	-	-
	22	0.0000	0.3200	0.0000	0.3200
		0.2000	1.0750	0.3000	0.4000
		0.6700	1.0750	1.0000	0.9040
		1.0000	0.9040	-	-
	27	0.0000	0.3625	0.0000	0.3625
		0.2000	1.1750	0.3000	0.4000
		0.7300	1.1750	1.0000	0.9818
		1.0000	0.9818	-	-
0.7	17	0.0000	0.2780	0.0000	0.2780
		0.1700	0.7000	0.3000	0.3000
		0.4000	0.8350	0.5000	0.3890
		0.6400	0.8350	0.5000	0.3890
		1.0000	0.7201	1.0000	0.7201
	22	0.0000	0.3000	0.0000	0.3000
		0.1000	0.5800	0.3000	0.3000
		0.3500	0.9150	0.6000	0.5100
		0.6800	0.9150	1.0000	0.8030
		1.0000	0.8030	-	-
	27	0.0000	0.2200	0.0000	0.2200
		0.1000	0.5400	0.3000	0.2600
		0.3500	1.0100	1.0000	0.9130
		0.7100	1.0100	-	-
		1.0000	0.9130	-	-
1.0	17	0.0000	0.2600	0.0000	0.2600
		0.1000	0.6000	0.3000	0.2800
		0.3500	0.8200	1.0000	0.7180
		0.6400	0.8200	-	-
		1.0000	0.7180	-	-
	22	0.0000	0.3500	0.0000	0.3500
		0.1000	0.6000	0.4300	0.3500
		0.5000	0.9400	1.0000	0.8400
		0.7300	0.9400	-	-
		1.0000	0.8400	-	-

TABLE VI - Continued

Blade Height (in.)	Corrected Work Output (Btu/lbm)	Suction		Pressure	
		Fractional Length	Mach Number	Fractional Length	Mach Number
	27	0.0000	0.3200	[illegible]	0.3200
		0.1500	0.7000	[illegible]	0.3200
		0.6000	1.0900	[illegible]	0.9660
		0.6700	1.0900	-	-
		1.0000	0.9660	-	-
0.7	17	0.0000	0.4400	0.0000	0.4400
		0.1000	0.8200	0.3000	0.4800
		0.6000	0.8200	1.0000	0.6510
		1.0000	0.6510	-	-
	22	0.0000	0.4800	0.0000	0.4800
		0.1000	0.9000	0.3000	0.5000
		0.6500	0.9000	1.0000	0.7340
		1.0000	0.7340	-	-
	27	0.0000	0.4500	0.0000	0.4500
		0.2000	1.0000	0.3000	0.4500
		0.6800	1.0000	1.0000	0.8530
		1.0000	0.8520	-	-
1.0	17	0.0000	0.5000	0.0000	0.5000
		0.1000	0.7300	0.7500	0.5000
		0.6000	0.7300	1.0000	0.5790
		1.0000	0.5790	-	-
	22	0.0000	0.6000	0.0000	0.6000
		0.1000	0.8600	0.7500	0.6000
		0.6000	0.8600	1.0000	0.6900
		1.0000	0.6900	-	-
	27	0.0000	0.7000	0.0000	0.7000
		0.1000	1.0200	0.7500	0.7000
		0.5600	1.0200	1.0000	0.8170
		1.0000	0.8170	-	-

TABLE VII. PRESCRIBED SURFACE MACH NUMBER DISTRIBUTIONS - ROTOR ROOTS

Blade Height (in.)	Corrected Work Output (Btu/lbm)	Suction		Pressure	
		Fractional Length	Mach Number	Fractional Length	Mach Number
0.7	17	0.0000	0.4400	0.0000	0.4400
		0.1000	0.8200	0.3000	0.4800
		0.6000	0.8200	1.0000	0.6510
		1.0000	0.6510	-	-
	22	0.0000	0.4800	0.0000	0.4800
		0.1000	0.9000	0.3000	0.5000
		0.6500	0.9000	1.0000	0.7340
		1.0000	0.7340	-	-
	27	0.0000	0.4500	0.0000	0.4500
		0.2000	1.0000	0.3000	0.4500
		0.6800	1.0000	1.0000	0.8530
		1.0000	0.8520	-	-
1.0	17	0.0000	0.5000	0.0000	0.5000
		0.1000	0.7300	0.7500	0.5000
		0.6000	0.7300	1.0000	0.5790
		1.0000	0.5790	-	-
	22	0.0000	0.6000	0.0000	0.6000
		0.1000	0.8600	0.7500	0.6000
		0.6000	0.8600	1.0000	0.6900
		1.0000	0.6900	-	-
	27	0.0000	0.7000	0.0000	0.7000
		0.1000	1.0200	0.7500	0.7000
		0.5600	1.0200	1.0000	0.8170
		1.0000	0.8170	-	-

TABLE VIII. BLADE GEOMETRIC DATA

Odd Cascade Numbers 1-17 - Stator Means
Even Cascade Numbers 2-18 - Rotor Means
Cascade Numbers 21-26 - Rotor Roots

Cascade Number	Blade Height (in.)	Corrected Work Output (Btu/lbm)	Pitch (s)	Pitch/Chord Ratio (s/c)	Aspect Ratio Blade (H/c)	Aspect Ratio Passage (H/o)
1	0.4	17	0.503	0.703	0.560	1.795
2	0.4	17	0.535	0.692	0.518	1.538
3	0.4	22	0.540	0.737	0.546	1.870
4	0.4	22	0.575	0.676	0.471	1.282
5	0.4	27	0.579	0.698	0.482	1.980
6	0.4	27	0.705	0.659	0.384	0.930
7	0.7	17	0.463	0.702	1.060	4.700
8	0.7	17	0.488	0.555	0.778	2.780
9	0.7	22	0.542	0.732	0.946	4.830
10	0.7	22	0.571	0.676	0.875	3.016
11	0.7	27	0.613	0.730	0.833	4.854
12	0.7	27	0.700	0.680	0.693	2.604
13	1.0	17	0.542	[illegible]	1.333	5.800
14	1.0	17	0.561	0.69[illegible]	[illegible].235	4.970
15	1.0	22	0.560	0.772	1.380	7.190
16	1.0	22	0.578	0.672	1.163	5.060
17	1.0	27	0.575	0.767	1.333	8.630
18	1.0	27	0.649	0.705	1.087	4.640
*						
21	0.7	17	0.510	0.548	0.753	2.825
22	0.7	22	0.512	0.563	0.770	2.965
23	0.7	27	0.637	0.601	0.660	2.480
24	1.0	17	0.449	0.528	1.178	5.896
25	1.0	22	0.476	0.523	1.100	5.967
26	1.0	27	0.547	0.547	1.000	5.397

*Cascades 19 and 20 are discussed in Appendix IV.

TABLE IX. DESIGN VALUES OF TOTAL-TO-STATIC PRESSURE RATIO

Cascade Number	$(P_o/P)_{EXIT}$	$(P_o/p)_{MAX}$
1	1.3022	1.4661
2	1.6173	1.9379
3	1.5396	1.7714
4	1.6987	2.0704
5	1.8732	2.1351
6	1.8538	2.3476
7	1.4111	1.5243
8	1.4124	1.5792
9	1.5568	1.6913
10	1.5289	1.7192
11	1.6695	1.8078
12	1.7154	1.9152
13	1.4468	1.5243
14	1.4098	1.5552
15	1.5743	1.6731
16	1.5873	1.7675
17	1.6950	1.8078
18	1.8201	2.1089
*	-	-
21	1.3294	1.5552
22	1.4307	1.6913
23	1.6072	1.8929
24	1.2550	1.4254
25	1.3748	1.6207
26	1.5505	1.9379

*Cascades 19 and 20 are discussed in Appendix IV.

TABLE X. EXPERIMENTAL RESULTS--TOTAL-PRESSURE-LOSS COEFFICIENTS

Cascade Number	Local Loss Coefficients at Immersion Depths (in.) A	B	C	D	Section Two-Dimensional Loss	Total Loss
	I. 0.4-in.-Height Cascades					
	A = 0.050	B = 0.100	C = 0.150	D = 0.200		
1	0.085	0.116	0.084	0.081	0.075	0.090
3	0.080	0.098	0.075	0.068	0.054	0.081
5	0.096	0.089	0.105	0.134	0.071	0.102
2	0.091	0.074	0.056	0.062	0.054	0.074
4	0.077	0.080	0.057	0.070	0.054	0.070
6	0.111	0.067	0.059	0.054	0.045	0.081
	II. 0.7-in.-Height Cascades					
	A = 0.050	B = 0.150	C = 0.250	D = 0.350		
7	0.123	0.090	0.085	0.065	0.073	0.094
9	0.076	0.061	0.057	0.051	0.088	0.063
11	0.102	0.084	0.094	0.088	0.124	0.093
8	0.100	0.146	0.119	0.098	0.117	0.119
10	0.074	0.089	0.112	0.080	0.089	0.091
12	0.064	0.079	0.107	0.096	0.069	0.087
	III. 1.0-in.-Height Cascades					
	A = 0.071	B = 0.214	C = 0.357	D = 0.500		
13	0.088	0.097	0.065	0.066	0.067	0.081
15	0.108	0.076	0.077	0.078	0.092	0.086
17	0.152	0.144	0.142	0.136	0.141	0.145
14	0.110	0.149	0.161	0.124	0.121	0.141
16	0.146	0.190	0.199	0.180	0.135	0.181
18	0.118	0.180	0.222	0.173	0.219	0.176

TABLE X - Continued

Cascade Number	Local Loss Coefficients at Immersion Depths (in.) A	B	C	D	Suction Test Midchannel Loss	Total Loss
	IV. 0.7-in.-Rotor Root Section Cascades					
	A = 0.058	B = 0.150	C = 0.250	D = 0.350		
21	0.160	0.174	0.200	0.145	0.161	0.174
22	0.110	0.147	0.215	0.152	0.150	0.159
23	0.139	0.126	0.180	0.190	0.109	0.156
	V. 1.0-in.-Rotor Root Section Cascades					
	A = 0.071	B = 0.214	C = 0.357	D = 0.500		
24	0.451	0.323	0.385	0.330	0.343	0.378
25	0.382	0.531	0.459	0.393	0.388	0.450
26	0.394	0.326	0.345	0.221	0.563	0.334

TABLE XI. SUCTION SURFACE DIFFUSION RATES

Cascade Number	$\frac{M_{max} - M_{ex}}{(M_{ex})(\Delta s/s)}$	$\frac{M_{max}}{M_{ex}}$
1	0.4281	1.2139
2	0.4731	1.1892
3	0.3256	1.1636
4	0.5732	1.1943
5	0.3670	1.1113
6	0.7288	1.2019
7	0.3755	1.1123
8	0.4432	1.1596
9	0.2928	1.0966
10	0.4359	1.1398
11	0.2534	1.0810
12	0.3664	1.1061
13	0.3862	1.0720
14	0.3946	1.1421
15	0.3872	1.0693
16	0.4409	1.1190
17	0.4287	1.0641
18	0.3890	1.1284
*	-	-
21	0.6490	1.2590
22	0.6462	1.2258
23	0.5428	1.1734
24	0.6520	1.2614
25	0.6159	1.2473
26	0.5647	1.2483

*Cascades 19 and 20 are discussed in Appendix IV.

TABLE XII. CONTRIBUTION OF MIXING LOSS TO FULLY MIXED LOSS COEFFICIENTS

Cascade Number	Total Loss	Mixing/ Total Loss	Mean-Line Loss (Solid)	Mixing/ Mean-Line Loss	Mean-Line Loss (Suction)	Mixing/ Mean-Line Loss
1	0.0897	0.0346	0.0815	0.0245	0.0761	0.0237
3	0.0806	0.0360	0.0676	0.0296	0.0544	0.0386
5	0.1017	0.1013	0.1337	0.0748	0.0707	0.1259
7	0.0937	0.0181	0.0651	0.0138	0.0730	0.0329
9	0.0629	0.0350	0.0514	0.0389	0.0877	0.0844
11	0.0926	0.0821	0.0879	0.0762	0.1242	0.1047
13	0.0807	0.0260	0.0657	0.0289	0.0673	0.0594
15	0.0855	0.0877	0.0777	0.0824	0.0920	0.1707
17	0.1446	0.1307	0.1363	0.1233	0.1411	0.3203
2	0.0740	0.0432	0.0619	0.0307	0.0543	0.0276
4	0.0701	0.0599	0.0699	0.0372	0.0536	0.0373
6	0.0811	0.0703	0.0537	0.0335	0.0453	0.0331
8	0.1188	0.0253	0.0984	0.0193	0.1169	0.0171
10	0.0914	0.0438	0.0795	0.0302	0.0887	0.0338
12	0.0868	0.0668	0.0959	0.0428	0.0688	0.0320
14	0.1407	0.0242	0.1237	0.0097	0.1211	0.0116
16	0.1814	0.0209	0.1802	0.0117	0.1350	0.0207
18	0.1759	0.0773	0.1733	0.0831	0.2188	0.0795
21	0.1741	0.0437	0.1454	0.0468	0.1605	0.0268
22	0.1589	0.0346	0.1524	0.0249	0.1500	0.0240
23	0.1556	0.0347	0.1898	0.0332	0.1090	0.0275
24	0.3784	0.0219	0.3296	0.0200	0.3427	0.0105
25	0.4500	0.0171	0.3927	0.0206	0.3877	0.0098
26	0.3344	0.0209	0.2207	0.0317	0.5630	0.0117

TABLE XIII. PERFORMANCE OF LEANED CASCADES

Streamtube Number	1	2	3	4	5	6	7
Flow Angle, deg							
0 deg lean	72.8	72.2	72.2	72.2	72.2	72.2	72.8
10 deg lean	78.4	77.4	76.9	75.8	73.7	72.6	71.5
20 deg lean	84.8	77.9	76.6	74.8	72.5	70.0	67.4
Axial Velocity, fps							
0 deg lean	316	329	329	330	329	326	316
10 deg lean	212	231	239	277	298	318	339
20 deg lean	86	218	249	282	322	368	416
Total-Pressure-Loss Coefficient							
0 deg lean	0.076	0.061	0.058	0.051	0.058	0.061	0.076
10 deg lean	0.121	0.114	0.112	0.057	0.073	0.106	0.062
20 deg lean	0.493	0.180	0.084	0.076	0.077	0.047	0.040

LITERATURE CITED

1. Rogo, C., and Tabbey, A., Experimental Investigation of Low Aspect Ratio and Tip Clearance on Turbine Performance and Aerodynamic Design (Report No. 1043), Continental Aviation and Engineering Corporation, Detroit, Michigan, 1967.

2. Analysis of Geometry and Design Point Performance of Axial Flow Turbines, Part I - Development of the Analysis Method and the Loss Coefficient Correlation (NREC Report No. 1125-1), Northern Research and Engineering Corporation, Cambridge, Massachusetts, September 14, 1967.

3. Analysis of Geometry and Design Point Performance of Axial Flow Turbines, Part II - Computer Program (NREC Report No. 1125-2), Northern Research and Engineering Corporation, Cambridge, Massachusetts, January 31, 1968.

4. Ainley, D. G., and Mathieson, G. C. R., A Method of Performance Estimation for Axial-Flow Turbines (R. & M. No. 2974), Aeronautical Research Council, London, 1957.

5. Stanitz, John D., and Sheldrake, Leonard J., Application of a Channel Design Method to High-Solidity Cascades and Tests of an Impulse Cascade with 90° of Turning (NACA Report No. 1116), National Advisory Committee for Aeronautics, 1953.

6. Stewart, W. L., Whitney, W. J., and Wong, R. Y., "A Study of Boundary Layer Characteristics of Turbomachine Blade Rows and Their Relation to Over-All Blade Loss", Trans. ASME, Journal of Basic Engineering, The American Society of Mechanical Engineers, Vol. 82, Series D, No. 3, September, 1960, pp. 588-592.

7. McEligot, D. M., et al, "Effect of Large Temperature Gradients on Convective Heat Transfer: The Downstream Region", Trans. ASME, The American Society of Mechanical Engineers, Series C, February, 1965, pp. 67-76.

8. Schlichting, Hermann, Boundary Layer Theory, McGraw-Hill Book Company, Inc., New York, 1960, pp. 321-323.

9. Schlichting, Hermann, Boundary Layer Theory, McGraw-Hill Book Company, Inc., New York, 1960, pp. 547-576.

10. Cooke, D. H., A Study of High-Mach-Number, High-Temperature Application of a Small, Single-Stage, Axial-Flow Gas Turbine (USAAVLABS TR 68-34), U. S. Army Aviation Materiel Laboratories, Fort Eustis, Virginia, June, 1968, AD 676184.

11. Wolf, H., Die Randverluste in Geraden Schaufelgittern, Wissenschaftliche Zeitschrift der Technischen Hochschule Dresden, 10, Heft 2, 1961.

APPENDIX I

ROTOR COOLING REQUIREMENTS

INTRODUCTION

An investigation of the efficiency limits of turbine stages operating at very high inlet temperatures should include an estimate of the performance penalty associated with any required coolant flows. The severity of this penalty is often great enough that an aerodynamically optimal design will require considerable modification to achieve the best overall cycle efficiency. For this reason, a preliminary cooling investigation was conducted as soon as the tentative stage and blade aerodynamic designs were established.

The two parameters of greatest importance in the aerothermodynamic analysis are normally the annulus height and the number of blades chosen for the design. The total heat transferred from the mainstream flow to the blades is directly proportional to the heat transfer surface area available, and thus to the annulus height; this parameter therefore indicates the gross cooling that a design will require. For a given pitch/chord ratio, on the other hand, the chosen number of blades fixes the blade chord and associated Reynolds number; this parameter therefore governs boundary-layer behavior on the blade surfaces and thus the heat transfer rates that will exist. In addition, for a given blade shape, the choice of blade number determines the cross-sectional area available for coolant passages and thus the maximum gross cooling that can be achieved.

In the present case, annulus heights and blade numbers have been chosen so as to span a reasonable range of aerodynamically efficient stage designs with high specific power outputs. It is still of importance, however, to consider the likely cooling penalties in addition to the experimentally determined aerodynamic losses when evaluating the overall performance that the various stages could be expected to achieve in practice. This appendix accordingly presents a preliminary analysis of three representative stages of differing annulus heights.

ANALYSIS MODEL

The objective of the simplified analysis is to determine the overall cooling flow requirement of a given stage, disregarding the detailed placement of the cooling passages within the blade profile. Thus, the blade may be replaced with a circular cylinder of equal height, H, and perimeter, P_s, and the following assumptions may be made:

1. The adiabatic wall temperature, T_s, is constant and equal to the row inlet relative total temperature at the hub (i.e., the recovery factor is unity).

2. The external heat transfer coefficient, h_s, is constant and equal to the area-weighted mean of the coefficients about the actual blade.

3. The net radial conduction of heat is zero.

4. The metal temperature, T_m, is a function of radius only.

5. The cooling configuration may be represented as a number, N_c, of equivalent standardized holes of perimeter, P_c, and heat transfer coefficient, h_c.

Since there is no net radial conduction, the steady-state heat balance equation at any radius r in the annulus may be written

$$h_s P_s [T_s - T_m(r)] = h_c P_c N_c [T_m(r) - T_c(r)] \qquad (16)$$

where $T_c(r)$ is the radial distribution of coolant temperature. This function must satisfy the following equation:

$$\frac{dT_c}{dr} = \frac{h_c P_c [T_m(r) - T_c(r)]}{w\, c_p} \qquad (17)$$

where w is the flow rate in each passage. Eliminating $T_m(r)$ between these equations yields

$$\frac{dT_c}{dr} = K [T_s - T_c(r)] \qquad (18)$$

where

$$K = \frac{h_s P_s h_c P_c}{w c_p (h_s P_s + N_c h_c P_c)}$$

This equation has the familiar solution

$$T_c(r) = (T_{co} - T_s) e^{-Kr} + T_s \qquad (19)$$

where T_{co} is the coolant temperature at the inlet to the blade. Finally, by inserting this result into Equation 16, the radial distribution of metal temperature as a function of the number of cooling passages in the blade may be obtained:

$$T_m(r) = \frac{1}{h_s P_s + N_c h_c P_c}\left[h_s P_s T_s + N_c h_c P_c \left\{(T_\infty - T_s)\exp\left[\frac{-h_s P_s h_c P_c r}{WC_p(h_s P_s + N_c h_c P_c)}\right] + T_s\right\}\right] \quad (20)$$

Thus, the minimum acceptable number of cooling passages, N_c^*, may be determined from Equation 20 if the maximum allowable metal temperature, T_m^*, is known as a function of radius. T_m^* may, of course, be calculated independently, since it can be assumed to depend only on the centrifugal stress at a given radius and the particular design life in hours for the given material.

RESULTS OF THE ANALYSIS

Although stator coolant flows are usually comparable in magnitude to those in the rotor, this analysis has been limited to a study of three typical rotor rows, so that centrifugal stress levels may be used to furnish a clear criterion of allowable metal temperatures.

Centrifugal stress at the root section has been plotted versus uncooled metal temperature in Figure 4 for each of the nine rotor designs. It will be seen that, with the exception of the most highly loaded 0.4-in.-annulus-height design, all the rotors lie within a band parallel to, and approximately 750°F higher than, the 1000-hr stress-to-rupture curve for the assumed material, MAR-M200. Since the wall, coolant, and allowable metal temperatures are all known at the blade hub, Equation 16 may be used to obtain a lower limit to the required number of coolant passages:

$$N_c^* \geq \frac{h_s P_s \left[T_s - T_m^*(0)\right]}{h_c P_c \left[T_m^*(0) - T_{c0}\right]} \quad (21)$$

It can be shown that cooling is most effective when each hole carries the minimum amount of coolant, insuring fully turbulent flow; this occurs at a Reynolds number of approximately 10,000. Thus,

$$Re = 10000 = \frac{4W}{\mu P_c} \quad (22)$$

and if the holes are 0.02 in. in diameter,

$$W = 2500 \mu P_c \cong 1 \ \text{LBM/HR} \quad (23)$$

The corresponding coolant conductance has been calculated by the method of Reference 7.

$$h_c P_c = 2.33 \quad BTU/FT\,HR\,^\circ R \tag{24}$$

Surface conductances for the three chosen rotor rows have been calculated by the method of Squire (Reference 8), for the laminar regime, and Truckenbrodt (Reference 9), after transition to turbulent flow has been predicted. Results are tabulated below.

Annulus Height, in.	0.4	0.7	1.0
Stage Specific Work Output, Btu/lbm	17	22	27
Suction Surface Length, ft	0.0726	0.1054	0.1370
Suction Surface Mean, $\bar{k}$, Btu/ft^2 hr $^\circ$F	574.4	439.3	397.9
Pressure Surface Length, ft	0.0629	0.0750	0.0882
Pressure Surface Mean, $\bar{k}$, Btu/ft^2 hr $^\circ$F	273.9	212.3	322.9
Leading-Edge Surface Length, ft	0.0050	0.0067	0.0083
Leading-Edge Mean, $\bar{k}$, Btu/ft^2 hr $^\circ$F	900	750	1100
Average Surface Conductance, Btu/ft^2 hr $^\circ$F	63.43	67.25	92.12

Assuming that the coolant is bled from a 10:1 pressure ratio compressor of 80-percent isentropic efficiency,

$$T_{C0} \cong 1200\ ^\circ R \tag{25}$$

Thus, from Equation 21, the minimum required number of passages for the 0.4-, 0.7-, and 1.0-in. designs are 28, 38, and 60, respectively.

To determine if these are the required numbers of passages, radial distributions of allowable metal temperature were calculated from the material property curve of Figure 4, assuming that stress is directly proportional to annulus area.

$$\sigma(r) = \sigma_{HUB} \frac{1 - \left(\frac{r}{r_{TIP}}\right)^2}{1 - \left(\frac{r_{HUB}}{r_{TIP}}\right)^2}$$

where

$$\sigma_{HUB} = 4.52\, \rho_m A \left(\frac{N}{1000}\right)^2 \left[1 - \frac{1-\xi}{3}\left(\frac{2+D}{1+D}\right)\right] \tag{26}$$

ρ_m is metal density, lbm/cu in.

A is annulus area, sq in.

N is rotational speed, rpm

ξ is area taper ratio

D is hub/tip ratio

Actual metal temperatures along the blade were then computed from Equation 20 and were superimposed on the allowable temperatures. The results have been plotted as a function of annulus height in Figure 25. It will be observed that the minimum number of passages proved to be clearly sufficient for 0.4-in. and 0.7-in. rotors and marginally sufficient in the case of the 1.0-in. rotor. Thus, final estimates of the percentage coolant flow requirements of each of the rotors may be obtained from

$$\omega_{C,\,TOTAL} = \frac{N_B N_C \omega}{5 \times 3600} \times 100 \qquad (27)$$

where N_B is the number of rotor blades chosen for each row. Therefore, the predicted values, in order of increasing annulus height, are 7.3 percent, 8.0 percent, and 10.3 percent, respectively.

APPENDIX II

CASCADE PROFILE COORDINATES

This appendix documents the profile shapes of each of the cascades tested in the experimental program. The blades are defined by the Cartesian coordinates, in inches, of 20 points equally spaced along each surface. Circular arcs were employed to complete the leading and trailing edges.

The following additional information is included:

1. Gas inlet and exit angles
2. Stagnation point location
3. Suction and pressure surface lengths
4. Profile area
5. Blade pitch and chord
6. Number of blades

Cascades 19 and 20, omitted from this tabulation, were identical in profile shape to cascade 9.

PROFILE COORDINATES FOR CASCADE NO. 1 (STATOR MEAN)

Blade Height = 0.4 in.

Stage Corrected work Output = 17 Btu/lb

Gas Inlet Angle = 0.0 deg

Gas Exit Angle = +63.6 deg

Normalized Length	Suction Surface		Pressure Surface	
	x	y	x	y
0.000	-0.261	0.126	-0.254	0.078
0.050	-0.230	0.157	-0.225	0.059
0.100	-0.194	0.178	-0.195	0.044
0.150	-0.154	0.190	-0.165	0.029
0.200	-0.112	0.190	-0.135	0.014
0.250	-0.072	0.178	-0.106	-0.001
0.300	-0.035	0.158	-0.076	-0.017
0.350	-0.001	0.134	-0.047	-0.034
0.400	0.029	0.106	-0.019	-0.052
0.450	0.059	0.076	0.008	-0.071
0.500	0.086	0.044	0.035	-0.091
0.550	0.111	0.010	0.061	-0.112
0.600	0.134	-0.024	0.087	-0.134
0.650	0.156	-0.059	0.112	-0.156
0.700	0.177	-0.096	0.136	-0.180
0.750	0.197	-0.133	0.159	-0.204
0.800	0.217	-0.170	0.181	-0.230
0.850	0.236	-0.207	0.203	-0.255
0.900	0.254	-0.245	0.223	-0.282
0.950	0.272	-0.283	0.244	-0.309
1.000	0.290	-0.321	0.263	-0.336

"Stagnation" Point, x = -0.286, y = 0.100

Suction Surface Length = 0.839 in.

Pressure Surface Length = 0.672 in.

Cross-Sectional Area = 0.0822 sq in.

Pitch = 0.503 in.

Chord = 0.715 in.

Number of Blades = 50

PROFILE COORDINATES FOR CASCADE NO. 2 (ROTOR MEAN)

Blade Height = 0.4 in.

Stage Corrected Work Output = 17 Btu/lbm

Gas Inlet Angle = -26.57 deg

Gas Exit Angle = -60.796 deg

Normalized Length	Suction Surface		Pressure Surface	
	x	y	x	y
0.000	-0.253	0.193	-0.264	0.152
0.050	-0.214	0.207	-0.240	0.123
0.100	-0.173	0.209	-0.213	0.098
0.150	-0.132	0.202	-0.185	0.074
0.200	-0.095	0.185	-0.156	0.051
0.250	-0.060	0.163	-0.127	0.028
0.300	-0.028	0.137	-0.098	0.006
0.350	0.002	0.110	-0.068	-0.015
0.400	0.031	0.081	-0.038	-0.037
0.450	0.058	0.050	-0.009	-0.059
0.500	0.085	0.019	0.019	-0.082
0.550	0.110	-0.013	0.048	-0.105
0.600	0.134	-0.046	0.076	-0.129
0.650	0.157	-0.080	0.104	-0.153
0.700	0.180	-0.115	0.130	-0.179
0.750	0.201	-0.150	0.157	-0.205
0.800	0.222	-0.185	0.182	-0.232
0.850	0.242	-0.221	0.206	-0.259
0.900	0.262	-0.257	0.230	-0.287
0.950	0.282	-0.293	0.254	-0.316
1.000	0.301	-0.329	0.276	-0.345

"Stagnation" Point, x = -0.284, y = 0.181

Suction Surface Length = 0.822 in.

Pressure Surface Length = 0.738 in.

Cross-Sectional Area = 0.0759 sq in.

Pitch = 0.535 in.

Chord = 0.773 in.

Number of Blades = 47

PROFILE COORDINATES FOR CASCADE NO. 3 (STATOR MEAN)

Blade Height = 0.4 in.

Stage Corrected Work Output = 22 Btu/lbm

Gas Inlet Angle = 0.0 deg

Gas Exit Angle = +67.8 deg

Normalized Length	Suction Surface		Pressure Surface	
	x	y	x	y
0.000	-0.255	0.137	-0.245	0.085
0.050	-0.224	0.170	-0.215	0.066
0.100	-0.186	0.194	-0.184	0.051
0.150	-0.144	0.206	-0.153	0.034
0.200	-0.100	0.205	-0.123	0.018
0.250	-0.057	0.192	-0.093	0.000
0.300	-0.020	0.168	-0.063	-0.017
0.350	0.118	0.138	-0.035	-0.037
0.400	0.040	0.105	-0.007	-0.058
0.450	0.067	0.069	0.018	-0.081
0.500	0.091	0.032	0.042	-0.105
0.550	0.114	-0.005	0.066	-0.130
0.600	0.135	-0.044	0.090	-0.155
0.650	0.155	-0.083	0.113	-0.181
0.700	0.174	-0.123	0.135	-0.208
0.750	0.192	-0.164	0.156	-0.236
0.800	0.210	-0.204	0.177	-0.264
0.850	0.227	-0.245	0.196	-0.292
0.900	0.244	-0.286	0.215	-0.321
0.950	0.261	-0.327	0.233	-0.351
1.000	0.277	-0.368	0.251	-0.381

"Stagnation" Point, x = 0.289, y = 0.108

Suction Surface Length = 0.885 in.

Pressure Surface Length = 0.693 in.

Cross-Sectional Area = 0.0849 sq in.

Pitch = 0.54 in.

Chord = 0.733 in.

Number of Blades = 50

PROFILE COORDINATES FOR CASCADE NO. 4 (ROTOR MEAN)

Blade Height = 0.4 in.

Stage Corrected Work Output = 22 Btu/lbm

Gas Inlet Angle = -3.23 deg

Gas Exit Angle = -57.26 deg

Normalized Length	Suction Surface		Pressure Surface	
	x	y	x	y
0.000	-0.321	0.146	-0.318	0.111
0.050	-0.281	0.172	-0.280	0.093
0.100	-0.237	0.189	-0.242	0.078
0.150	-0.190	0.195	-0.204	0.063
0.200	-0.143	0.191	-0.166	0.046
0.250	-0.099	0.176	-0.129	0.029
0.300	-0.057	0.154	-0.093	0.010
0.350	-0.018	0.128	-0.057	-0.010
0.400	0.018	0.098	-0.023	-0.032
0.450	0.052	0.067	0.010	-0.055
0.500	0.086	0.033	0.043	-0.079
0.550	0.118	-0.000	0.076	-0.104
0.600	0.148	-0.036	0.108	-0.129
0.650	0.178	-0.073	0.139	-0.156
0.700	0.206	-0.110	0.170	-0.184
0.750	0.234	-0.149	0.199	-0.212
0.800	0.260	-0.188	0.228	-0.241
0.850	0.286	-0.227	0.256	-0.271
0.900	0.311	-0.267	0.284	-0.301
0.950	0.336	-0.307	0.311	-0.332
1.000	0.361	-0.347	0.337	-0.364

"Stagnation" Point, x = -0.349, y = 0.127

Suction Surface Length = 0.942 in.

Pressure Surface Length = 0.820 in.

Cross-Sectional Area = 0.0828 sq in.

Pitch = 0.575 in.

Chord = 0.850 in.

Number of Blades = 47

PROFILE COORDINATES FOR CASCADE NO. 5 (STATOR MEAN)

Blade Height = 0.4 in.

Stage Corrected Work Output = 27 Btu/lbm

Gas Inlet Angle = 0.0 deg

Gas Exit Angle = 69.55 deg

Normalized Length	Suction Surface		Pressure Surface	
	x	y	x	y
0.000	-0.289	0.156	-0.275	0.100
0.050	-0.253	0.193	-0.240	0.080
0.100	-0.210	0.220	-0.206	0.060
0.150	-0.161	0.233	-0.172	0.040
0.200	-0.110	0.231	-0.138	0.020
0.250	-0.062	0.216	-0.104	-0.000
0.300	-0.019	0.190	-0.071	-0.022
0.350	0.017	0.156	-0.039	-0.045
0.400	0.049	0.116	-0.007	-0.069
0.450	0.078	0.075	0.021	-0.096
0.500	0.105	0.032	0.049	-0.124
0.550	0.130	-0.011	0.077	-0.152
0.600	0.154	-0.056	0.104	-0.181
0.650	0.176	-0.101	0.130	-0.211
0.700	0.198	-0.147	0.155	-0.242
0.750	0.218	-0.193	0.179	-0.273
0.800	0.238	-0.240	0.202	-0.305
0.850	0.256	-0.287	0.224	-0.338
0.900	0.274	-0.335	0.245	-0.372
0.950	0.292	-0.382	0.264	-0.407
1.000	0.310	-0.430	0.284	-0.441

"Stagnation" Point, x = -0.336, y = 0.124

Suction Surface Length = 1.012 in.

Pressure Surface Length = 0.792 in.

Cross-Sectional Area = 0.1084 sq in.

Pitch = 0.579 in.

Chord = 0.830 in.

Number of Blades = 50

PROFILE COORDINATES FOR CASCADE NO. 6 (ROTOR MEAN)

Blade Height = 0.4 in.

Stage Corrected Work Output = 27 Btu/lb

Gas Inlet Angle = 14.92 deg

Gas Exit Angle = -52.56 deg

Normalized Length	Suction Surface		Pressure Surface	
	x	y	x	y
0.000	-0.433	0.101	-0.421	0.068
0.050	-0.389	0.144	-0.367	0.063
0.100	-0.338	0.178	-0.315	0.058
0.150	-0.281	0.200	-0.262	0.052
0.200	-0.220	0.209	-0.210	0.043
0.250	-0.160	0.202	-0.158	0.030
0.300	-0.102	0.184	-0.108	0.015
0.350	-0.046	0.158	-0.059	-0.005
0.400	0.006	0.127	-0.012	-0.029
0.450	0.056	0.092	0.033	-0.055
0.500	0.103	0.054	0.078	-0.082
0.550	0.149	0.013	0.123	-0.111
0.600	0.193	-0.028	0.166	-0.141
0.650	0.236	-0.072	0.208	-0.173
0.700	0.277	-0.116	0.250	-0.206
0.750	0.318	-0.163	0.290	-0.240
0.800	0.356	-0.210	0.330	-0.275
0.850	0.394	-0.258	0.368	-0.312
0.900	0.431	-0.307	0.406	-0.349
0.950	0.467	-0.356	0.443	-0.386
1.000	0.504	-0.405	0.480	-0.424

"Stagnation" Point, x = -0.464, y = 0.074

Suction Surface Length = 1.222 in.

Pressure Surface Length = 1.058 in.

Cross-Sectional Area = 0.1193 sq in.

Pitch = 0.705 in.

Chord = 1.07 in.

Number of Blades = 41

PROFILE COORDINATES FOR CASCADE NO. 7 (STATOR MEAN)

Blade Height = 0.7 in.

Stage Corrected Work Output = 17 Btu/lbm

Gas Inlet Angle = 0.0 deg

Gas Exit Angle = 71.2 deg

Normalized Length	Suction Surface		Pressure Surface	
	x	y	x	y
0.000	-0.241	0.124	-0.231	0.078
0.050	-0.211	0.154	-0.203	0.061
0.100	-0.177	0.176	-0.176	0.046
0.150	-0.138	0.189	-0.148	0.031
0.200	-0.097	0.191	-0.121	0.015
0.250	-0.057	0.183	-0.094	-0.000
0.300	-0.020	0.165	-0.068	-0.017
0.350	0.010	0.139	-0.042	-0.034
0.400	0.038	0.108	-0.017	-0.053
0.450	0.062	0.075	0.006	-0.074
0.500	0.084	0.041	0.029	-0.095
0.550	0.105	0.006	0.051	-0.117
0.600	0.124	-0.030	0.073	-0.140
0.650	0.142	-0.066	0.094	-0.163
0.700	0.159	-0.104	0.114	-0.188
0.750	0.175	-0.141	0.133	-0.212
0.800	0.190	-0.180	0.151	-0.238
0.850	0.204	-0.218	0.169	-0.264
0.900	0.217	-0.257	0.185	-0.291
0.950	0.230	-0.296	0.200	-0.318
1.000	0.243	-0.334	0.216	-0.346

"Stagnation" Point, x = -0.274, y = 0.099

Suction Surface Length = 0.819 in.

Pressure Surface Length = 0.628 in.

Cross-Sectional Area = 0.0775 sq in.

Pitch = 0.463 in.

Chord = 0.66 in.

Number of Blades = 40

PROFILE COORDINATES FOR CASCADE NO. 8 (ROTOR MEAN)

Blade Height = 0.7 in.

Stage Corrected Work Output = 17 Btu/lbm

Gas Inlet Angle = 34.98 deg

Gas Exit Angle = 64.08 deg

Normalized Length	Suction Surface		Pressure Surface	
	x	y	x	y
0.000	-0.351	0.038	-0.319	-0.008
0.050	-0.328	0.093	-0.274	-0.010
0.100	-0.295	0.142	-0.231	-0.010
0.150	-0.251	0.181	-0.187	-0.011
0.200	-0.198	0.206	-0.144	-0.015
0.250	-0.140	0.214	-0.101	-0.022
0.300	-0.081	0.208	-0.058	-0.033
0.350	-0.025	0.190	-0.018	-0.048
0.400	0.025	0.161	0.021	-0.067
0.450	0.072	0.125	0.059	-0.088
0.500	0.113	0.084	0.096	-0.112
0.550	0.152	0.039	0.130	-0.138
0.600	0.187	-0.007	0.164	-0.166
0.650	0.220	-0.056	0.195	-0.196
0.700	0.250	-0.106	0.226	-0.228
0.750	0.279	-0.158	0.255	-0.260
0.800	0.307	-0.210	0.283	-0.294
0.850	0.334	-0.262	0.309	-0.328
0.900	0.359	-0.315	0.335	-0.364
0.950	0.385	-0.368	0.360	-0.400
1.000	0.410	-0.422	0.384	-0.436

"Stagnation" Point, x = -0.364, y = -0.003

Suction Surface Length = 1.026 in.

Pressure Surface Length = 0.755 in.

Cross-Sectional Area = 0.1358 sq in.

Pitch = 0.488 in.

Chord = 0.88 in.

Number of Blades = 38

PROFILE COORDINATES FOR CASCADE NO. 9 (STATOR MEAN)

Blade Height = 0.7 in.

Stage Corrected Work Output = 22 Btu/lb

Gas Inlet Angle = 0.0 deg

Gas Exit Angle = 74.5 deg

Normalized Length	Suction Surface		Pressure Surface	
	x	y	x	y
0.000	-0.259	0.142	-0.242	0.090
0.050	-0.228	0.178	-0.212	0.072
0.100	-0.190	0.207	-0.182	0.053
0.150	-0.146	0.223	-0.153	0.034
0.200	-0.100	0.225	-0.125	0.014
0.250	-0.054	0.213	-0.097	-0.005
0.300	-0.013	0.191	-0.069	-0.026
0.350	0.021	0.160	-0.042	-0.048
0.400	0.049	0.123	-0.016	-0.070
0.450	0.074	0.083	0.008	-0.094
0.500	0.096	0.042	0.033	-0.119
0.550	0.117	0.000	0.057	-0.144
0.600	0.136	-0.042	0.079	-0.171
0.650	0.154	-0.085	0.100	-0.199
0.700	0.170	-0.129	0.120	-0.227
0.750	0.185	-0.173	0.139	-0.256
0.800	0.200	-0.218	0.158	-0.285
0.850	0.213	-0.262	0.175	-0.315
0.900	0.226	-0.307	0.192	-0.346
0.950	0.239	-0.353	0.207	-0.377
1.000	0.251	-0.398	0.223	-0.408

"Stagnation" Point, x = -0.308, y = 0.112

Suction Surface Length = 0.936 in.

Pressure Surface Length = 0.694 in.

Cross-Sectional Area = 0.0989 sq in

Pitch = 0.542 in

Chord = 0.740 in

Number of Blades = 40

PROFILE COORDINATES FOR CASCADE NO. 10 (ROTOR MEAN)

Blade Height = 0.7 in.

Stage Corrected Work Output = 22 Btu/lbm

Gas Inlet Angle = 39.0 deg

Gas Exit Angle = 66.02 deg

Normalized Length	Suction Surface		Pressure Surface	
	x	y	x	y
0.000	-0.336	0.038	-0.294	-0.017
0.050	-0.319	0.095	-0.251	-0.020
0.100	-0.287	0.145	-0.210	-0.020
0.150	-0.243	0.183	-0.168	-0.020
0.200	-0.190	0.209	-0.126	-0.024
0.250	-0.133	0.220	-0.085	-0.031
0.300	-0.075	0.216	-0.045	-0.042
0.350	-0.019	0.198	-0.007	-0.058
0.400	0.030	0.167	0.029	-0.078
0.450	0.074	0.129	0.064	-0.100
0.500	0.114	0.086	0.098	-0.125
0.550	0.150	0.039	0.131	-0.151
0.600	0.183	-0.008	0.162	-0.178
0.650	0.215	-0.057	0.192	-0.207
0.700	0.244	-0.108	0.221	-0.238
0.750	0.271	-0.160	0.248	-0.269
0.800	0.297	-0.213	0.274	-0.302
0.850	0.322	-0.266	0.298	-0.336
0.900	0.347	-0.319	0.322	-0.370
0.950	0.370	-0.373	0.345	-0.405
1.000	0.393	-0.427	0.367	-0.440

"Stagnation" Point, x = -0.344, y = -0.009

Suction Surface Length = 1.173 in.

Pressure Surface Length = 0.834 in.

Cross-Sectional Area = 0.1392 sq in.

Pitch = 0.571 in.

Chord = 0.845 in.

Number of Blades = 38

PROFILE COORDINATES FOR CASCADE NO. 11 (STATOR MEAN)

Blade Height = 0.7 in.

Stage Corrected Work Output = 27 Btu/lbm

Gas Inlet Angle = 0.0 deg

Gas Exit Angle = 76.375 deg

Normalized Length	Suction Surface		Pressure Surface	
	x	y	x	y
0.000	-0.294	0.164	-0.271	0.109
0.050	-0.258	0.207	-0.236	0.088
0.100	-0.215	0.241	-0.202	0.066
0.150	-0.164	0.259	-0.170	0.043
0.200	-0.110	0.260	-0.137	0.018
0.250	-0.058	0.245	-0.106	-0.006
0.300	-0.011	0.217	-0.075	-0.032
0.350	0.029	0.181	-0.046	-0.059
0.400	0.062	0.138	-0.017	-0.088
0.450	0.089	0.091	0.010	-0.116
0.500	0.113	0.042	0.038	-0.145
0.550	0.135	-0.007	0.065	-0.175
0.600	0.156	-0.057	0.091	-0.205
0.650	0.175	-0.108	0.115	-0.238
0.700	0.192	-0.160	0.137	-0.271
0.750	0.209	-0.212	0.158	-0.305
0.800	0.224	-0.264	0.179	-0.340
0.850	0.238	-0.317	0.198	-0.376
0.900	0.251	-0.370	0.216	-0.412
0.950	0.264	-0.423	0.233	-0.448
1.000	0.277	-0.476	0.249	-0.485

"Stagnation" Point, x = -0.347, y = 0.131

Suction Surface Length = 1.089 in.

Pressure Surface Length = 0.804 in.

Cross-Sectional Area = 0.1288 sq in.

Pitch = 0.613 in.

Chord = 0.840 in.

Number of Blades = 40

PROFILE COORDINATES FOR CASCADE NO. 12 (ROTOR MEAN)

Blade Height = 0.7 in.

Stage Corrected Work Output = 27 Btu/lbm

Gas Inlet Angle = 38.12 deg

Gas Exit Angle = 67.39 deg

Normalized Length	Suction Surface		Pressure Surface	
	x	y	x	y
0.000	-0.384	0.044	-0.346	-0.001
0.050	-0.363	0.113	-0.294	0.000
0.100	-0.330	0.175	-0.244	0.001
0.150	-0.279	0.225	-0.193	-0.002
0.200	-0.217	0.258	-0.143	-0.010
0.250	-0.148	0.271	-0.094	-0.023
0.300	-0.078	0.262	-0.047	-0.042
0.350	-0.013	0.234	-0.003	-0.067
0.400	0.042	0.191	0.037	-0.096
0.450	0.090	0.139	0.077	-0.127
0.500	0.133	0.083	0.116	-0.160
0.550	0.173	0.024	0.153	-0.195
0.600	0.209	-0.036	0.189	-0.231
0.650	0.244	-0.097	0.223	-0.268
0.700	0.277	-0.160	0.255	-0.307
0.750	0.308	-0.224	0.286	-0.347
0.800	0.338	-0.288	0.316	-0.389
0.350	0.367	-0.353	0.344	-0.431
0.900	0.394	-0.418	0.370	-0.474
0.950	0.421	-0.483	0.396	-0.518
1.000	0.448	-0.549	0.421	-0.562

"Stagnation" Point, x = -0.411, y = -0.010

Suction Surface Length = 1.416 in.

Pressure Surface Length = 1.014 in.

Cross-Sectional Area = 0.1818 sq in.

Pitch = 0.7 in.

Chord = 1.03 in.

Number of Blades = 35

PROFILE COORDINATES FOR CASCADE NO. 13 (STATOR MEAN)

Blade Height = 1.0 in.

Stage Corrected Work Output = 17 Btu/lbm

Gas Inlet Angle = 0.0 deg

Gas Exit Angle = 74.7 deg

Normalized Length	Suction Surface		Pressure Surface	
	x	y	x	y
0.000	-0.273	0.145	-0.255	0.097
0.050	-0.239	0.180	-0.222	0.079
0.100	-0.199	0.208	-0.190	0.061
0.150	-0.153	0.224	-0.159	0.043
0.200	-0.105	0.226	-0.128	0.023
0.250	-0.058	0.215	-0.098	0.002
0.300	-0.016	0.193	-0.069	-0.019
0.350	0.020	0.162	-0.042	-0.043
0.400	0.050	0.124	-0.015	-0.068
0.450	0.075	0.082	0.010	-0.093
0.500	0.098	0.040	0.036	-0.119
0.550	0.119	-0.003	0.061	-0.145
0.600	0.139	-0.047	0.085	-0.173
0.650	0.157	-0.091	0.107	-0.201
0.700	0.175	-0.136	0.128	-0.231
0.750	0.192	-0.181	0.148	-0.262
0.800	0.207	-0.227	0.166	-0.293
0.850	0.222	-0.273	0.184	-0.325
0.900	0.235	-0.320	0.201	-0.357
0.950	0.248	-0.366	0.216	-0.390
1.000	0.261	-0.413	0.231	-0.423

"Stagnation" Point, x = -0.319, y = 0.117

Suction Surface Length = 0.965 in.

Pressure Surface Length = 0.728 in.

Cross-Sectional Area = 0.1003 sq in.

Pitch = 0.5416 in

Chord = 0.75 in

Number of Blades = 29

PROFILE COORDINATES FOR CASCADE NO. 14 (ROTOR MEAN)

Blade Height = 1.0 in.

Stage Corrected Work Output = 17 Btu/lbm

Gas Inlet Angle = 55.07 deg

Gas Exit Angle = 67.8 deg

Normalized Length	Suction Surface		Pressure Surface	
	x	y	x	y
0.000	-0.331	-0.049	-0.300	-0.075
0.050	-0.323	0.014	-0.259	-0.061
0.100	-0.307	0.076	-0.218	-0.051
0.150	-0.275	0.130	-0.177	-0.044
0.200	-0.232	0.177	-0.135	-0.042
0.250	-0.180	0.212	-0.093	-0.044
0.300	-0.119	0.230	-0.051	-0.051
0.350	-0.056	0.228	-0.011	-0.065
0.400	0.003	0.206	0.026	-0.082
0.450	0.055	0.171	0.063	-0.102
0.500	0.102	0.127	0.099	-0.125
0.550	0.142	0.078	0.133	-0.150
0.600	0.179	0.026	0.165	-0.177
0.650	0.212	-0.027	0.196	-0.206
0.700	0.243	-0.082	0.225	-0.236
0.750	0.271	-0.139	0.252	-0.269
0.800	0.298	-0.197	0.278	-0.302
0.850	0.323	-0.255	0.303	-0.336
0.900	0.348	-0.314	0.326	-0.371
0.950	0.372	-0.373	0.348	-0.407
1.000	0.395	-0.431	0.370	-0.444

"Stagnation" Point, x = -0.340, y = -0.089

Suction Surface Length = 1.270 in.

Pressure Surface Length = 0.843 in.

Cross-Sectional Area = 0.1545 sq in.

Pitch = 0.561 in.

Chord = 0.81 in.

Number of Blades = 28

PROFILE COORDINATES FOR CASCADE NO. 15 (STATOR MEAN)

Blade Height = 1.0 in.

Stage Corrected Work Output = 22 Btu/lbm

Gas Inlet Angle = 0.0 deg

Gas Exit Angle = 76.9 deg

Normalized Length	Suction Surface		Pressure Surface	
	x	y	x	y
0.000	-0.246	0.152	-0.217	0.092
0.050	-0.218	0.192	-0.188	0.073
0.100	-0.182	0.222	-0.161	0.053
0.150	-0.137	0.237	-0.134	0.033
0.200	-0.091	0.236	-0.107	0.012
0.250	-0.046	0.221	-0.081	-0.008
0.300	-0.008	0.194	-0.057	-0.031
0.350	0.024	0.160	-0.034	-0.056
0.400	0.049	0.121	-0.011	-0.081
0.450	0.071	0.079	0.010	-0.106
0.500	0.091	0.037	0.032	-0.131
0.550	0.110	-0.005	0.054	-0.157
0.600	0.128	-0.049	0.075	-0.184
0.650	0.145	-0.093	0.094	-0.211
0.700	0.161	-0.137	0.112	-0.240
0.750	0.175	-0.182	0.130	-0.268
0.800	0.189	-0.227	0.146	-0.298
0.850	0.201	-0.272	0.162	-0.327
0.900	0.213	-0.318	0.177	-0.358
0.950	0.224	-0.364	0.191	-0.388
1.000	0.234	-0.409	0.205	-0.419

"Stagnation" Point, x = -0.286, y = 0.117

Suction Surface Length = 0.940 in.

Pressure Surface Length = 0.673 in.

Cross-Sectional Area = 0.0973 sq in.

Pitch = 0.5596 in.

Chord = 0.725 in.

Number of Blades = 32

PROFILE COORDINATES FOR CASCADE NO. 16 (ROTOR MEAN)

Blade Height = 1.0 in.

Stage Corrected Work Output = 22 Btu/lbm

Gas Inlet Angle = 58.5 deg

Gas Exit Angle = 69.4 deg

Normalized Length	Suction Surface		Pressure Surface	
	x	y	x	y
0.000	-	-0.094	-0.333	-0.123
0.050	-0.358	-0.024	-0.289	-0.107
0.100	-0.337	0.042	-0.246	-0.091
0.150	-0.304	0.104	-0.201	-0.079
0.200	-0.262	0.160	-0.156	-0.070
0.250	-0.208	0.205	-0.110	-0.066
0.300	-0.145	0.236	-0.064	-0.066
0.350	-0.076	0.247	-0.018	-0.071
0.400	-0.007	0.237	0.026	-0.081
0.450	0.056	0.208	0.069	-0.097
0.500	0.112	0.165	0.109	-0.119
0.550	0.159	0.113	0.148	-0.145
0.600	0.200	0.056	0.184	-0.174
0.650	0.237	-0.003	0.218	-0.205
0.700	0.271	-0.064	0.250	-0.238
0.750	0.303	-0.127	0.280	-0.273
0.800	0.331	-0.191	0.309	-0.309
0.850	0.359	-0.256	0.335	-0.347
0.900	0.384	-0.322	0.360	-0.386
0.950	0.409	-0.388	0.384	-0.425
1.000	0.433	-0.454	0.407	-0.466

"Stagnation" Point, x = -0.375, y = -0.136

Suction Surface Length = 1.406 in.

Pressure Surface Length = 0.922 in.

Cross-Sectional Area = 0.1922 sq in.

Pitch = 0.5776 in.

Chord = 0.86 in.

Number of Blades = 31

PROFILE COORDINATES FOR CASCADE NO. 17 (STATOR MEAN)

Blade Height = 1.0 in.

Stage Corrected Work Output = 27 Btu/lbm

Gas Inlet Angle = 0.0 deg

Gas Exit Angle = 78.375 deg

Normalized Length	Suction Surface		Pressure Surface	
	x	y	x	y
0.000	-0.254	0.162	-0.218	0.097
0.050	-0.227	0.205	-0.189	0.076
0.100	-0.189	0.236	-0.161	0.055
0.150	-0.142	0.251	-0.134	0.033
0.200	-0.093	0.249	-0.107	0.011
0.250	-0.047	0.231	-0.080	-0.011
0.300	-0.008	0.202	-0.055	-0.035
0.350	0.025	0.165	-0.032	-0.061
0.400	0.053	0.125	-0.009	-0.087
0.450	0.075	0.081	0.013	-0.114
0.500	0.096	0.036	0.035	-0.141
0.550	0.115	-0.008	0.058	-0.168
0.600	0.133	-0.054	0.078	-0.196
0.650	0.150	-0.100	0.097	-0.225
0.700	0.166	-0.147	0.115	-0.255
0.750	0.181	-0.194	0.133	-0.285
0.800	0.194	-0.241	0.150	-0.316
0.850	0.207	-0.289	0.166	-0.347
0.900	0.218	-0.337	0.181	-0.378
0.950	0.228	-0.385	0.195	-0.410
1.000	0.238	-0.433	0.209	-0.442

"Stagnation" Point, x = -0.293, y = 0.124

Suction Surface Length = 0.985 in

Pressure Surface Length = 0.698 in.

Cross-Sectional Area = 0.1054 sq in.

Pitch = 0.5745 in.

Chord = 0.75 in.

Number of Blades = 35

PROFILE COORDINATES FOR CASCADE NO. 18 (ROTOR MEAN)

Blade Height = 1.0 in.

Stage Corrected Work Output = 27 Btu/lbm

Gas Inlet Angle = 59.84 deg

Gas Exit Angle = 70.20 deg

Normalized Length	Suction Surface		Pressure Surface	
	x	y	x	y
0.000	-0.381	-0.100	-0.341	-0.127
0.050	-0.367	-0.023	-0.295	-0.107
0.100	-0.349	0.051	-0.249	-0.091
0.150	-0.320	0.122	-0.201	-0.078
0.200	-0.278	0.186	-0.152	-0.071
0.250	-0.221	0.238	-0.103	-0.069
0.300	-0.152	0.271	-0.053	-0.072
0.350	-0.075	0.279	-0.005	-0.080
0.400	-0.001	0.259	0.041	-0.096
0.450	0.064	0.220	0.085	-0.119
0.500	0.120	0.167	0.125	-0.147
0.550	0.169	0.108	0.164	-0.178
0.600	0.212	0.044	0.201	-0.211
0.650	0.251	-0.022	0.235	-0.246
0.700	0.286	-0.091	0.268	-0.284
0.750	0.318	-0.161	0.299	-0.322
0.800	0.348	-0.232	0.328	-0.362
0.850	0.377	-0.303	0.356	-0.403
0.900	0.404	-0.376	0.382	-0.446
0.950	0.430	-0.448	0.406	-0.488
1.000	0.456	-0.521	0.430	-0.532

"Stagnation" Point, x = -0.390, y = -0.148

Suction Surface Length = 1.542 in.

Pressure Surface Length = 0.989 in

Cross-Sectional Area = 0.2208 sq in.

Pitch = 0.6486 in.

Chord = 0.92 in.

Number of Blades = 31

PROFILE COORDINATES FOR CASCADE NO. 21 (ROTOR ROOT)

Blade Height = 0.7 in.

Stage Corrected Work Output = 17 Btu/lbm

Gas Inlet Angle = 49.23 deg

Gas Exit Angle = 60.94 deg

Normalized Length	Suction Surface		Pressure Surface	
	x	y	x	y
0.000	-0.390	0.006	-0.341	-0.049
0.050	-0.380	0.068	-0.295	-0.051
0.100	-0.349	0.123	-0.249	-0.047
0.150	-0.302	0.164	-0.204	-0.045
0.200	-0.245	0.191	-0.158	-0.045
0.250	-0.184	0.204	-0.112	-0.048
0.300	-0.121	0.205	-0.067	-0.054
0.350	-0.059	0.195	-0.022	-0.063
0.400	0.000	0.177	0.021	-0.076
0.450	0.057	0.150	0.064	-0.091
0.500	0.110	0.117	0.106	-0.109
0.550	0.160	0.079	0.147	-0.129
0.600	0.206	0.036	0.187	-0.152
0.650	0.248	-0.009	0.225	-0.177
0.700	0.287	-0.059	0.262	-0.204
0.750	0.323	-0.110	0.297	-0.233
0.800	0.357	-0.163	0.331	-0.263
0.850	0.389	-0.217	0.364	-0.295
0.900	0.420	-0.272	0.395	-0.328
0.950	0.450	-0.327	0.425	-0.363
1.000	0.479	-0.383	0.454	-0.398

"Stagnation" Point, x = -0.383, y = -0.036

Suction Surface Length = 1.256 in.

Pressure Surface Length = 0.914 in.

Cross-Sectional Area = 0.1700 sq in.

Pitch = 0.51 in.

Chord = 0.93 in.

Number of Blades = 32

PROFILE COORDINATES FOR CASCADE NO. 22 (ROTOR ROOT)

Blade Height = 0.7 in.

Stage Corrected Work Output = 22 Btu/lbm

Gas Inlet Angle = 52.66 deg

Gas Exit Angle = 62.41 deg

Normalized Length	Suction Surface		Pressure Surface	
	x	y	x	y
0.000	-0.382	-0.002	-0.330	-0.057
0.050	-0.375	0.060	-0.285	-0.057
0.100	-0.346	0.116	-0.240	-0.052
0.150	-0.302	0.161	-0.195	-0.048
0.200	-0.247	0.192	-0.150	-0.047
0.250	-0.186	0.208	-0.105	-0.050
0.300	-0.123	0.211	-0.061	-0.055
0.350	-0.060	0.202	-0.017	-0.065
0.400	-0.000	0.183	0.026	-0.078
0.450	0.056	0.155	0.068	-0.094
0.500	0.109	0.121	0.109	-0.112
0.550	0.158	0.081	0.149	-0.133
0.600	0.204	0.037	0.187	-0.156
0.650	0.246	-0.010	0.224	-0.182
0.700	0.284	-0.060	0.260	-0.209
0.750	0.319	-0.112	0.294	-0.239
0.800	0.352	-0.166	0.327	-0.269
0.850	0.383	-0.221	0.358	-0.302
0.900	0.413	-0.277	0.388	-0.335
0.950	0.442	-0.334	0.417	-0.370
1.000	0.471	-0.390	0.445	-0.405

"Stagnation" Point, x = -0.374, y = -0.045

Suction Surface Length = 1.265 in.

Pressure Surface Length = 0.900 in.

Cross-Sectional Area = 0.1719 sq in.

Pitch = 0.512 in.

Chord = 0.91 in.

Number of Blades = 38

PROFILE COORDINATES FOR CASCADE NO. 23 (ROTOR ROOT)

Blade Height = 0.7 in.

Stage Corrected Work Output = 27 Btu/lb

Gas Inlet Angle = 52.86 deg

Gas Exit Angle = 63.7 deg

Normalized Length	Suction Surface		Pressure Surface	
	x	y	x	y
0.000	-0.439	-0.036	-0.392	-0.083
0.050	-0.421	0.038	-0.337	-0.075
0.100	-0.390	0.108	-0.284	-0.064
0.150	-0.346	0.172	-0.230	-0.056
0.200	-0.290	0.223	-0.176	-0.052
0.250	-0.220	0.253	-0.122	-0.053
0.300	-0.144	0.263	-0.068	-0.060
0.350	-0.068	0.253	-0.016	-0.072
0.400	0.004	0.227	0.035	-0.093
0.450	0.070	0.189	0.085	-0.111
0.500	0.131	0.142	0.133	-0.136
0.550	0.186	0.089	0.179	-0.164
0.600	0.237	0.032	0.224	-0.195
0.650	0.284	-0.028	0.266	-0.228
0.700	0.327	-0.092	0.307	-0.264
0.750	0.367	-0.157	0.346	-0.302
0.800	0.405	-0.224	0.383	-0.342
0.850	0.441	-0.291	0.418	-0.383
0.900	0.476	-0.360	0.452	-0.425
0.950	0.510	-0.429	0.485	-0.469
1.000	0.543	-0.498	0.516	-0.513

"Stagnation" Point, x = -0.441, y = -0.085

Suction Surface Length = 1.535 in.

Pressure Surface Length = 1.085 in.

Cross-Sectional Area = 0.2323 sq in.

Pitch = 0.637 in.

Chord = 1.06 in.

Number of Blades = 35

PROFILE COORDINATES FOR CASCADE NO. 24 (ROTOR ROOT)

Blade Height = 1.0 in.

Stage Corrected Work Output = 17 Btu/lbm

Gas Inlet Angle = 65.42 deg

Gas Exit Angle = 67.8 deg

Normalized Length	Suction Surface		Pressure Surface	
	x	y	x	y
0.000	-0.382	-0.114	-0.346	-0.143
0.050	-0.380	-0.048	-0.303	-0.131
0.100	-0.363	0.015	-0.262	-0.115
0.150	-0.333	0.074	-0.220	-0.101
0.200	-0.291	0.125	-0.178	-0.090
0.250	-0.238	0.165	-0.135	-0.083
0.300	-0.178	0.191	-0.091	-0.078
0.350	-0.113	0.205	-0.047	-0.078
0.400	-0.047	0.208	-0.003	-0.081
0.450	0.017	0.200	0.039	-0.087
0.500	0.080	0.180	0.082	-0.096
0.550	0.139	0.150	0.124	-0.109
0.600	0.192	0.111	0.165	-0.126
0.650	0.238	0.064	0.204	-0.145
0.700	0.279	0.011	0.242	-0.168
0.750	0.314	-0.044	0.278	-0.194
0.800	0.346	-0.102	0.311	-0.223
0.850	0.375	-0.161	0.341	-0.254
0.900	0.401	-0.222	0.370	-0.287
0.950	0.426	-0.283	0.397	-0.322
1.000	0.450	-0.344	0.422	-0.358

"Stagnation" Point, x = -0.376, y = -0.146

Suction Surface Length = 1.322 in.

Pressure Surface Length = 0.878 in.

Cross-Sectional Area = 0.1944 sq in.

Pitch = 0.4488 in.

Chord = 0.85 in.

Number of Blades = 28

PROFILE COORDINATES FOR CASCADE NO. 25 (ROTOR ROOT)

Blade Height = 1.0 in.

Stage Corrected Work Output = 22 Btu/lbm

Gas Inlet Angle = 67.67 deg

Gas Exit Angle = 69.40 deg

Normalized Length	Suction Surface		Pressure Surface	
	x	y	x	y
0.000	-0.403	-0.136	-0.376	-0.162
0.050	-0.406	-0.063	-0.330	-0.147
0.100	-0.392	0.007	-0.285	-0.128
0.150	-0.363	0.075	-0.240	-0.113
0.200	-0.321	0.134	-0.194	-0.100
0.250	-0.264	0.179	-0.146	-0.092
0.300	-0.198	0.209	-0.099	-0.087
0.350	-0.127	0.225	-0.050	-0.086
0.400	-0.054	0.228	-0.003	-0.089
0.450	0.017	0.219	0.044	-0.096
0.500	0.087	0.197	0.091	-0.107
0.550	0.152	0.164	0.137	-0.122
0.600	0.210	0.120	0.181	-0.141
0.650	0.260	0.067	0.223	-0.163
0.700	0.303	0.008	0.264	-0.188
0.750	0.341	-0.053	0.302	-0.217
0.800	0.375	-0.118	0.338	-0.250
0.850	0.405	-0.184	0.371	-0.285
0.900	0.433	-0.252	0.401	-0.322
0.950	0.458	-0.320	0.430	-0.361
1.000	0.484	-0.388	0.456	-0.401

"Stagnation" Point, x = -0.401, y = -0.168

Suction Surface Length = 1.459 in.

Pressure Surface Length = 0.961 in.

Cross-Sectional Area = 0.2306 sq in.

Pitch = 0.4763 in.

Chord = 0.91 in.

Number of Blades = 31

PROFILE COORDINATES FOR CASCADE NO. 26 (ROTOR ROOT)

Blade Height = 1.0 in.

Stage Corrected Work Output = 27 Btu/lbm

Gas Inlet Angle = 68.80 deg

Gas Exit Angle = 70.20 deg

Normalized Length	Suction Surface		Pressure Surface	
	x	y	x	y
0.000	-0.424	-0.146	-0.404	-0.175
0.050	-0.434	-0.064	-0.353	-0.161
0.100	-0.424	0.016	-0.303	-0.142
0.150	-0.398	0.094	-0.252	-0.126
0.200	-0.355	0.164	-0.201	-0.114
0.250	-0.291	0.215	-0.148	-0.107
0.300	-0.215	0.246	-0.096	-0.103
0.350	-0.135	0.261	-0.043	-0.105
0.400	-0.052	0.262	0.009	-0.110
0.450	0.027	0.247	0.061	-0.120
0.500	0.104	0.219	0.112	-0.134
0.550	0.175	0.177	0.162	-0.152
0.600	0.237	0.123	0.210	-0.175
0.650	0.290	0.060	0.256	-0.201
0.700	0.336	-0.007	0.300	-0.231
0.750	0.377	-0.079	0.341	-0.264
0.800	0.413	-0.153	0.378	-0.301
0.850	0.446	-0.228	0.413	-0.341
0.900	0.476	-0.305	0.446	-0.383
0.950	0.504	-0.382	0.476	-0.427
1.000	0.531	-0.459	0.504	-0.472

"Stagnation" Point, x = -0.427, y = -0.183

Suction Surface Length = 1.645 in.

Pressure Surface Length = 1.059 in

Cross-Sectional Area = 0.2897 sq in

Pitch = 0.5472 in.

Chord = 1.00 in.

Number of Blades = 31

APPENDIX III

TOTAL-PRESSURE PROFILE MIXING LOSS

INTRODUCTION

The data obtained in the cascade tests consist of distributions of total pressure, static pressure, and flow angle in the plane traversed by the probe. Since the traverse plane was located one chord length downstream of the trailing-edge plane, some loss due to mixing of the total-pressure profiles is included in the measured data. However, a considerably greater flow length would have been required to eliminate all variations in the observed total pressures, particularly in the pitchwise direction. Thus, it is impractical to measure directly the fully mixed loss coefficients of the cascades; excessive duct losses in the downstream smoothing region would be unavoidable. On the other hand, simple mass-averaging of the profiles observed at the traverse plane is not sufficient, because the overall mixing loss can be considerable when the traversed profiles show large total-pressure variation. Hence, the additional mixing loss occurring downstream of the traverse plane was calculated by an analytic procedure. This appendix presents the equations that govern this mixing process and discusses the results obtained when the procedure was applied to the data from each of the cascade tests.

PROBLEM STATEMENT

The traverse plane is designated station 1, and a parallel downstream plane at which fully uniform conditions may be assumed to exist, station 2. Conditions at station 1 are defined by the measured pitchwise (y) and spanwise (z) distributions of total pressure, $P_{01}(y,z)$, static pressure, $p_1(y,z)$, and flow angle with respect to the x-direction, $\beta_1(y,z)$, and by the total temperature, T_{01}, assumed to be a constant. Assuming that the flow is two-dimensional and has no component of velocity in the z-direction, the four equations relating conditions at the two stations are the following:

1. Conservation of momentum in the x-direction

$$g_0 p_2 + \rho_2 V_2^2 \cos^2\beta_2 = \frac{1}{SH}\int_0^H\int_0^S (g_0 p_1 + \rho_1 V_1^2 \cos^2\beta_1)\,dz\,dy \qquad (28)$$

where S is pitch
H is span

2. Conservation of momentum in the y-direction

$$\rho_2 V_2^2 \sin\beta_2 \cos\beta_2 = \frac{1}{SH} \int_0^{H} \int_0^{s} (\rho_1 V_1^2 \sin\beta_1 \cos\beta_1)\, dx\, dy \qquad (29)$$

3. Continuity

$$\rho_2 V_2 \cos\beta_2 = \frac{1}{SH} \int_0^{H} \int_0^{s} (\rho_1 V_1 \cos\beta_1)\, dx\, dy \qquad (30)$$

4. Conservation of energy

$$T_{02} = T_{01} \qquad (31)$$

METHOD OF SOLUTION

The downstream static pressure may be eliminated from Equation 28 by applying the equation of state, the definition of total temperature, and Equation 31:

$$p_2 = R\rho_2 T_2 = R\rho_2 \left[T_{02} - \frac{V_2^2}{2g_0 J C_p}\right] = R\rho_2 \left[T_{01} - \frac{V_2^2}{2g_0 J C_p}\right] \qquad (32)$$

where it is assumed that the specific heat is a given constant. Then, by denoting the known definite integrals appearing on the right-hand sides of the first three equations by I_1, I_2, and I_3, respectively, we may reduce the equations to the following simplified form:

$$\begin{aligned} g_0 R\rho_2 \left[T_{01} - \frac{V_2^2}{2g_0 J C_p}\right] + \rho_2 V_2^2 \cos^2\beta_2 &= \frac{I_1}{SH} \\ \rho_2 V_2^2 \sin\beta_2 \cos\beta_2 &= \frac{I_2}{SH} \\ \rho_2 V_2 \cos\beta_2 &= \frac{I_3}{SH} \end{aligned} \qquad (33)$$

These equations have the following solution, as may be verified by direct substitution:

$$\beta_2 = \text{Arc Sin}\sqrt{A}$$
$$V_2 = I_2/(I_3 \sin\beta_2)$$
$$\rho_2 = I_3/(SH\, V_2 \cos\beta_2) \qquad (34)$$

where

$$A = \frac{M^2 - 2KL + M(M^2 - 4KL - 4L^2)^{1/2}}{2(K^2 + M^2)}$$

and

$$K \equiv g_0 R T_{01} I_3^2 - I_2^2$$
$$L \equiv (\gamma+1) I_2^2/2\gamma$$
$$M \equiv I_1 I_2$$

Hence, the fully mixed static pressure can be obtained from Equations 32 and 34, and the fully mixed total pressure can be obtained from

$$P_{02} = p_2 \left(\frac{P_0}{p}\right)_2 = \frac{p_2}{\left(1 - \frac{V_2^2}{2 g_0 J C_p T_{01}}\right)^{\gamma/\gamma-1}} \qquad (35)$$

RESULTS

A short computer program, designated Program MIXLOS, was written to perform the above calculation. The resulting fully mixed loss coefficients were employed without exception as the data for the new loss correlation. On the whole, the contribution of the mixing process to the final loss coefficients was small; in general, the increase in loss varied between 1 and 10 percent of the overall loss. In several cases, however, where the observed pressure and angle profiles were more severe, the mixing loss amounted to as much as 32 percent of the fully mixed loss. (Mixing loss was defined as the difference between the mass-averaged total pressure at station 1 and the total pressure at station 2 given by Equation 35.)

Table XII presents the fully mixed loss coefficients for each of the cascades, together with the percentages of these loss coefficients, which represented mixing loss downstream of the traverse plane. Data from each of the three major tests are included. These were the tests for the total losses, the mean-line losses, and the mean-line losses with boundary-layer suction.

In general, the percentage of mixing loss was found to increase with stage loading for both the stator and the rotor rows. Mixing loss constituted more than 10 percent of fully mixed loss in only four cases. Cascades 5 and 17, the most highly loaded 0.4- and 1.0-in.-height stators, showed high mixing losses in all three tests. The remaining two cascades exhibiting large mixing loss were the most highly loaded 0.7-in. stator and the high-deflection, 22-Btu/lbm, 1.0-in.-height stator. It is probable that all of these rows operated partially separated, particularly during the suction tests when additional diffusion was imposed because of the boundary-layer bleed. Hence, large mixing losses would be anticipated for these cascades.

APPENDIX IV

PERFORMANCE OF LEANED CASCADES

INTRODUCTION

The secondary flows that occur in the actual turbine stage environment are often particularly severe at the exit from the stator rows. Large static pressure gradients, which result from the high level of tangential velocity, transport low-momentum fluid on the blade surfaces toward the hub of the row. When the accumulated loss cores subsequently enter the rotating row, large additional losses can occur because of positive incidence on the highly loaded hub section and centrifugation of the low-velocity fluid.

If this model of secondary flow is correct, an obvious remedy would be to reduce the driving pressure gradient by leaning the blading with respect to the radial direction. Two leaned versions of the 22-Btu/lbm, 0.7-in.-height stator were accordingly included in the cascade test program. Lean angles with respect to a normal to the end walls of 10 and 20 deg were specified for the cascades. Profile shape, channel height, and test total-to-static pressure ratio were identical to those employed for cascade 9.

RESULTS OF CASCADE TESTS

The average total-pressure-loss coefficients for the cascades with 0, 10, and 20 deg of lean were 0.063, 0.092, and 0.109, respectively. Corresponding values of exit flow angle for the three rows were 72.4, 75.1, and 74.8 deg.

The detailed variation of measured performance is presented in Table XIII. The channel was divided horizontally into seven streamtubes of equal height, with the first streamtube located adjacent to the upper wall of the cascade. Values of fully mixed flow angle and total-pressure-loss coefficient were calculated for each streamtube as described in Appendix III. Meridional velocity was computed from the known exit dynamic head and flow angle. Symmetry about the mean line of the unleaned cascade was assumed; the remainder of the data represents results from actual traverses.

As the angle of lean was increased, considerably higher losses and flow angles at the upper wall and slightly lower losses and flow angles at the lower wall were observed. As mentioned earlier, the net result of these changes was to increase the average values of both deflection and loss level over those measured in the datum configuration. In addition, the through-flow velocity distribution, essentially constant for the unleaned cascade, became highly skewed at the high angle of lean.

DISCUSSION OF RESULTS

Although a rigorous treatment of nonisentropic flow conditions within a leaned blade row is beyond the scope of this report, a qualitative explanation of the experimental data may be attempted with the assistance of the schematic sketch below. The horizontal lines represent the walls of the cascade as viewed from downstream. Exit flow proceeds toward the left.

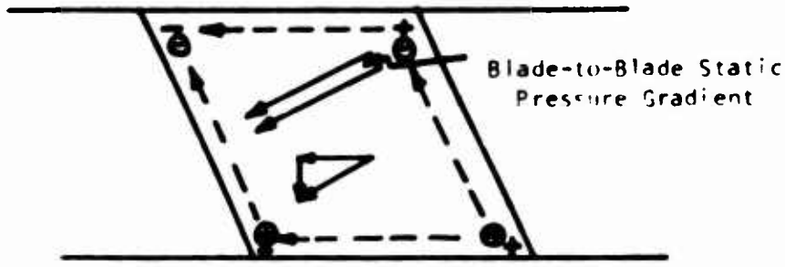

Hence, the pressure surface of the blade is on the right side of the channel. Under the influence of the blade-to-blade static pressure gradient, a fluid particle is accelerated in the direction indicated by the arrow. Hence, it tends to develop a downward velocity component. Since the particle is constrained by the lower wall from maintaining this downward component, a secondary static pressure field arises which elevates the pressure at the lower wall above that of the upper wall. This field has been indicated in the sketch by the circled signs.

Thus, the result of leaning a planar cascade is to create a spanwise pressure variation which tends to transport the blade surface boundary layers outward, as indicated by the dashed arrows. Therefore, accumulation of this low-velocity fluid led to the very high total-pressure loss and flow deflection recorded near the upper wall. The secondary flow in a leaned planar cascade is thus similar to, but opposite in direction from, that occurring in an unleaned annular cascade. In a leaned annular cascade, however, the result would have been to reduce the intensity of secondary flow through cancellation of the opposing pressure gradients.

Unclassified

Security Classification

DOCUMENT CONTROL DATA - R & D

(Security classification of title, body of abstract and indexing annotation must be entered when the overall report is classified)

1. ORIGINATING ACTIVITY (Corporate author)

Northern Research and Engineering Corporation
219 Vassar Street
Cambridge, Massachusetts 02139

2a. REPORT SECURITY CLASSIFICATION

Unclassified

2b. GROUP

3. REPORT TITLE

An Investigation of Efficiency Limits for Small, Cooled Turbines

4. DESCRIPTIVE NOTES (Type of report and inclusive dates)

Final Technical Report

5. AUTHOR(S) (First name, middle initial, last name)

Carter, Anthony F.
Lenherr, Fred K.

6. REPORT DATE	7a. TOTAL NO OF PAGES	7b. NO OF REFS
August 1970	122	11

8a. CONTRACT OR GRANT NO	9a. ORIGINATOR'S REPORT NUMBER(S)
DAAJ02-68-C-0050	USAAVLABS Technical Report 70-14
b. PROJECT NO Task 1G162203D14413	
c.	9b. OTHER REPORT NO(S) (Any other numbers that may be assigned this report) NREC Report No. 1137-1
d.	

10. DISTRIBUTION STATEMENT

This document is subject to special export controls, and each transmittal to foreign governments or foreign nationals may be made only with prior approval of U. S. Army Aviation Materiel Laboratories, Fort Eustis, Virginia 23604.

11. SUPPLEMENTARY NOTES	12. SPONSORING MILITARY ACTIVITY
	U. S. Army Aviation Materiel Laboratories Fort Eustis, Virginia

13. ABSTRACT

For engines with specific powers in excess of 200 hp sec/lbm and mass flow rates in the 2 to 5 lbm/sec range, small, cooled turbines are required. For axial turbines, the low blading aspect ratios and high trailing-edge blockages lead to relatively low efficiencies. A combined analytical and experimental investigation has been undertaken to define achievable efficiency limits for a particular engine requirement. Cascade tests of blade sections from nine designs of differing annulus height and corrected work output level have been used to obtain a total-pressure-loss correlation. This correlation, together with additional secondary loss factors derived from stage test data, has been used to predict achievable efficiencies. The results of the investigation show that the aspect ratio penalty is insufficient to offset the advantage of reduced stage loading factor for the range of annulus heights considered. Although an efficiency penalty of approximately 4 points was predicted for the smallest annulus height designs (compared with larger uncooled gas turbines), the smallest height considered produced the highest level of predicted achievable efficiency. (U)

DD FORM 1 NOV 68 1473 REPLACES DD FORM 1473, 1 JAN 64, WHICH IS OBSOLETE FOR ARMY USE.

Unclassified

Security Classification

14 KEY WORDS	LINK A		LINK B		LINK C	
	ROLE	WT	ROLE	WT	ROLE	WT
Small, cooled turbines						
Cascade tests						
Aspect ratio						
Secondary losses						
Total-pressure-loss correlation						
Achievable turbine efficiency						